UNIVERSITY OF THESSALY

POLYTECHNIC SCHOOL

DEPARTMENT OF MECHANICAL ENGINEERING

LABORATORY OF MATERIALS

Diploma Thesis

Integrated Modelling of the heat treatment of low-alloy TRIP steels

By

Kalamvokas Ioannis

Supervisor:

Dr. Helen Kamoutsi

Submitted for the Partial Fulfilment of the requirements for

the degree of Diploma in Mechanical Engineering

Certified by the members of the Thesis Committee:

First Examiner (Supervisor)

Dr. Helen Kamoutsi

Lab Teaching Staff,

Department of Mechanical Engineering,

University of Thessaly

Second Examiner

Dr. Nikolaos Aravas

Professor of Computational Mechanics of Structures

Department of Mechanical Engineering

University of Thessaly

Third Examiner

Dr. Dimitris Pantelis

Associate Professor of Stochastic Models of Operations Research in Industrial Management

Department of Mechanical Engineering

University of Thessaly

Acknowledgements

First and foremost, I would like to thank my supervisor, Dr. Helen Kamoutsi. Her continuous support during, not only the time of developing this work, but the whole period of my undergrad studies, has been a much needed asset. The completion of this work would not have been possible without her.

I would also like to thank Prof. G. Haidemenopoulos for his crucial inputs and constructive critisism throughout the whole process.

In addition, I would like to thank the personnel of the Physical Metallurgy Lab, for treating me as a member of the team and always offering a helping hand.

Finally, I would like to thank my family for always believing in me. Their constant sacrifices paved the way for me to follow my dreams, under any circumstances. Their love and support will always drive me forward, even in memory.

ABSTRACT

When designing high strength alloys, controlling the formation and development of phases that strengthen the microstructure is the most important part of the analysis. In an effort to carefully control the transformation and precipitation of phases, a lot of effort has been put through to simulate such procedures. This thesis is the continuance of efforts made to simulate the heat treatment of bainite strengthening alloys such as Dual Phase and TRIP steels. To achieve this, a MATLAB algorithm has been created, integrating calculations of paraequilibrium energies by pairing MATLAB with the Thermocalc Software. For the bainitic transformation, the Azuma model was used, and developed for both isothermal and continuous cooling processes. A series of experimental data was used as validation, from a DP and a TRIP steel alloy. The model was later applied to a TRIP 700 alloy. The results include volume fractions of all phases (austenite, ferrite, bainitic ferrite, cementite precipitates, and martensite), composition in Carbon, size of bainite platelets and yield strength of austenite.

Table of Contents

1 Theoretical Background

1.1 Introduction

In recent years the automotive industry strives to meet the demands for vehicle weight reduction to improve fuel economy and enhanced crash performance and passenger safety. Furthermore, the competition between steel and low-density metals (Al and Mg) has been growing. This demand has been passed on to steel manufactures, for new improved advanced high strength sheet steels (AHSS).

Methods for dealing with the high demands, except from alloying modification also involve processing combinations in order to produce unique microstructural combinations like DP (dual-phase), TRIP (transformation induced plasticity), HSLA (high strength low alloy), CP (complex phase), TWIP (twinning induced plasticity), and martensitic steels. The properties of these multi-phase steels are derived from appropriate combinations of phases and strengthening mechanisms. Continued developments of AHSS steels, require careful microstructure control to optimize the specific strengthening mechanisms responsible for the desirable final properties [1].

DP steels are currently the most applied AHSS grades. Interest in DP steels resulted from the combination of continuous yielding with an increase in strength while maintaining or improving ductility [2]. One important finding during research on DP steels was the contribution of retained austenite on the deformation behavior, as illustrated in the data in Figure 1.1-1. Marder observed that DP steels, that contain retained austenite had increased ductility relative to the increase in retained austenite [3]. Figure 1.1-1 illustrates the basis on which new developments in AHSS, especially transformation induced plasticity (TRIP) steels, were based.

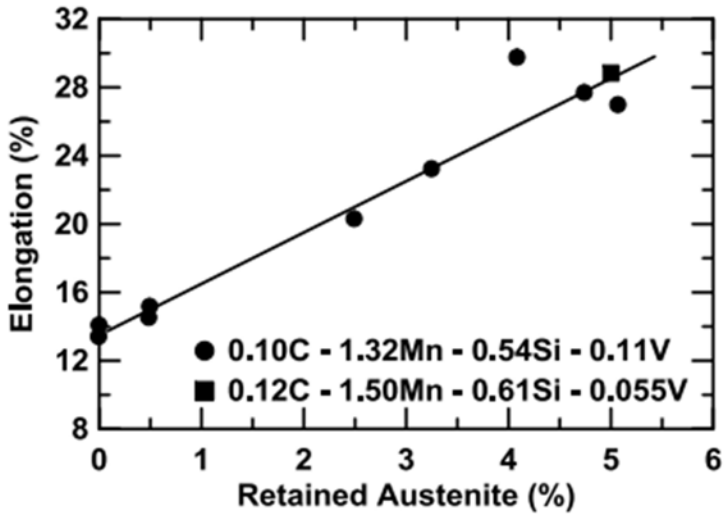

Figure 1.1-1 The effects of retained austenite on the ductility of two low carbon dual-phase steels [3].

In addition to DP steels, AHSS grades that are currently investigated by steel manufactures among others are TRansformation Induced Plasticity (TRIP) steels. These steel grades are part of the "first generation" AHSS. The "second generation" AHSS steels include, austenitic stainless steels,

Twinning Induced Plasticity (TWIP) steels, lightweight steels with induced plasticity (L-IP) and shear band strengthened steels (SIP) as illustrated in Figure 1.1-2.

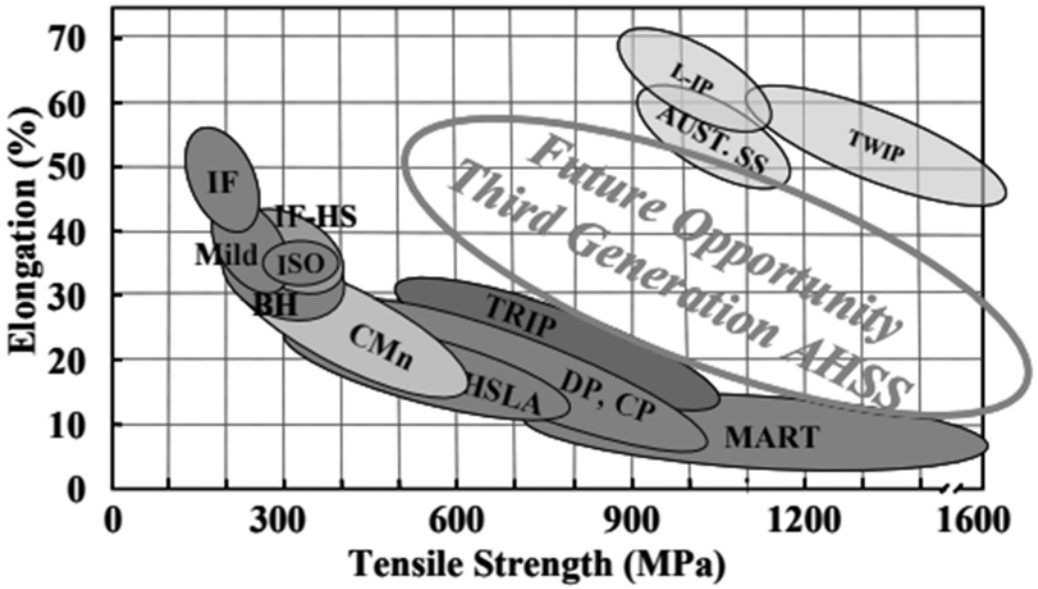

Figure 1.1-2 Overview of tensile strength and total elongation combinations for various classes of conventional and advanced high strength sheet steel (AHSS) grades [4, 5].

Enhanced strength/elongation combinations are clearly obtained for TRIP steel grades where strain-induced transformation of retained austenite into martensite results in increased strain hardening.

The second generation AHSS steels exhibit superior mechanical properties, high alloying results in a significant cost increase. Furthermore, TWIP steels with high manganese contents, have been shown to be prone to delayed cracking [6]. From Figure 1.1-2 it is clear that a property gap exists between the currently available AHSS grades of the first and second generations and defines a property band for future "Third Generation" AHSS. Current research is focused on this property window using modified or novel processing routes where [4, 7]. More specifically, ongoing AHSS research is focused on increasing strength and/or ductility to higher levels than exhibited by the first generation AHSS without significantly enriching the alloy compositions. Simultaneously it is also aimed at reducing the alloying levels in second generation AHSS grades. These strategies include: processing to enhance properties of DP steels; modifications to traditional TRIP steel processing; development of high strength steels with ultrafine bainitic microstructures; implementation of new processing routes including quenching and partitioning (Q&P); and development of high Mn content TRIP steels.

1.1.1 Enhanced DP Steels

Increase in the strength of a Dual Phase steels can be obtained by increasing the martensite volume fraction, altering carbon content and/or modifying the intercritical annealing temperature. Through this methodology Dual Phase steels with increased mechanical properties, DP780 and DP980, have been developed. A strength increase can also been obtained by microstructural refinement resulting from special hot deformation practices [8, 9].

1.1.2 Modified TRIP Steels

Early TRIP steel research was performed on grades with higher carbon contents than currently used in commercially available grades. Matsumura et al. investigated 0.4CMnSi grades [10, 11] and the high carbon level results in properties that merit consideration in the context of third generation AHSS objectives. Grain refinement of TRIP steels by microalloying has also been investigated [12]. Tensile strength levels up to 1 GPa with ductility levels of about 20 % total elongation have been obtained.

1.1.3 Ultrafine Bainite

Recent work has been conducted to create ultrafine bainitic microstructures [13, 14]. Low transformation temperatures in the range 125-325 °C were employed in a 0.98C-1.89Mn-1.46Si-1.26Cr-0.26Mo-0.09V alloy (in wt pct) which exhibited 600HV hardness and strength in excess of 2.5 GPa. The microstructure was obtained after a 15 day heat treatment, thus further work has been done on increasing bainite kinetics, reducing heat treatment to hours rather than days by alloying with Al and/or Co [15, 16].

1.1.4 Quenching and Partitioning

Quenching & Partitioning (Q&P) has been proposed recently as a new way of producing martensitic steels containing enhanced levels of retained austenite [17]. The process, consists of a two step thermal treatment where the steel is quenched to a predetermined temperature (quench temperature, QT) in the M_s-M_f range to produce a partially martensitic, partially austenitic microstructure. The second step, aims at carbon enrichment of the austenite by (partial) carbon depletion of the martensite and carbon transport to the austenite. The addition of molybdenum retards bainite transformation kinetics and has been shown to increase the retained austenite volume fraction whereas aluminum substitution for silicon has been found to accelerate the bainite reaction, and reduce the retained austenite fractions .

1.1.5 High Mn TRIP

An alternative processing concept has been proposed by Merwin [18] based on earlier work by Grange and Miller [19] to produce fine grained or ultra fine grained duplex ferrite-austenite microstructures based on “medium” manganese (5-7 wt pct), low carbon (0.1 wt pct) compositions. Manganese enrichment of austenite during intercritical annealing was recently applied to a cold rolled 0.1-C 7.1-Mn (wt pct) steel to produce a range of microstructures with varying austenite fraction and stability [18]. Based on equilibrium thermodynamic predictions samples of the steel were annealed for 168 hr at temperatures between 575^{o}C and 675^{o}C [20]. The long annealing times were employed to facilitate Mn partitioning. The resulting microstructures included between 2 and 43 pct retained austenite in a fine grained ferrite matrix (between 0.9 and 1.5 µm).

1.2 Bainite Transformation and modelling

As descripted above TRIP steels, with alloying process routes modifications are major players in the development for new steels “Third Generation” AHSS.

1.2.1 TRIP Steels

When austenite is deformed at temperatures above M_S but below the critical M_D temperature, it can transform to martensite if a critical stress or strain have been attained. TRIP phenomenon implies that the local transformation of metastable austenite to martensite hardens the portion of material where this transformation is occurring, thus preventing further strain localization in this region (Figure 1.2-1). The same behaviour then recurs in the next local region and over the entire specimen ensuring very high strain-hardening rate that facilitates very high uniform elongation in the material.

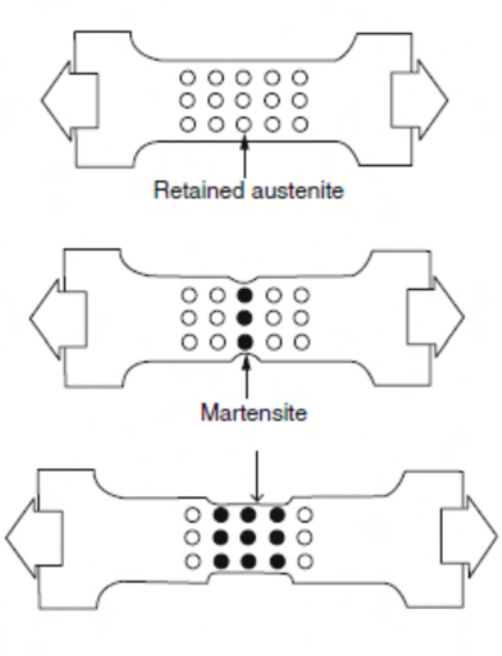

Figure 1.2-1 TRIP phenomenon: dark circles designate points where austenite has transformed to martensite

So, the precondition for the TRIP phenomenon is that the M_S temperature of retained austenite (RA) should be below the room temperature. M_S value can be estimated from equations [21, 22]. The M_D temperature depends on chemical composition of RA and its size. In comparison with the “classical” high-alloyed TRIP steels, the retention of austenite in low-alloyed steels requires the occurrence of certain transformation reactions that can lead to artificial “forced” carbon enrichment of the remaining austenite fraction the first carbon enrichment of austenite can take place during holding steel in the two-phase ferrite + austenite region due to partitioning of carbon to austenite.

For example, annealing at temperature that produces only 50 % of austenite doubles the carbon concentration in austenite with respect to the total carbon content in steel. This is followed by the second enrichment during initial slow cooling of steel when a portion of austenite transforms into new ferrite. Carbon, rejected from the newly formed ferrite, additionally enriches the remainder of austenite. The third step of austenite enrichment with carbon occurs during isothermal soak in the bainite region. Due to the transformation of major part of the available austenite to low-carbon bainite, practically all of the carbon that has been in steel is now concentrated in the remaining

retained austenite. The important finding though was the necessity to alloy the steel by strong ferrite stabilizers that facilitate formation of “carbon-free” bainite preventing potential losses of carbon in austenite.

1.2.2 Metallurgy of Manufacturing of TRIP Steels

The presence of retained austenite in final microstructure is the key point of the TRIP steel concept. Therefore, it is imperative to achieve maximum possible carbon content in the final portions of austenite to reduce the M_S temperature down to below the ambient temperature in steels that contain only about 0.2 % C. The thermal processing of TRIP steels must utilize all the possibilities to enrich the γ-phase with carbon during phase transformations occurring at consecutive stages of heat treatment.

1.2.3 Phase Transformations During Heat Treatment to Produce TRIP Steels

Three processes take place during heating to intercritical temperatures: recrystallization of ferrite, dissolution of cementite, and formation of austenite. All these processes are significantly affected by the preliminary structure and the heating rate. For example, if an initial content of ~0.2 % C in steel is assumed and a ferrite volume fraction of 50 % is achieve during intercritical annealing. The resulting strength of the steel shows that the (double) enrichment with carbon due to its partitioning to austenite during intercritical annealing is insufficient to approach the necessary carbon content in austenite portion.

Partial ferrite formation during slow cooling can increase carbon by another ~10–15 % which is still insufficient. Thus, to achieve maximum enrichment of austenite with carbon, to prevent martensitic transformation during final cooling to room temperature, an additional stage of carbon enrichment is needed. It is well known that during bainitic transformation, carbon is redistributed and ferrite/cementite (carbide) mixture is formed. Only additions of strong ferrite forming elements, like Si and Al, that inhibit carbide precipitations can result in the formation of “free carbon bainite” or “bainitic ferrite” and can thus promote further partitioning of carbon to the remaining austenite during bainite reaction.

1.2.4 Effect of Steel Composition

Effects of the steel composition on microstructure and properties of TRIP steels include A_{C1}–A_{C3} range and therefore on kinetics of austenitization, as well as the effects on recrystallization. The same factors (raising A_{C1} and expanding A_{C1}–A_{C3} temperature range) produce strong effects of chemical composition on the kinetics of austenitization. Since the main features of TRIP steels are based on the presence of retained austenite, the most important role of alloying is to enhance hardenability of γ-phase, to prevent pearlite formation during initial cooling from intercritical temperature down to IBT so that to preserve all carbon in the remaining austenite, and to ensure the necessary kinetics of bainite formation and proper enrichment of remaining austenite with carbon to decrease M_S below room temperature.

The presence of Si, Al, and other ferrite stabilizers in TRIP steel composition is necessary to suppress the formation of carbides during the bainitic reaction, thus preserving all carbon in the remaining austenite and facilitating the formation of bainitic ferrite. All of the initial TRIP designs were based on alloying with 1.0–2.0 % Si. Since high Si is not desirable for galvanizing process, other ferrite forming elements began to draw attention, including Al, P, V, Cr, Mo, Ti, and Nb.

The most successful substitutes of Si turned out to be Al and P individually and/or in various combinations with Si. Silicon is the key element in TRIP steels that makes the retention of austenite feasible at relatively low carbon content. The additions of Si facilitate enrichment of austenite with carbon and thus impact the stability of remaining austenite leading to higher volume fraction of retained austenite.

Additions of more than 1 % Si strongly retard the precipitation of carbides. In the presence of Si, the formation of cementite in bainite is shifted to higher temperatures and longer times, contributing to lowering M_S of remaining austenite. Matsumura et al. showed that the increase in Si content from 1.2 to 1.5 and 2.0 % resulted in increase in volume fraction of retained austenite at the same maximum carbon content in γ-phase indicating the enhanced retardation of carbide precipitation by Si. The increase in Si also retarded the completion of bainitic reaction, thereby increasing processing window: allowable holding at IBT was shifted to longer times where drastic decrease in RA volume fraction can be observed at lower Si contents [11].

Numerous comparisons of Si- and Al-added TRIP steels showed that by adjustment of chemical composition (C, Mn) and isothermal holding temperature/ time, the similar combinations of strength and ductility can be achieved in Al-bearing steels at higher uniform elongation and carbon content in austenite. The effects of Si and Al are illustrated in [23] showing the product of the amount of retained austenite and its carbon content against austempering time at 400^{o}C. Girault et al. concluded that Al as strong carbide inhibitor is less efficient than Si in the same concentration, although this contradiction with numerous literature data can be in part related to low carbon content (0.11 %) in steel used for this study [24]

Carbon is the most powerful element for enhancing the hardenability of austenite. Increase of C content also lowers the temperature of transition from upper to lower bainite. Carbon content in steel controls the amount of initial austenite at annealing of TRIP steels, its carbon content, possible amount of retained austenite in final microstructure, and potential strength of steel. The important drawback of higher carbon content is strong retardation of bainitic transformation kinetics [25]. Restrictions for carbon content are also determined by manufacturability limitations (such as, e.g., weldability). This motivates seeking the ways to achieve the prescribed strength at lower carbon content.

Manganese is an austenite stabilizer. Austenite hardenability is increased with increase in Mn content. Its presence prevents pearlite formation allowing for slower cooling from annealing temperatures, decreases the M_S temperature, but retards bainite formation. Typical Mn content in TRIP steels is 1.3–1.7 %. Manganese increases the strength of steel by solid solution strengthening. However, excessive manganese should be avoided because the inhibition of ferrite formation by Mn can reduce carbon enrichment of austenite during initial cooling.

1.3 Bainite

A phase that administers the benefit of added hardness is bainite. The transformation of bainite plays a significant role in the final mechanical characteristics of TRIP steels but is also found frequently in other types of high strength steels. Two types of morphologies exist; upper and lower bainite.

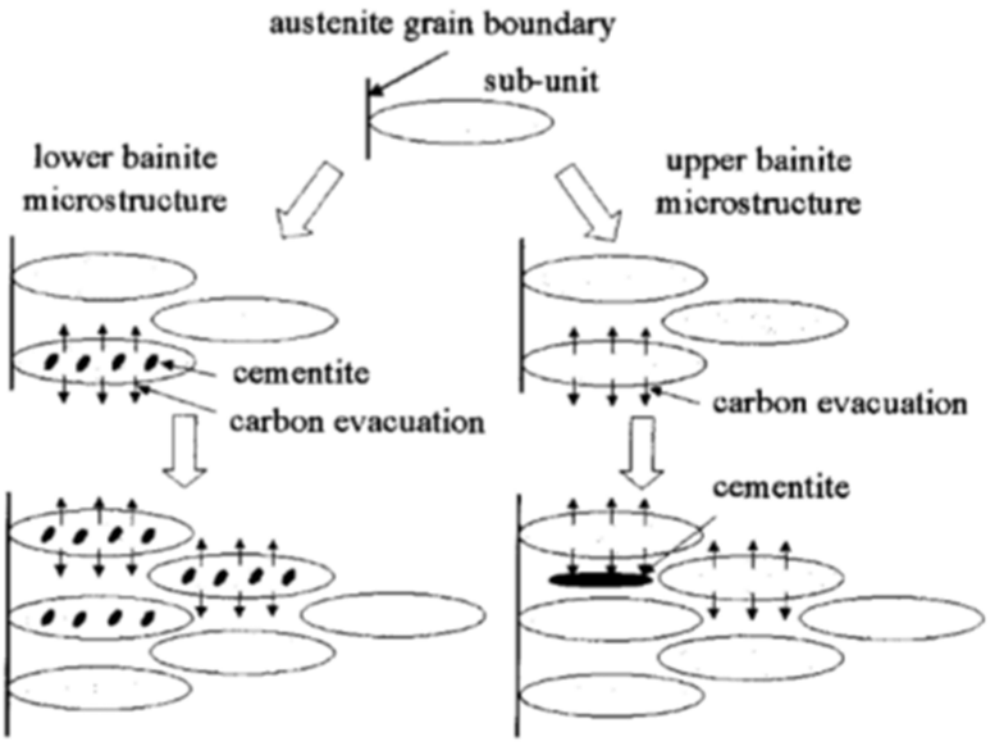

Figure 1.3-1 Bainite Transformation [26]

The transformation of the former evolves in two distinct stages. At first, nucleation of ferrite plates occurs at the austenite grain boundaries. Due to the very low solubility for carbon of the bainitic ferrite, the growth is accompanied with the enrichment of the austenite. Eventually, cementite precipitates from the residual austenite layers in between the ferrite. The amount of cementite depends mainly on the carbon concentration of the alloy. Upper bainite is formed in clusters of parallel plates called bainite sheaves. The formation of these plates causes change in the shape of the region, which can be described as an invariant-plane strain (IPS) with large shear component, identical to that of martensitic transformation. The strains put on the transformation region causes the deformation of the austenite grains, which in turn causes the increase of the density of dislocations. This blocks the growth of bainitic ferrite plates, causing the sheaves to grow to very small sizes compared to the austenite [26].

Lower bainite has similar characteristics to upper bainite. The major difference between them is that at the case of lower bainite cementite particles precipitate outside as well as inside of the ferrite plates. This means that all in all there are two kinds of cementite precipitates, one present at the carbon-rich austenite and one at the bainitic ferrite due to supersaturation.

However, when considering TRIP AL alloys, because of the aluminium present, such carbides are prevented from forming. This leads to the enrichment of the austenite at a greater extend, thus greatly reducing its ability to transform to martensite by quenching. The result is a complete lack of martensite in the microstructure, giving better formability to the end product.

The bainitic transformation proceeds by the nucleation and growth mechanisms. Two opposing doctrines have been proposed, regarding the controlling process of the bainitic transformation: diffusion-controlled growth and nucleation-control. According to the first approach, the rate of the

transformation is determined by the growth-rate of bainitic ferrite laths in austenite, which is considered to take place under diffusion-control. The opposing approach supports the idea that the overall transformation rate is determined by the rate at which bainitic ferrite nucleates in austenite. Up to now the controversy among the metallurgical community about these two opposing views remains unsolved.

Published modelling approaches are based either on the diffusion-control or on the nucleation-control mechanism. Most of the models however are based on the nucleation-control mechanism, which presents certain advantages over diffusion-control.

The most complete existing model is the one presented by Azuma et al [27]. Its major advantage over other existing models is that it takes into account and quantifies the precipitation of cementite during the bainitic transformation. This allows for a more realistic modelling of the bainitic transformation overall and, furthermore, it widens the range of applicability of the model to practically any steel composition and heat-treatment route (e.g. holding time in transformation temperature).

Other proposed models [28-30] which neglect carbide precipitation and focus solely on the kinetics of bainitic ferrite, are inevitably limited to be best applicable only to steel compositions for which carbide precipitation is severely suppressed, e.g. in steels containing Si and/or Al in excess of 1 mass %. But even in these cases, cementite will eventually precipitate at prolonged transformation times, which means that neglecting carbide precipitation poses limitations not only with respect to steel composition, but also with respect to heat-treatment conditions.

The model of Azuma et al [27] also manages to account for a number of significant aspects of the bainitic transformation. Due to its structure it can discriminate and identify the evolution of upper and lower bainite, depending on the chemistry of the steel and transformation temperature. Furthermore, it takes into account and calculates important microstructural features of bainite, such as the size of bainitic ferrite platelets and the size of cementite particles, as well as the variation of these microstructural features during the transformation (e.g. gradual refinement of bainitic ferrite platelets due to the gradual enrichment of untransformed austenite in carbon). Finally, although lacking in the form presented in reference [27], the model can be easily modified, in order to be applied for continuous cooling transformation.

Besides calculating vol. fractions, the model of reference [27] manages to provide quantitative information about a series of very interesting features, such as the average carbon content and yield strength of untransformed austenite, the average size of cementite precipitates, the average size of ferrite platelets, etc, all as functions of temperature and time. In conclusion, concerning the evaluation of existing models retrieved from literature, the model by Azuma et al seems to be the most complete, and presents the greatest potential for wide applicability in comparison to the other reported models.

1.4 Paraequilibrium Calculations

In order to apply and exploit the selected kinetic model for the bainitic transformation in the steels of interest, a series of cumbersome thermodynamic calculations have to be performed. For example, calculation of the thermodynamic driving-forces for the nucleation of the product phases (i.e. bainitic ferrite and cementite) in paraequilibrium with the respective parent phases, as functions of transformation temperature and C-content of parent austenite, is necessary, since these functions are required input to the kinetic model.

The kinetic theories of diffusional phase transformations in alloys containing both substitutional and interstitial elements are well developed [31]. An important feature of various kinetic models is the assumption of local equilibrium at the interface. Depending on the interface velocity during transformation, it is convenient to classify the kinetics into two distinct modes:

Partitioning local equilibrium is characterized by low interface velocity while maintaining local equilibrium at the interface. This condition is also referred to as orthoequilibrium (OE). The overall kinetics of OE transformation is governed by the slowest diffusing specie (substitutional element). The thermodynamic condition for OE between ferrite (α) and cementite (θ) in steels is given by

$$\mu_j^{\alpha} = \mu_j^{\theta} \tag{1}$$

where μi is the chemical potential of element i (=C, Co, Cr, Fe, Mn, Mo, Ni, Si) .

paraequilibrium (PE) is a kinetically constrained equilibrium when the diffusivity of the substitutional species is negligible compared to that of interstitial species. The kinetics of PE is governed by the fastest diffusing specie, which is either C or N in steels. Hultgren [32] argued that if carbon diffuses appreciably faster than the substitutional alloying elements, then the growing phase inherits the substitutional alloy contents. Furthermore, if the substitutional alloying elements are not allowed to partition, their individual chemical potentials have no physical relevance and thus the thermodynamic behavior of these elements can be expressed by one hypothetical element, Z. Then, PE is defined by a uniform carbon potential and a uniform site fraction of substitutional elements across the transforming interface. For example, in the case of α/θ transformation, the thermodynamic conditions for PE are given by

$$\mu_C^{\alpha} = \mu_C^{\theta} \tag{2}$$

$$y_C^{\alpha} = y_C^{\theta} \tag{3}$$

$$\mu_Z^{\alpha}\left(\equiv \sum y_j \mu_j^{\alpha}\right) = \mu_Z^{\theta}\left(\equiv \sum y_j \mu_j^{\theta}\right) \tag{4}$$

where the yj terms are the site fractions of substitutional element j (representing Co, Cr, Fe, Ni, Mo, V, and W). For a system containing both substitutional (j) and interstitial elements (C or N), the site fractions are related to the ordinary mole fractions (x) as follows.

$$y_j = \frac{x_j}{1 - x_C - x_N} \tag{5}$$

$$y_{C\text{ or }N} = \frac{p}{q}\frac{x_{C\text{ or }N}}{1 - x_C - x_N} \quad (6)$$

According to the two-sublattice model [8] used here to express substitutional alloying, p= 1 and q= 3 for ferrite, and p =q=1 for austenite.

Driving-forces under paraequilibrium are of special importance in the kinetic model and the method to calculate them has to be extended to all the major alloying elements in the steels under consideration. It is also necessary to calculate paraequilibrium concentrations between the involved phases, as well as the molar volumes of the product phases. Since there is no readily available computational thermodynamics software to implement the aforementioned calculations automatically, a methodology had to be developed towards this direction.

As the bainitic transformation in steels evolves, three simultaneous phase-transformations take place in the system (Figure 1.3-1):

$\gamma \rightarrow \gamma' + \alpha B$ (7)
$\gamma' \rightarrow \gamma'' + \theta\gamma$ (8)
$\alpha B \rightarrow \alpha' B + \theta\alpha$ (9)

In transformation (7), parent austenite (γ) of nominal C-content transforms to bainitic ferrite (αB). The untransformed fraction of austenite (γ′) is substantially enriched in C compared to parent austenite, due to the carbon rejected by bainitic ferrite.

In transformation (8), cementite (θγ) precipitates from C-rich austenite (γ′). Precipitation takes place within the austenitic grains, leading to the morphology known as upper bainite. The precipitation of cementite reduces drastically the C-content of austenite, so that the remaining austenite (γ′′) contains substantially lower amounts of carbon.

In transformation (9), cementite (θα) precipitates in bainitic ferrite, leading to the morphology known as lower bainite. As in the case of austenite, cementite draws carbon from bainitic ferrite, leaving the later with even lower C-content (α′B).

During the bainitic transformation, the aforementioned phase-transformations take place under paraequilibrium conditions. Calculation of paraequilibrium driving-forces (Figure 1.2, Figure 1.3) for the nucleation of the product phases is not a straightforward task and cannot be performed directly in Thermo-Calc software. In order to perform these calculations a modification was necessary, by intervening in the Gibbs Energy System (GES) module of Thermo-Calc software.

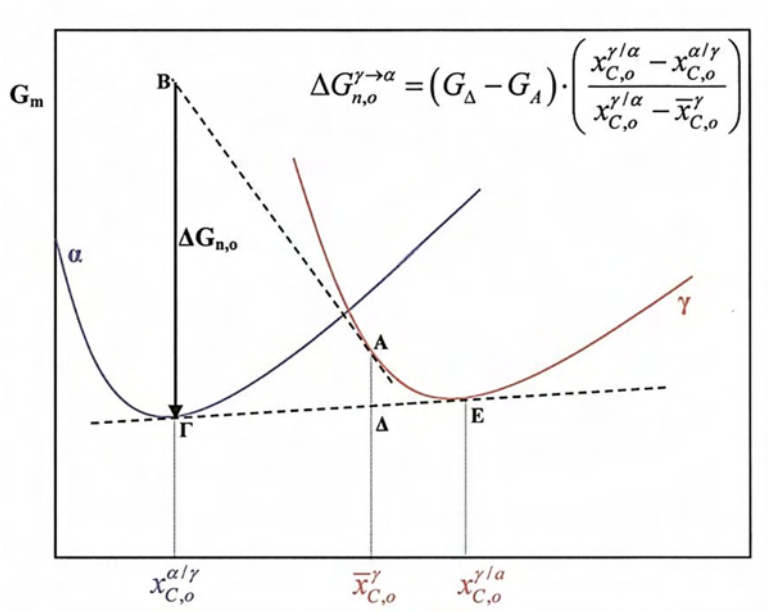

Figure 1.2 The driving force for nucleation of (α) in para-equilibrium with austenite (γ) is determined (Thermo-Calc).

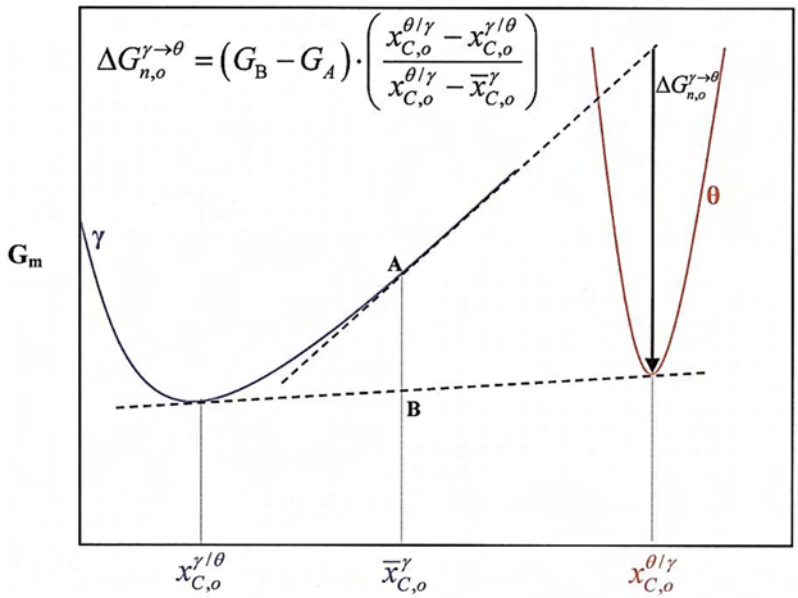

Figure 1.3 The driving force for nucleation of (ϑ) in para-equilibrium with austenite (γ) is determined (problem with Thermo-Calc!).

Haidemenopoulos et al. [33] and Olson et al. [31, 34, 35] established a technique, by which paraequilibrium thermodynamic calculations can be performed in multicomponent steels, containing various substitutional alloying elements. The fundamental idea behind this technique is that in a multicomponent steel Fe-C-M1-M2-…-Mn, where Mi represent the substitutional alloying elements of the steel, all substitutional elements (including Fe) can be replaced by a fictitious element, Z, so that the alloy reduces to a pseudo-binary Z-C system.

The thermodynamic conditions for two multi-component solid phases, α1 and α2, to exist in paraequilibrium are the following:

$$\mu_C^{\alpha 1} = \mu_C^{\alpha 2} \quad (10)$$

$$y_j^{\alpha 1} = \mu y_j^{\alpha 2} \quad (11)$$

In order for these two phases to exist in paraequilibrium, the chemical potential of C (μ_C) has to be the same in the two phases, and the site-fractions of each substitutional element (yj) have to be the same in the two phases.

The site-fraction of a substitutional element j, yj, is defined by:

$$y_j = \frac{x_j}{1 - x_C} \quad (12)$$

In Eq. (12) x_j and x_C are the usual mole-fractions of substitutional element j and of carbon, respectively.

The chemical potential of the fictitious element Z, which replaces all substitutional elements of the steel, is defined by:

$$\mu_Z^{\alpha 1} = \sum y_j \mu_j^{\alpha 1} \quad (13)$$

$$\mu_Z^{\alpha 2} = \sum y_j \mu_j^{\alpha 2} \quad (14)$$

Now, paraequilibrium conditions for the actual steel reduce to the corresponding orthoequilibrium condition for the pseudo-binary Z-C system:

$$\mu_C^{\alpha 1} = \mu_C^{\alpha 2} \quad (15)$$

$$\mu_Z^{\alpha 1} = \mu_Z^{\alpha 2} \quad (16)$$

The molar Gibbs free energy of a phase (α) in the pseudo-binary Z-C system is given by the following expression:

$$G_m^a = y_C \sum y_j \cdot G_{j:C}^{0,a} + y_{Va} \sum y_j \cdot G_{j:Va}^{0,a} + R \cdot T \left(\sum y_j \ln y_j \cdot + 3 y_C \ln y_C + 3 y_{Va} \ln y_{Va} \right) + G_m^{xs,a} + G_m^{mag,a} \quad (17)$$

In Eq. (17), yj, yC and yVa represent the site-fractions of substitutional elements, carbon and vacancies, respectively, $G_{j:C}^{o,\alpha}$ and $G_{j:Va}^{o,\alpha}$ are the lattice-stability parameters of substitutional element j with carbon atoms and vacancies, respectively, $G_m^{xs,\alpha}$ is the term representing the excess Gibbs energy of mixing and $G_m^{mag,\alpha}$ is the magnetic ordering energy contribution term. In the CALPHAD method, the excess Gibbs energy of mixing term ($G_m^{xs,\alpha}$) is approximated by a Redlich-Kister-Muggianu polynomial expansion [35].

2 Bainite Model Analysis

Evidently, due to the different stages and types of the bainitic transformation and its overall complexity, creating a model that considers every aspect of the evolution, has been a demanding task. Past models had to compromise, by either neglecting the precipitation of cementite, or treating the whole process as a single event. But, as clearly explained earlier, cementite precipitation is a key event in an overall transformation characterized by distinct stages. This need for a complete mathematical model simulating the bainitic transformation was ended in 2003 with the introduction of the Azuma model. In contrast with other models, the Azuma model takes into account and quantifies the precipitation of cementite during the transformation. This enables more realistic modelling of the transformation and widens the range of applicability of the model to practically any steel composition. Other published models, which focus solely on the kinetics of bainitic ferrite, are inevitably limited to cases where carbide precipitation is severely suppressed, e.g. in steels containing Si and/or Al. Furthermore, the model proposed for a number of significant aspects of the bainitic transformation. It identifies the formation of upper or lower bainite by their structural differences, depending on the chemistry of the steel and transformation temperature. It calculates the volume fractions of every phase present, as well as the carbon concentration in relation to time. It also calculates important microstructural features of bainite, such as the size of bainitic ferrite platelets, and the variation of these features during the transformation (e.g. gradual refinement of bainitic ferrite platelets due to the gradual enrichment of untransformed austenite in carbon). Finally, the model calculates the strength of austenite. This plethora of data is the reason the Azuma is the most complete model to date, and why it was chosen in favor of others.

For our calculations we decided to use MATLAB software due to its user friendly coding environment and good handling of large matrices. Taking a look at the algorithm itself, it consists of a series of time discriminated equations. Given a fixed timestep, it will calculate the appropriate values at any given time, using data from the previous timestep, and all of the necessary parameters of the transformation needed. The termination criterion is the completion of the transformation time. Our model is able to do two types of calculations, one for the isothermal transformation and one for the continuous cooling of samples, with their differentiation being analysed later on. Described below is a detailed explanation of the algorithm developed, accompanied by the calculation steps of the model in the case of isothermal transformation.

2.1 Zones Division

The composition inside the grain is not a fixed value; rather it is a function of distance. All elements have a variable value from one grain barrier to the other. As explained earlier, our algorithm is composed of discriminated equations. This limits our ability to apply the model to the function of composition itself, so, we are forced to consider distinct values. To do this, we divide areas of space, zones, and calculate the mean composition of every element in that particular area. This division is performed by hand, in an effort to balance the accuracy of the final result and the time needed to complete all calculations. By doing this, we can run our calculations for each zone separately, and then compose our now transformed grain by multiplying our results with the percentage of the participation of the zone in the whole grain and summing up. This might seem as an inaccurate approach at first, but given the results we are able to produce we believe it to be a fine compromise between accuracy and process time. Besides dividing the zones, we use Lee's [36]

equation for calculating the Bs Temperature. This way can have an early prediction as to what the response of the metal should be after every treatment.

2.2 Calculation Parameters

The actual algorithm used, takes into consideration a lot of parameters in order to produce the specified results. First and foremost, the alloy composition is inserted. The values of nucleation rate of the bainitic ferrite, cementite in both bainitic ferrite and austenite are also considered ($N_{\alpha/\gamma}$, $N_{\alpha/cem}$, $N_{\gamma/cem}$). Other very important factors include the activation energies for the diffusion of carbon in austenite and bainitic ferrite, the activation energies for ferrite nucleation in paraequilibrium and cementite precipitations (ΔG^*). Of course, the actual percentages of carbon in each phase are considered at the time of initiation. Lastly, the interfacial energies ($\sigma_{\alpha/\gamma}$, $\sigma_{\alpha/cem}$, $\sigma_{\gamma/cem}$) between all phases are used in the calculation process.

All in all, the algorithm is very sensitive. Meaning that, most of the above parameters have a great influence in the end result of the calculation. A tiny alteration of their values can cause a change to the time of the initiation, the time of completion of the transformation or change the final values of the results. This forces us to be very precise and careful about which values we should assign to every parameter. The actual determination of the values of these parameters is somewhat diverse, in the sense that not all are pinpointed the same way. Some are already available through thermodynamic calculations, such as the activation energies (ΔG^*) for the formation of ferrite, cementite in austenite and cementite in ferrite. Others like the autocatalytic nucleation factor β are generally treated as fix parameters.

Concerning the calculation of the interfacial energies ($\sigma_{\alpha/\gamma}$, $\sigma_{\alpha/cem}$, $\sigma_{\gamma/cem}$), we used data from RWTH. During an RFCS project, RWTH went on to calculate interfacial energies by using the commercial software MatCalc. This software is able to describe the formation and growth of precipitates within a given matrix as a function of time and temperature. In this software is integrated also a model for calculating interfacial energies. The generalized nearest-neighbor broken-bond model by B. Sonderegger and E. Kozeschnik employed in the program is an extension of the classical nearest neighbor broken-bond model [37] and gives good estimation for the interfacial energies. The interfacial energies for TRIP-Al were calculated as a function of carbon content and temperature over a wide range. The interfacial energies were calculated in the temperature range between 350°C and 600°C as this is the region of major interest concerning the bainitic transformation. The carbon enrichment of the retained austenite during the transformation was taken into account by calculating the interfacial energy as a function of carbon content and temperature as the transformation progresses. Evaluating this parameter correctly is of major importance. As of this work, we were able to eliminate the uncertainty from a parameter of vast significance to our model. As can be seen in the equations used by Azuma in the following paragraphs, the interfacial energies are raised to the third power when calculating nucleation-rate densities, meaning that very small changes can have major impact on the final outcome.

The remaining parameters, the nucleation rates ($N_{\alpha/\gamma}$, $N_{\alpha/cem}$, $N_{\gamma/cem}$), are treated more as fluctuating variables, to adjust the model on the experimental dilation curves, than actual parameters. This leaves us with an algorithm that is not independent of experiments and cannot predict on its own the parameters we seek with enough accuracy. However, there is a small range of nucleation rate values in which the Azuma model produces valid results from a logical point of view.

So, as long all other variables are determined, the nucleation rates can be evaluated by trial and error. For example, consider the TRIP-Al and the isothermal transformation at 400°C. If we set the nucleation rate of ferrite $N_{\alpha/\gamma}$=1E18 the model gives negative values for the volume fraction of austenite. At $N_{\alpha/\gamma}$=1E19, almost no bainitic ferrite is transformed. But at $N_{\alpha/\gamma}$=1E20 the results match almost perfectly the dilatometric data. Unfortunately, as of now, there is not a model that can calculate the Nucleation rates. These parameters are complex functions that depend on temperature, composition and many other factors. Although there are some theoretical nucleation models, the nucleation density is not easy to predict properly at the moment.

2.3 Evaluation of Thermodynamic Parameters - Thermocalc Implementation

To calculate most of the parameters mentioned above, we need to compute several paraequilibrium states. For this purpose, we use Thermocalc Software. Because of the amount of information needed to be taken into consideration, and the large number of variables that we need to calculate (every zone is matched with 11 additional variables other than their original composition), it became apparent that a method of implementation of those calculations must be developed and attached to our MATLAB code. To achieve this, we developed a series of functions, with the task to create the appropriate Thermocalc (.tcm) files. These files are then run by Thermocalc through our MATLAB code. We use the Thermocalc Console, specifically Thermocalc S, as it pairs excellent with the MATLAB environment and can use the MATLAB console as a screen output.

The first step of computations is the determination of mean X_C percentage in the austenite matrix. After this step is complete, we can now define the boundaries of X_C and Temperature within which we will run our paraequilibrium calculations. Given the complete chemical composition of the zone, in our case this result comes from the kinetic calculations done in Dictra, the algorithm creates a range of alloy compositions with different carbon percentages X_C. The range is selected to be wide enough to include all possible compositions the alloy zone might go through as the bainitic transformation progresses. With an equally wide range of temperature, we create a 2D mesh of composition-temperature, which we use to calculate the necessary parameters for the Azuma Model.

The different compositions are created by considering simple equilibrium, and we use Thermocalc to export a number of files containing the compositions. These files are then read by MATLAB, where we calculate the site-fraction of every substitutional element, as explained earlier. This is the final step before computing one of the parameters of the paraequilibrium. As before, we use MATLAB to create the appropriate .tcm file and Thermocalc S to run it. For every chemical composition of the mesh, a different .tcm file must be created and run.

When the value of the desired parameter in paraequilibrium has been calculated for every composition X_C and temperature of our mesh, it is now a matter of finding the correct fit. Because of the nature of the parameters, we can predict their behaviour regarding the 2 variables. This means we can predetermine the type of fitting needed, and not have to evaluate random types of fitting in order to find the best suited for each parameter. We use polynomial fits, different for every

parameter. The advantage of using a polynomial fit is the ease of how we can calculate the value of the parameter, by just knowing the power and coefficients of the polynomial. This way, we can easily implement the evaluation of the parameter in the Azuma algorithm for every possible state the zone passes, as it is being transformed.

The process described above, needs to be repeated for each parameter of every zone. The variables include the activation energies (ΔG*), the molecular volume of each phase (V_m) and chemical compositions of every phase in carbon (X_c). In total, 10 parameters are calculated with this method. Considering an alloy divided in 10 zones and a mesh of 30 different X_c percentages, the number of different files Thermocalc needs to run is well over 1000. This goes to show the importance of coupling of the two softwares, and the time saved by this implementation.

For a more thorough examination of the method, the Appendix attached includes parts of the code developed. However, the Thermocalc codes, due to their size, are omitted.

2.4 Azuma Model

Now that all the necessary parameters have been evaluated, the Azuma Model can be applied. Every run starts with the initiation of the parameters. Time is set to zero (t=0), a fix time step is decided, e.g. step=0.01sec, and the duration of the transformation, i.e. how long the specimen will stay in the furnace, is inserted along with the temperature. Variables calculated at the previous step are also inserted into the Azuma model.

2.4.1 Description

To briefly describe how the model works, consider that every time step is paired with a specific carbon composition. As time progresses, the austenite matrix is enriched with carbon leaving the bainite phase. At the very start, we consider that the zone consists completely of austenite. Meaning that, the volume fraction of austenite is f_γ=1, and all other volume fractions are zero, $f_{\alpha b}$=0 $f_{\theta,\gamma}$=0 $f_{\theta,\alpha}$=0. For each phase involved in the bainitic transformation, a series of calculations are performed.

Starting with the bainite phase, the activation energy is calculated. By definition, ΔG_v is given by dividing the molar thermodynamic driving-force for ferrite nucleation in paraequilibrium with austenite, ΔG_n, by the molar volume of the product phase (i.e. ferrite), $V_{m,\alpha}$:

$$\Delta G_{v,o}^{\gamma\to\alpha} = \frac{\Delta G_{n,o}^{\gamma\to\alpha}}{V_m^{\alpha}} \tag{18}$$

The activation energy, ΔG*, is a function of thermodynamic driving-force and surface energy:

$$\Delta G^*_{\gamma\to\alpha_B,o} = \frac{16\pi\cdot(\sigma^{\alpha/\gamma})^3}{3\left(\Delta G_{v,o}^{\gamma\to\alpha}\right)^2}\cdot N_A - \left[3.637\cdot\left(T-273.18\right)-2540\right] \qquad (in\ \ J/mol) \tag{19}$$

In eq. **(20)** N_A is the Avogadro number, $\sigma^{\alpha/\gamma}$ the ferrite/austenite interfacial energy and ΔG_v the initial thermodynamic driving-force, per unit volume, for the nucleation of ferrite in paraequilibrium with austenite. The latter is a result of the Thermocalc-MATLAB pairing we discussed, and is a strong function of chemical composition. Thus, it will decrease with time, as parent austenite becomes gradually enriched in carbon during the transformation.

The initial primary nucleation-rate density is given by nucleation theory:

$$I_{o,pr}^{\alpha_B} = N_o \cdot \frac{kT}{h} \cdot \exp\left(-\frac{Q_C^{\gamma}}{RT}\right) \cdot \exp\left(-\frac{\Delta G^{*}_{\gamma \to \alpha_B, o}}{RT}\right) \quad (in\ \ m^{-3}\sec^{-1}) \tag{21}$$

Where $Q_{C,\gamma}$ represents the activation energy for carbon diffusion in austenite, ΔG* the activation energy for ferrite nucleation *in paraequilibrium* with parent austenite and N_o the initial nucleation-site density for ferrite. Constants k, h and R have their usual meanings.

The overall (i.e. primary and autocatalytic) nucleation-rate density of bainitic ferrite (α_B) platelets is given by:

$$I_o^{\alpha_B} = (1 + \beta \cdot f_o^{\alpha_B}) \cdot I_{o,pr}^{\alpha_B} \quad (in\ \ m^{-3}\sec^{-1}) \tag{22}$$

Where $f^{\alpha B}$ is the vol. fraction and $I_{\alpha B,pr}$ the *primary* nucleation-rate density of bainitic ferrite, both functions of time. β is a constant accounting for the contribution of *autocatalytic* nucleation during the transformation.

Calculation of the thermodynamic driving-forces under paraequilibrium conditions has been implemented, through evaluating the fitting equation we created earlier, at the Thermocalc-MATLAB pairing procedure.

The vol. fraction of bainitic ferrite is calculated at the end of each time increment, by first determining the number of platelets that nucleated within this time interval. This is done by employing eq. (22) to (23). Each individual platelet is considered to have a volume:

$$v_{\alpha_B,1} = L_{\alpha_B,1} \cdot W_{\alpha_B,1} \cdot s_{\alpha_B,1} \tag{24}$$

with L, W and s being the length, width and thickness of each platelet, respectively. The spatial dimensions of each individual platelet will vary with time, since they depend on the mechanical strength of surrounding austenite, within which they grow. The yield strength of austenite increases during the transformation, mainly due to carbon enrichment, and can be calculated by the following empirical expression:

$$\begin{aligned} S_{\gamma,o} = {} & [1 - 0.26\times10^{-2}\cdot(T-298) + 0.47\times10^{-5}\cdot(T-298)^2 - \\ & - 0.326\times10^{-8}\cdot(T-298)^3]\cdot 15.4\cdot(3.6 + 23\overline{w}_{C,o}^{\gamma} + 1.3w_{Si} + 0.65w_{Mn}) \quad (in\ MPa) \end{aligned} \tag{25}$$

The dimensions of the platelets can subsequently be calculated by the following empirical equations:

$$\begin{aligned} W_{\alpha_B,o} &= \left[0.478 + 1.2\times10^{-4}T + 1.25\times10^{-4}\left(T - \Delta G_{n,o}^{\gamma\to a}\right) - 2.2\times10^{-3}S_{\gamma,o}\right]\cdot10^{-6} \quad (in\ m) \\ L_{\alpha_B,o} &= 6W_{\alpha_B,o} \\ s_{\alpha_B,o} &= 0.12W_{\alpha_B,o} \end{aligned} \tag{26}$$

Once the nucleation-rate density (i.e. the number of platelets formed per unit time and volume) and the volume each individual platelet have been calculated for the running time increment, the *extended* vol. fraction increment of bainitic ferrite, which formed within this time increment, is given by:

$$\Delta f_{0-1}^{\alpha_B,ext} = I_o^{\alpha_B} \cdot v_{\alpha_B,o} \cdot \Delta t \tag{27}$$

Subsequently, the corresponding *real* vol. fraction increment of bainitic ferrite is calculated:

$$\Delta f_{0-1}^{\alpha_B} = \Delta f_{0-1}^{\alpha_B,ext} \cdot \left(1 - f_o^{\alpha_B} - f_o^{\theta/\gamma} - f_o^{\theta/\alpha}\right) \tag{28}$$

where the f's denote the vol. fractions of the respective phases that had already formed until that moment.

The new value of the vol. fraction of bainitic ferrite is then given by:

$$f_1^{\alpha_B} = f_o^{\alpha_B} + \Delta f_{0-1}^{\alpha_B} \tag{29}$$

A similar approach is used for the calculation of the vol. fraction of cementite, which may precipitate either within ferrite or in austenite during the transformation. For example, the nucleation-rate density of cementite in austenite, under paraequilibrium conditions, is given by:

$$I_o^{\theta/\gamma} = N_o^{\theta/\gamma} \cdot \frac{kT}{h} \cdot \exp\left(-\frac{Q_C^{\gamma}}{RT}\right) \cdot \exp\left(-\frac{\Delta G^*_{\gamma\to\theta,o}}{RT}\right) \quad (in\ \ m^{-3}\sec^{-1}) \tag{30}$$

Similarly to eq. **(21)**, $Q_{C,\gamma}$ in eq. **(30)** represents the activation energy for carbon diffusion in austenite, ΔG* the activation energy for cementite nucleation *in paraequilibrium* with parent austenite and $N_{o,\theta/\gamma}$ the initial nucleation-site density for cementite.

The *extended* vol. fraction increment of cementite precipitated in austenite, which formed within the time increment under consideration, is then given by:

$$\Delta f_{0-1}^{\theta/\gamma,ext} = \frac{25\pi}{4} I_o^{\theta/\gamma} \cdot \Delta t \cdot \left[\frac{\left(\bar{x}_{C,o}^{\gamma} - x_{C,o}^{\gamma/\theta}\right)^2 \cdot D_C^{\gamma} \cdot \Delta t}{\left(x_{C,o}^{\theta/\gamma} - \bar{x}_{C,o}^{\gamma}\right) \cdot \left(x_{C,o}^{\theta/\gamma} - x_{C,o}^{\gamma/\theta}\right)}\right]^{3/2} \tag{31}$$

In eq. **(31)** $x^{\gamma/\theta}$ and $x^{\theta/\gamma}$ stand for the paraequilibrium carbon concentrations between cementite and austenite, x^{γ} is the average carbon concentration in parent austenite and D_C the diffusivity of carbon in austenite.

The corresponding *real* vol. fraction increment of cementite in austenite is calculated by:

$$\Delta f_{0-1}^{\theta/\gamma} = \Delta f_{0-1}^{\theta/\gamma,ext} \cdot \left(1 - f_o^{\alpha_B} - f_o^{\theta/\gamma} - f_o^{\theta/\alpha}\right) \tag{32}$$

and, the overall vol. fraction, up to that moment, is equal to:

$$f_1^{\theta/\gamma} = f_o^{\theta/\gamma} + \Delta f_{0-1}^{\theta/\gamma} \tag{33}$$

A corresponding set of equations is used for the calculation of cementite precipitation in ferrite.

Through the above described calculational process, which is repeated with updated parameter values for every new time increment, the vol. fractions of the involved phases are calculated with respect to time. This way the kinetics of the bainitic transformation is quantitatively determined. In addition, results are obtained regarding the evolution of the chemical composition of the phases and the microstructural features of ferrite platelets and cementite particles.

2.4.2 Calculation Procedure

The major steps of the algorithm are listed below:

1. Transformation temperature (T) and time-step (Δt) for the calculations are set.
2. The C-contents of ferrite ($x_{C,o}^{\alpha/\gamma}$) and austenite ($x_{C,o}^{\gamma/\alpha}$) in paraequilibrium are calculated.
3. The thermodynamic driving-force for nucleation of ferrite ($\Delta G_{n,o}^{\gamma\to\alpha}$) in paraequilibrium with austenite is calculated.
4. Values are set for the ferrite/austenite ($\sigma^{\alpha/\gamma}$), cementite/austenite ($\sigma^{\theta/\gamma}$) and cementite/ferrite ($\sigma^{\theta/\alpha}$) interfacial energies and the corresponding nucleation-site densities (N_o, $N_o^{\theta/\gamma}$, $N_o^{\theta/\alpha}$).
5. The activation energy for paraequilibrium nucleation of ferrite in austenite is calculated: $\Delta G^{*}_{\gamma\to\alpha_B,o} = \frac{16\pi\cdot(\sigma^{\alpha/\gamma})^3}{3\left(\Delta G_{v,o}^{\gamma\to\alpha}\right)^2}\cdot N_A - \left[3.637\cdot(T-273.18)-2540\right]$
6. The initial primary nucleation-rate density of ferrite is calculated: $I_{o,pr}^{\alpha_B} = N_o\cdot\frac{kT}{h}\cdot\exp\left(-\frac{Q_C^{\gamma}}{RT}\right)\cdot\exp\left(-\frac{\Delta G^{*}_{\gamma\to\alpha_B,o}}{RT}\right)$ The initial overall nucleation-rate density of ferrite is calculated: $I_o^{\alpha_B} = (1+\beta\cdot f_o^{\alpha_B})\cdot I_{o,pr}^{\alpha_B}$
8. The initial yield-stress of austenite is calculated: $S_{\gamma,o} = [1-0.26\times10^{-2}\cdot(T-298)+0.47\times10^{-5}\cdot(T-298)^2 - -0.326\times10^{-8}\cdot(T-298)^3]\cdot15.4\cdot(3.6+23\overline{w}_{C,o}^{\gamma}+1.3w_{Si}+0.65w_{Mn})$
9. The size of the bainitic ferrite platelet is calculated: $W_{\alpha_B,o} = \left[0.478+1.2\times10^{-4}T+1.25\times10^{-4}\left(T-\Delta G_{n,o}^{\gamma\to a}\right)-2.2\times10^{-3}S_{\gamma,o}\right]\cdot10^{-6}$
10. The C-contents of cementite ($x_{C,o}^{\theta/\gamma}$) and austenite ($x_{C,o}^{\gamma/\theta}$) in para-equilibrium are calculated.

11. The thermodynamic driving-force for nucleation of cementite ($\Delta G_{n,o}^{\gamma\to\theta}$) in paraequilibrium with austenite is calculated.
12. The activation energy for paraequilibrium nucleation of cementite in austenite is calculated: $\Delta G^{*}_{\gamma\to\theta,o}=\frac{16\pi\cdot(\sigma^{\theta/\gamma})^{3}}{3\left(\Delta G_{v,o}^{\gamma\to\theta}\right)^{2}}\cdot N_{A}$
13. The initial nucleation-rate density of cementite in austenite is calculated: $I_o^{\theta/\gamma}=N_o^{\theta/\gamma}\cdot\frac{kT}{h}\cdot\exp\left(-\frac{Q_C^{\gamma}}{RT}\right)\cdot\exp\left(-\frac{\Delta G^{*}_{\gamma\to\theta,o}}{RT}\right)$
14. The C-contents of cementite ($x_{C,o}^{\theta/\alpha}$) and ferrite ($x_{C,o}^{\alpha/\theta}$) in paraequilibrium are calculated.
15. The thermodynamic driving-force for nucleation of cementite ($\Delta G_{n,o}^{\alpha\to\theta}$) in paraequilibrium with ferrite is calculated.
16. The activation energy for paraequilibrium nucleation of cementite in ferrite is calculated: $\Delta G^{*}_{\alpha\to\theta,o}=\frac{16\pi\cdot(\sigma^{\theta/\alpha})^{3}}{3\left(\Delta G_{v,o}^{\alpha\to\theta}\right)^{2}}\cdot N_{A}$
17. The initial nucleation-rate density of cementite in ferrite is calculated: $I_o^{\theta/\alpha}=N_o^{\theta/\alpha}\cdot\frac{kT}{h}\cdot\exp\left(-\frac{Q_C^{\alpha}}{RT}\right)\cdot\exp\left(-\frac{\Delta G^{*}_{\alpha\to\theta,o}}{RT}\right)$
18. Time is increased by Δt.
19. The extended vol. fraction increment of bainitic ferrite is calculated: $\Delta f_{0-1}^{\alpha_B,ext}=I_o^{\alpha_B}\cdot v_{\alpha_B,o}\cdot\Delta t$
20. The real vol. fraction increment of bainitic ferrite is calculated: $\Delta f_{0-1}^{\alpha_B}=\Delta f_{0-1}^{\alpha_B,ext}\cdot\left(1-f_o^{\alpha_B}-f_o^{\theta/\gamma}-f_o^{\theta/\alpha}\right)$
21. The vol. fraction of bainitic ferrite at time t_1 is calculated: $f_1^{\alpha_B}=f_o^{\alpha_B}+\Delta f_{0-1}^{\alpha_B}$
22. The extended vol. fraction increment of cementite in austenite is calculated: $\Delta f_{0-1}^{\theta/\gamma,ext}=\frac{25\pi}{4}I_o^{\theta/\gamma}\cdot\Delta t\cdot\left[\frac{\left(\overline{x}_{C,o}^{\gamma}-x_{C,o}^{\gamma/\theta}\right)^{2}\cdot D_C^{\gamma}\cdot\Delta t}{\left(x_{C,o}^{\theta/\gamma}-\overline{x}_{C,o}^{\gamma}\right)\cdot\left(x_{C,o}^{\theta/\gamma}-x_{C,o}^{\gamma/\theta}\right)}\right]^{3/2}$
23. The real vol. fraction increment of cementite in austenite is calculated: $\Delta f_{0-1}^{\theta/\gamma}=\Delta f_{0-1}^{\theta/\gamma,ext}\cdot\left(1-f_o^{\alpha_B}-f_o^{\theta/\gamma}-f_o^{\theta/\alpha}\right)$

24. The vol. fraction of cementite in austenite at time t_1 is calculated: $f_1^{\theta/\gamma} = f_o^{\theta/\gamma} + \Delta f_{0-1}^{\theta/\gamma}$

25. The extended vol. fraction increment of cementite in ferrite is calculated:

$$\Delta f_{0-1}^{\theta/\alpha,ext} = \frac{25\pi}{4} I_o^{\theta/\alpha} \cdot \Delta t \cdot \left[\frac{\left(\overline{x}_{C,o}^{\alpha} - x_{C,o}^{\alpha/\theta}\right)^2 \cdot D_C^{\alpha} \cdot \Delta t}{\left(x_{C,o}^{\theta/\alpha} - \overline{x}_{C,o}^{\alpha}\right) \cdot \left(x_{C,o}^{\theta/\alpha} - x_{C,o}^{\alpha/\theta}\right)} \right]^{3/2}$$

26. The real vol. fraction increment of cementite in ferrite is calculated:

$$\Delta f_{0-1}^{\theta/\alpha} = \Delta f_{0-1}^{\theta/\alpha,ext} \cdot \left(1 - f_o^{\alpha_B} - f_o^{\theta/\gamma} - f_o^{\theta/\alpha}\right)$$

27. The vol. fraction of cementite in ferrite at time t_1 is calculated: $f_1^{\theta/\alpha} = f_o^{\theta/\alpha} + \Delta f_{0-1}^{\theta/\alpha}$

Important notice: As the transformation proceeds in time, new cementite particles will nucleate and grow during every time-step, but also already existing (i.e. formed in previous timesteps) cementite particles will continue to grow. In order to take these processes simultaneously into account, it can be shown that the vol. fraction of cementite at time t_n is given by:

$$f_n^{\theta/\gamma} = f_{n-1}^{\theta/\gamma} + \frac{25\pi}{4} \cdot \sum_{i=0}^{n} \left(I_i^{\theta/\gamma} \cdot \Delta t_i \right) \cdot \left[\frac{\left(\overline{x}_{C,n-1}^{\gamma} - x_{C,n-1}^{\gamma/\theta}\right)^2 \cdot D_C^{\gamma} \cdot \Delta t_{n-1}}{\left(x_{C,n-1}^{\theta/\gamma} - \overline{x}_{C,n-1}^{\gamma}\right) \cdot \left(x_{C,n-1}^{\theta/\gamma} - x_{C,n-1}^{\gamma/\theta}\right)} \right]^{3/2} \cdot \left(1 - f_{n-1}^{\alpha_B} - f_{n-1}^{\theta/\gamma} - f_{n-1}^{\theta/\alpha}\right)$$

for cementite in austenite, and by:

$$f_n^{\theta/\alpha} = f_{n-1}^{\theta/\alpha} + \frac{25\pi}{4} \cdot \sum_{i=0}^{n} \left(I_i^{\theta/\alpha} \cdot \Delta t_i \right) \cdot \left[\frac{\left(\overline{x}_{C,n-1}^{\alpha} - x_{C,n-1}^{\alpha/\theta}\right)^2 \cdot D_C^{\alpha} \cdot \Delta t_{n-1}}{\left(x_{C,n-1}^{\theta/\alpha} - \overline{x}_{C,n-1}^{\alpha}\right) \cdot \left(x_{C,n-1}^{\theta/\alpha} - x_{C,n-1}^{\alpha/\theta}\right)} \right]^{3/2} \cdot \left(1 - f_{n-1}^{\alpha_B} - f_{n-1}^{\theta/\gamma} - f_{n-1}^{\theta/\alpha}\right)$$

for cementite in ferrite.

28. The average mole-fraction of C in austenite is updated: $\overline{x}_{C,1}^{\gamma} = \dfrac{\overline{x}_{C,o}^{\gamma} - \left(f_1^{\alpha_B} \cdot x_{C,o}^{\alpha/\gamma} + f_1^{\theta/\gamma} \cdot x_{C,o}^{\theta/\gamma}\right)}{1 - f_1^{\alpha_B} - f_1^{\theta/\gamma}}$

29. The average mole-fraction of C in ferrite is updated: $\overline{x}_{C,1}^{\alpha} = \dfrac{\overline{x}_{C,o}^{\alpha} - f_1^{\alpha/\gamma} \cdot x_{C,o}^{\theta/\alpha}}{1 - f_1^{\theta/\alpha}}$

30. The new values of activation energies for paraequilibrium nucleation are calculated.

31. The procedure is repeated for the next timestep.

3 Martensite Transformation

During cooling after the isothermal holding at the bainitic transformation temperature, the austenite-martensite transformation in carbon steels begins at a certain temperature designated as the M_S, temperature and proceeds only upon continuous cooling below this temperature. For the cooling part of the control process, a semi empirical Matlab model is employed. In order to determine the M_S temperature in austenite and the transformation fraction profiles of the final

microstructure, the Barbier equation and the Koistinen-Marburger model are incorporated into the Matlab code [22].

The raw data produced by the Azuma mole are processed to determine the fraction of austenite and its stability, as a function of cooling temperature and chemical composition [38].

To determine the M_S temperature of the austenite at a given time, as a function of distance in the simulation cell, the Barbier Equation was employed, resulting in an M_S profile.

$$M_s(x,t) = 545 - 601.2(1 - \exp(-0.868C)) - 34.4Mn - 13.7Si - 1.4Al$$

Then using the Koistinen-Marburger model it is possible to calculate the profile of the transformation fraction, which describes the austenite to martensite transformation kinetics.

$$f_T(x,t) = 1 - \exp\big(-0.011(M_s(x,t) - T_R)\big), \qquad M_S \geq T_R$$

where T_R indicates the ambient temperature of 25℃.

The total volume fraction of martensite $f_M(t)$ at a given time interval is then given by

$$f_M(t) = \frac{f_\gamma(t)}{x_I(t)} \int_0^{x_I(t)} f_T(x,t)\, dx$$

where $f_\gamma(t) = \frac{x_I(t)}{x_L}$ is the total austenite volume fraction, $x_I(t)$ is the position of the interface at a given time and x_L is the total simulation cell length. Finally the total volume fraction of retained austenite is given by subtracting the fraction of martensite from that of the austenite as

$$f_{\gamma R}(t) = f_\gamma(t) - f_M(t)$$

It is also important to calculate the mean concentration ($\bar{X}_i$) of the elements in ferrite, martensite and retained austenite, as a function of the heat treatment time. The following relation can be used to obtain the mean concentration values from a profile at a given time.

$$\bar{X}_i^{bcc}(t) = \frac{\int_{x_I(t)}^{x_L} X_i(x,t)\, dx}{x_L - x_I(t)}$$

$$\bar{X}_i^{fccR}(t) = \frac{\int_0^{x_I(t)} \big(1 - f_T(x,t)\big)\, X_i(x,t)\, dx}{\int_0^{x_I(t)} \big(1 - f_T(x,t)\big)\, dx}$$

$$\bar{X}_i^{Mart}(t) = \frac{\int_0^{x_I(t)} f_T(x,t)\, X_i(x,t)\, dx}{\int_0^{x_I(t)} f_T(x,t)\, dx}$$

4 Validation of modelling process (Integrated model)

In order to validate the proposed integrated model that was developed during this thesis, two sets of data were used. In the work performed previously by the Laboratory of Materials, RWTH and Voestalpine during an RFCS Project [39], a TRIP steel enriched in aluminium (TRIP-Al) and a Dual phase steel (VA_DP_Mn2.2) enriched in manganese were studied. In the case of DP steel, a heat treatment of full annealing, subsequent cooling to the bainitic transformation temperature and isothermal holding was performed, using a Bähr dilatometer DIL805 A/D. In the case of TRIP-Al steel a heat treatment of intrecritical annealing, subsequent cooling to the bainitic transformation temperature and isothermal holding was performed. In both cases the formation of austenite during intercritical annealing, bainitic ferrite, retained austenite and martensite was studied both by dilatometry as well as quantitative metallographic investigation.

4.1 Dual Phase steel VA_DP_2.2Mn_0.8Cr

The Dual Phase steel VA_DP_2.2Mn_0.8Cr was provided by Voestalpine [39] and its chemical composition is presented in the following table:

Table 4.1-1 VA DP Composition

C (%wt.)	Mn (%wt.)	Cr (%wt.)	Si (%wt.)	Nb (%wt.)
0.146	2.39	0.77	0.13	0.021

The heat treatment consisted of heating with 20°C/sec to the full annealing temperature of 850 °C for 60sec, subsequent cooling with a rate of 20°C/sec to the bainitic transformation temperature and isothermal holding there. The thermal cycle is depicted below in Figure 4.1-1

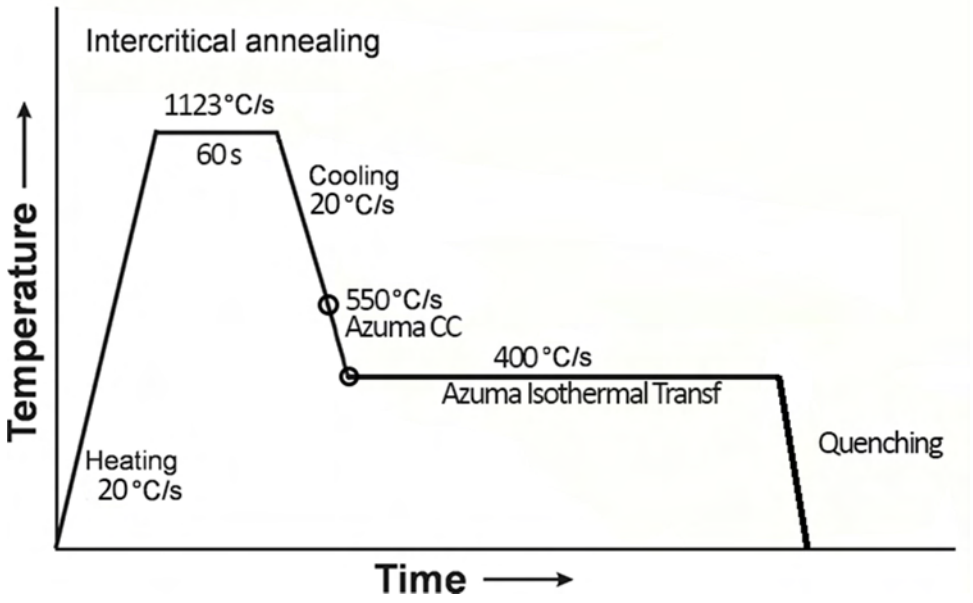

Figure 4.1-1 Thermal Cycle of Dual Phase steel VA DP2.2Mn_0.8Cr

4.1.1 Kinetic Results-Zone Division

As mentioned above the part of the heat treatment involving the initial stages of heating, annealing and cooling to the bainite start temperature were investigated with the help of thermodynamics and kinetics and the commercial software Thermocalc and Dictra. The kinetics of formation of austenite during annealing and cooling were studied. The initial microstructure was ferrite-pearlite similar to that produced during hot-rolling of DP-steels. Concerning the kinetic model, the initial grain size of the material was taken into account in the region size used by the model, as well as the initial ferrite perlite microstructure.

The initial conditions (initial phase composition) were evaluated using the thermodynamic software THERMOCALC. It was assumed that the perlite fraction of the microstructure is spontaneously converted into austenite upon exposure to the A_{C1} temperature; this is illustrated in Table 4.1-2. Kinetic calculations were performed with the software Dictra and the volume fraction of austenite (100%), as well as the composition profiles (Mn, C, Si, Cr) of a supposed austenite grain was evaluated, as depicted in Figure 4.1-3. The IA temperature, heating and cooling rates as well as the final temperature of the simulation is presented in Table 4.1-2. Heating and cooling rates were the same at 20K/s and the annealing holding time 60sec. It was not possible for the simulation to be performed lower than 550^{o}C so this is the final temperature reached by cooling.

Table 4.1-2 Annealing Process

Heating		Holding		Cooling	
Initial Temp (^{o}C)	**Rate (K/s)**	**Holding Temp (^{o}C)**	**Holding Time (s)**	**Final Temp (^{o}C)**	**Rate (K/s)**
705	20	850	60	550	20

Representative results of the kinetic calculations are presented in Figure 4.1-2. Austenite volume fraction increases during heating, full annealing is achieved, and ferrite is formed during cooling.

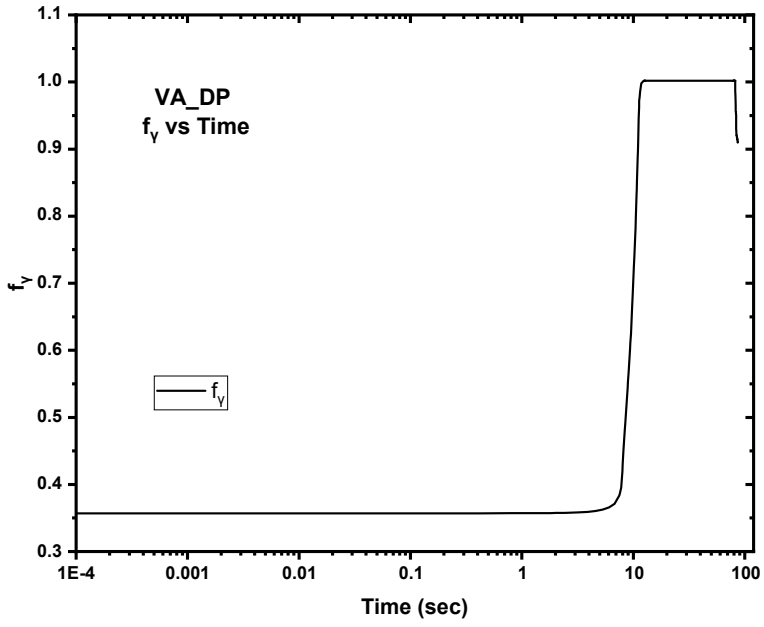

Figure 4.1-2 The evolution of austenite volume fraction for Dual Phase steel VA DP2.2Mn_0.8Cr after heating with a rate of 20K/sec, and isothernal holding at 850^{o}C versus time.

At the end of cooling the element profiles are calculated. They are presented in Figure 4.1-3. Mn, Cr and C enrich austenite while Al prefers to partition into the new forming ferrite. These results in three distinct composition zones to be developed in austenite as illustrated in Figure 4.1-3.

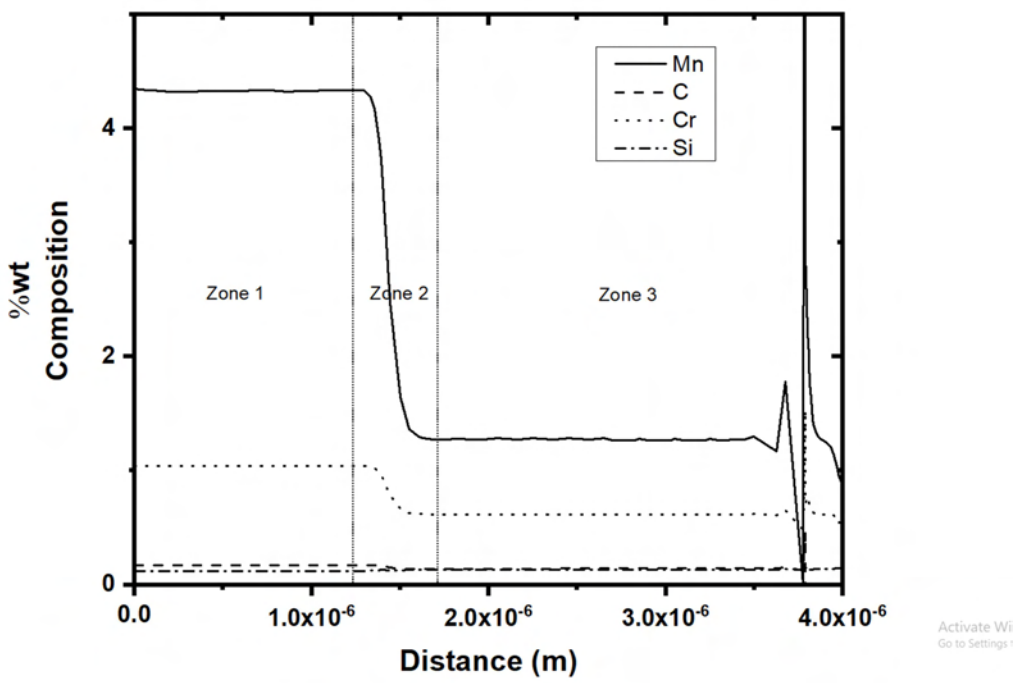

Figure 4.1-3 Composition Profiles for Dual Phase steel VA DP2.2Mn_0.8Cr at the end of cooling at 550^{o}C

The end of Zone 3 is defined by the boundary between the austenite that remains (on the left) and the newly formed ferrite (on the right). By dividing the distance of each phase with the total distance (Table 4.1-5), one can calculate the respective size of each zone, and proceed to calculate the mean composition of every zone (Table 4.1-4).

Table 4.1-3 Volume Fractions post Annealing

f_α	f_γ
0.0530231	0.9469764

Table 4.1-4 Zone Compositions

	C (%wt.)	Mn (%wt.)	Cr (%wt.)	Si (%wt.)	Nb (%wt.)	Al (%wt.)
Zone 1	0.170147	4.315651	1.038796	0.120027	0.021	0
Zone 2	0.152609	2.626343	0.806076	0.12906	0.021	0
Zone 3	0.142927	1.288764	0.619198	0.135774	0.021	0

Table 4.1-5 Zone Length, Percentages and Bainite start (B_s) Temperature

	Length (nm)	Length Percentage	B_s (°C)
Zone 1	1394.20	0.36	407.5
Zone 2	211.87	0.06	522.5
Zone 3	2181.83	0.58	613.4

4.1.2 Azuma Continuous Cooling

During cooling to the desired temperature of 400°C for the isothermal bainitic transformation, the modified Azuma model for the case of Continuous Cooling was applied. The starting temperature resulting from the final step of the kinetic calculation was 550°C and the final 400°C, with a steady cooling rate of 20K/s. The continuous cooling method was applied to all three zones, the results are illustrated in the figures below. The volume fraction of bainitic ferrite ($f_{\alpha b}$) for each respective zone, versus time, during Continuous Cooling is illustrated in Figure 4.1-4. Volume fraction of austenite (f_γ) is illustrated in Figure 4.1-5, while the respective mean Carbon concentration ($X_{c\gamma}$) is illustrated in Figure 4.1-6.

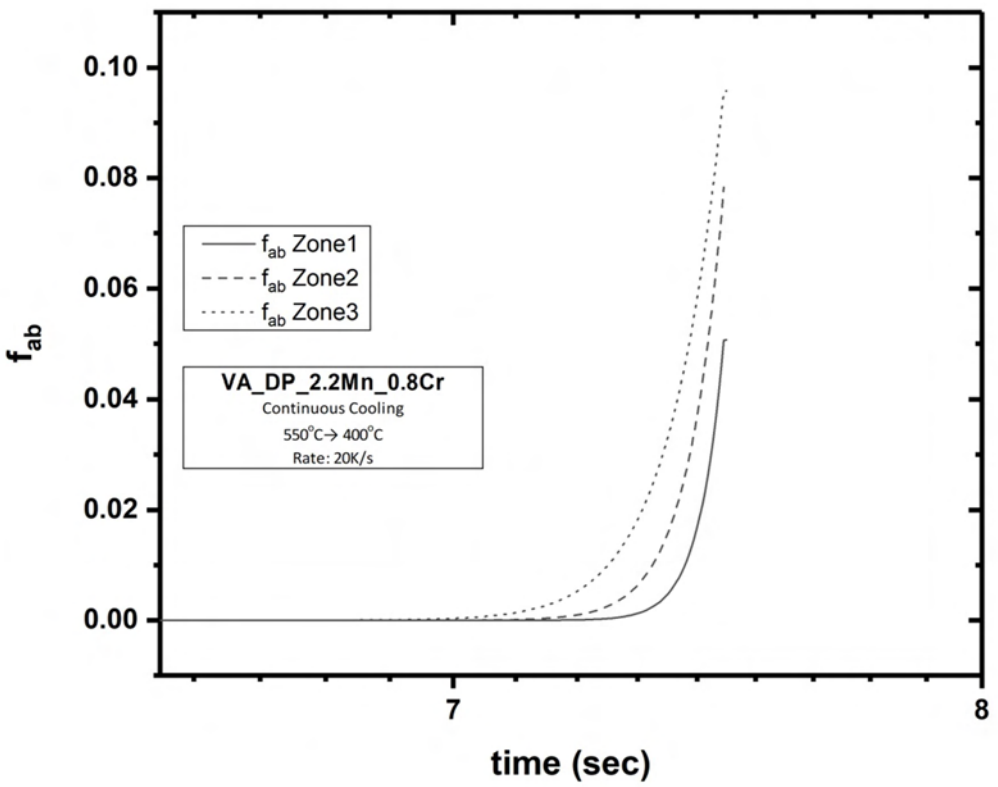

Figure 4.1-4 Volume fraction of bainitic ferrite ($f_{\alpha b}$) for each respective zone versus time during Continuous Cooling

As predicted by the B_s temperature, the zone with the lowest one, is the one that makes the least amount of bainite. The following Figure 4.1-6 shows the change in carbon composition that occurs, as a result of the transformation.

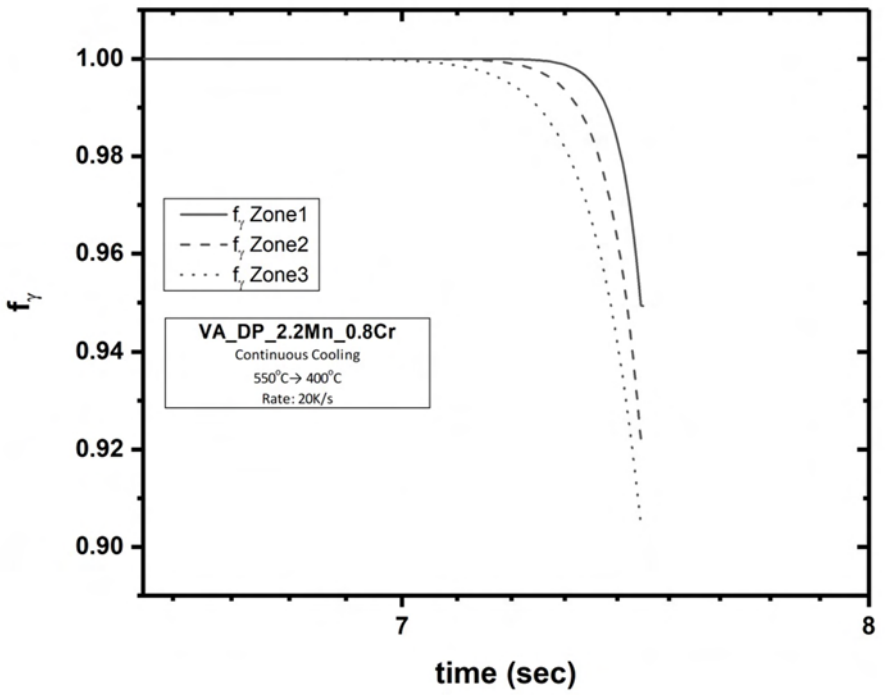

Figure 4.1-5 Volume fraction of austenite (f_γ) for each respective zone versus time during Continuous Cooling

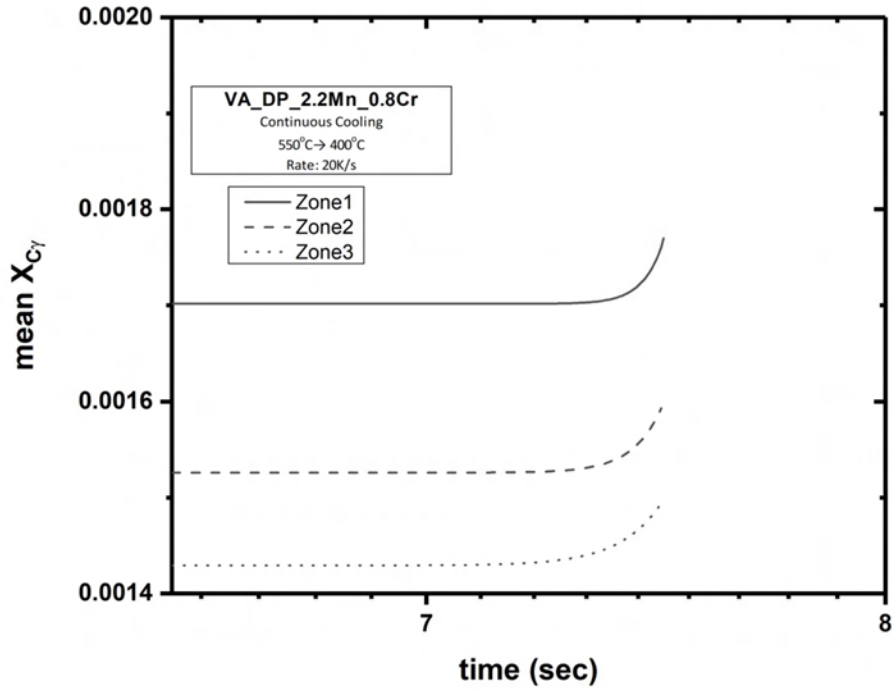

Figure 4.1-6 Mean Carbon concentration ($X_{c\gamma}$) versus time, during Continuous Cooling of Dual Phase steel VA-DPMn2.2

4.1.3 Azuma Isothermal Transformation

The simulation was continued, by using the composition evaluated from the continuous cooling model as the input for the isothermal bainitic transformation. The temperature is set at 400 ^{o}C and the duration is 2000 sec.

The figures below depict the results of the isothermal Azuma simulation with respect to the three zones. The volume fraction of bainitic ferrite ($f_{\alpha b}$) for each respective zone versus time during Isothermal Holding is depicted in Figure 4.1-7. The volume fraction of austenite (f_{γ}) is depicted in Figure 4.1-8 and Carbon concentration ($X_{c\gamma}$) versus time is depicted in Figure 4.1-9. These results are presented in relation to every zone.

In Figure 4.1-9 the mean Carbon concentration ($X_{c\gamma}$) of all participating zones is also presented versus time. In the figures that follow the mean value of every parameter is presented. Figure 4.1-10 depicts the mean volume fraction of bainitic ferrite ($f_{\alpha b}$) and the mean volume fraction of austenite (f_{γ}). Figure 4.1-11 depicts the mean volume fraction of austenite (f_{γ}) and the corresponding austenite enrichment of all contributing zones versus time during Isothermal Holding.

During this simulation no carbides were formed in either austenite or bainitic ferrite, as is evident in Figure 4.1-12. In Figure 4.1-13 and Figure 4.1-14 the microstructural characteristics of bainitic ferrite and the mechanical characteristics of austenite are presented. The platelet size of bainitic ferrite is presented in Figure 4.1-13 and the tensile Yield Strength of retained austenite in comparison with the enrichment of austenite in Carbon presented in Figure 4.1-14.

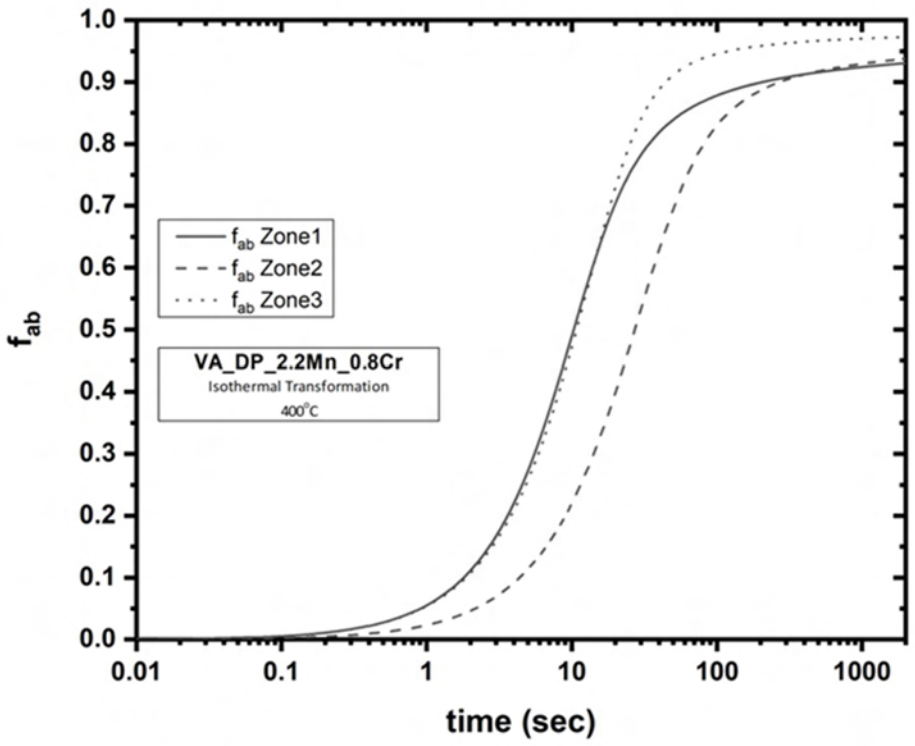

Figure 4.1-7 Volume fraction of bainitic ferrite ($f_{\alpha b}$) for each respective zone versus time during Isothermal Holding

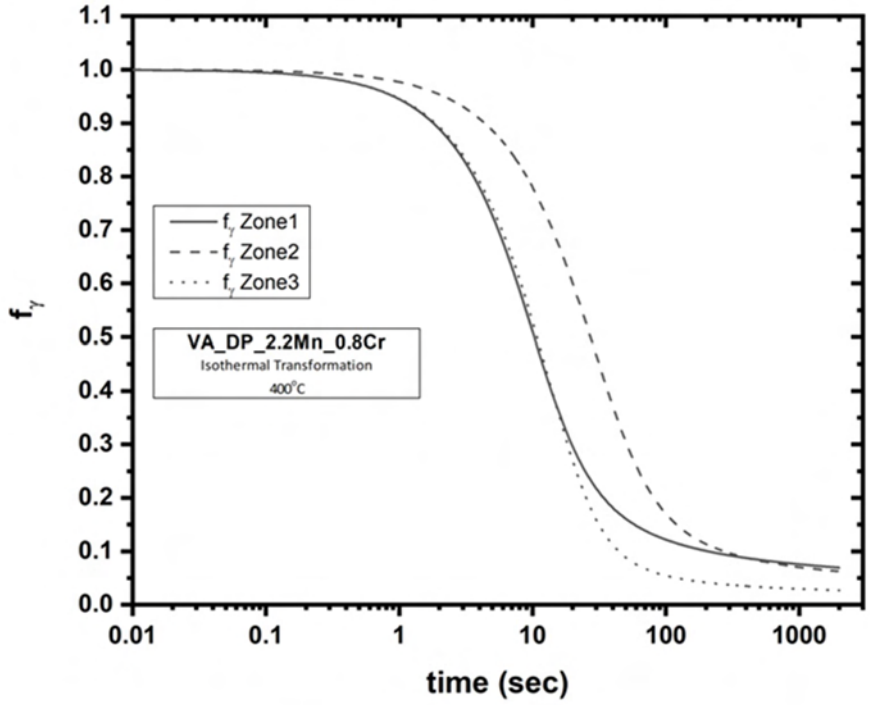

Figure 4.1-8 Volume fraction of austenite (f_γ) for each respective zone versus time during Isothermal Holding

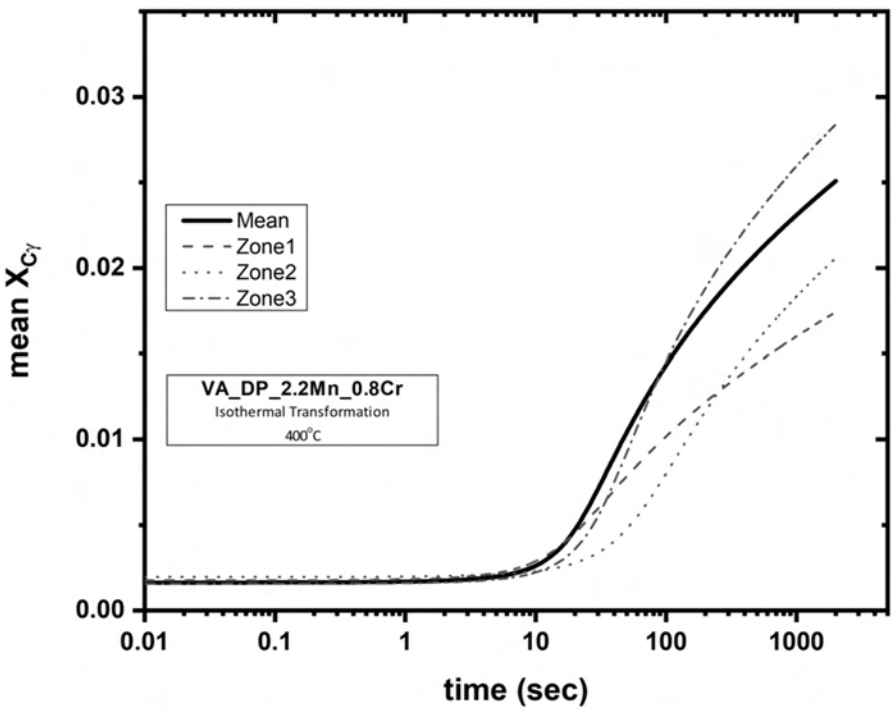

Figure 4.1-9 Mean Carbon concentration ($X_{C\gamma}$) versus time, during Isothermal Holding

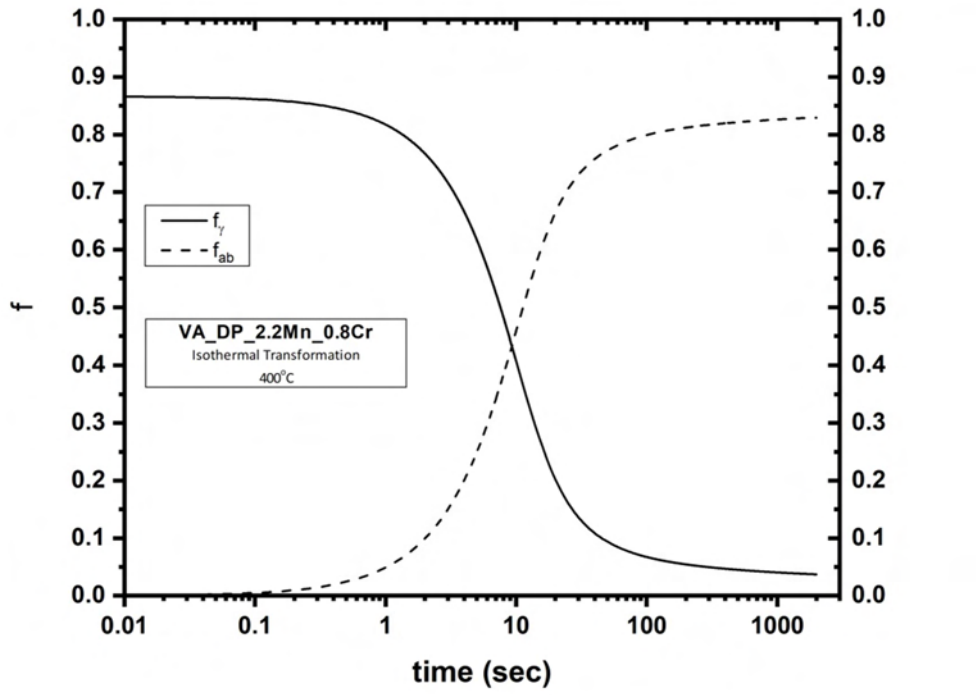

Figure 4.1-10 Mean volume fraction of bainitic ferrite ($f_{\alpha b}$) and mean volume fraction of austenite (f_γ) of all contributing zones versus time during Isothermal Holding

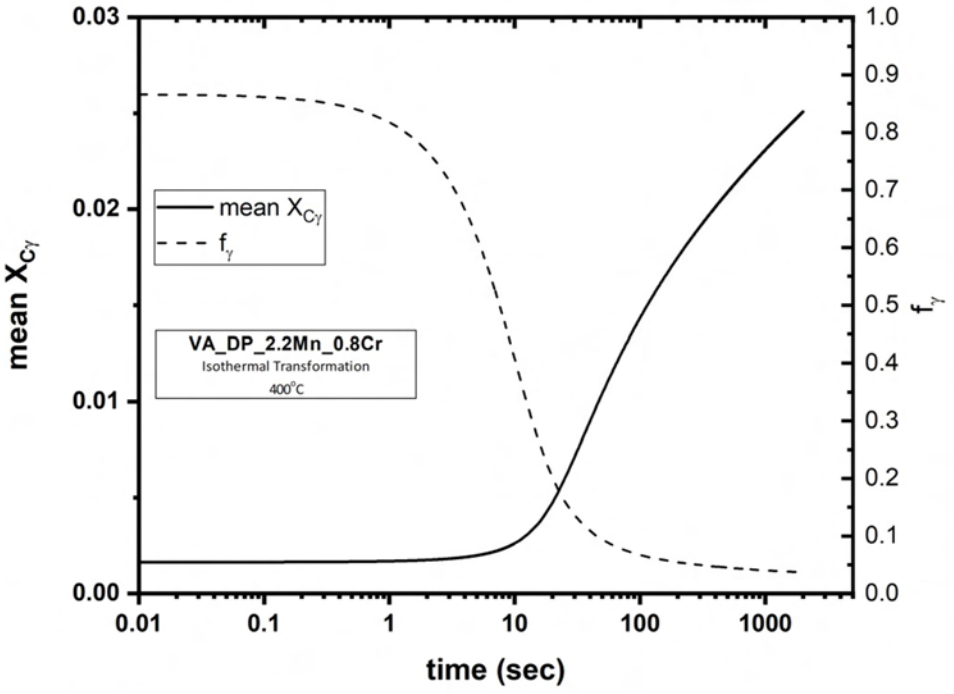

Figure 4.1-11 Mean volume fraction of austenite (f_γ) and corresponding austenite enrichment of all contributing zones versus time during Isothermal Holding

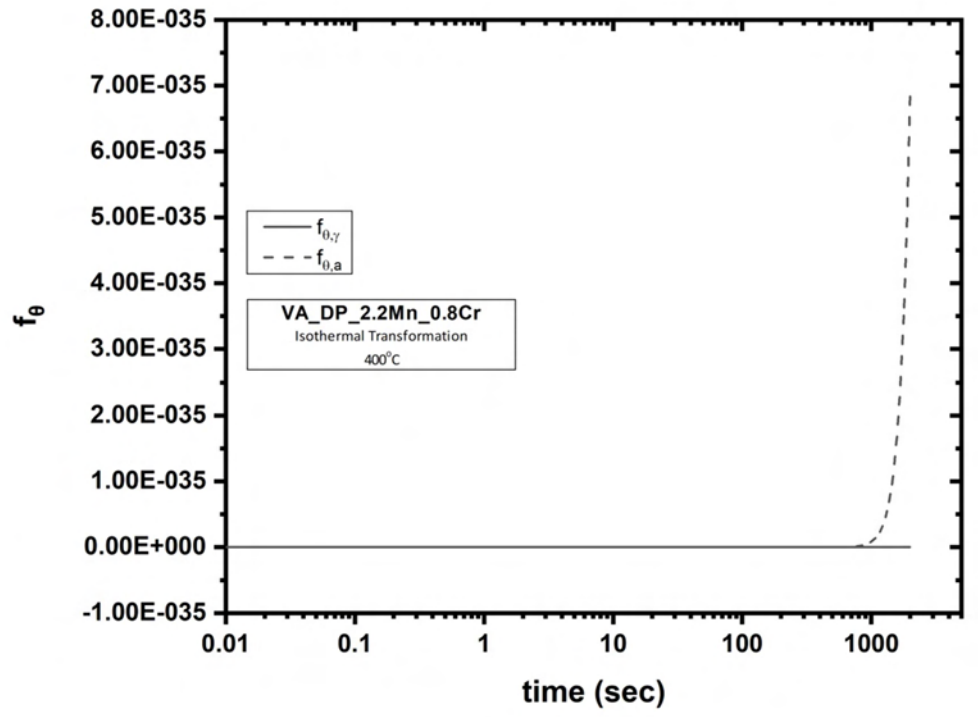

Figure 4.1-12 Cementite Precipitates: In both austenite and bainitic ferrite. There are virtually no carbides formed

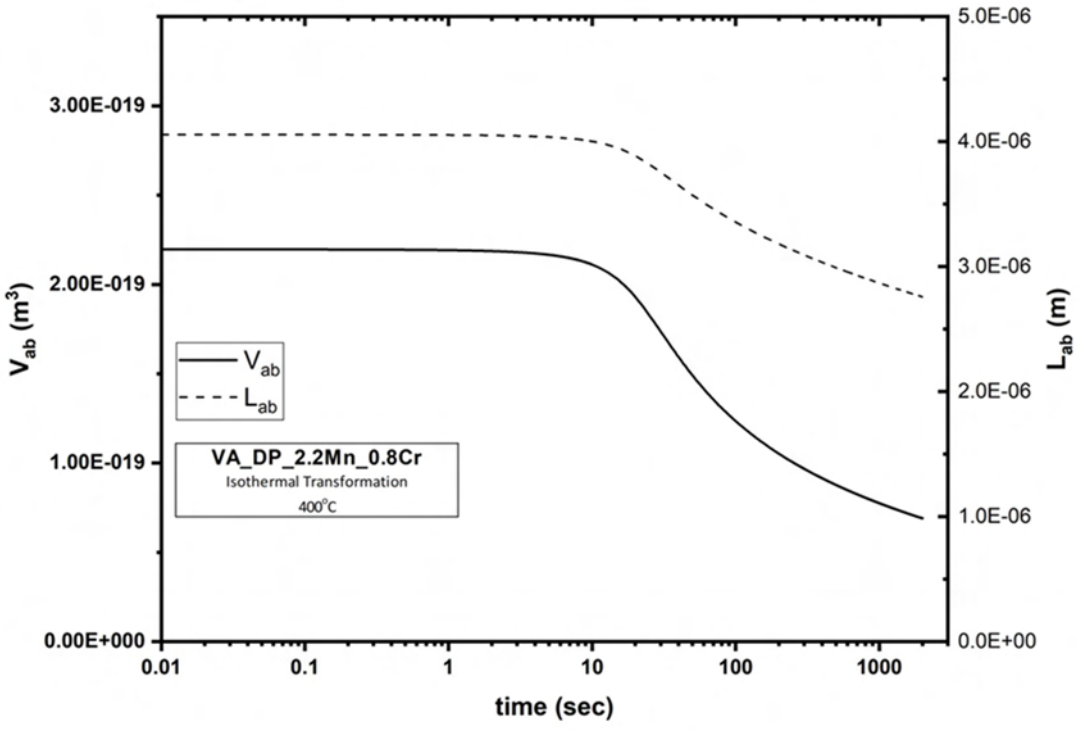

Figure 4.1-13 Platelet Size of bainitic ferrite

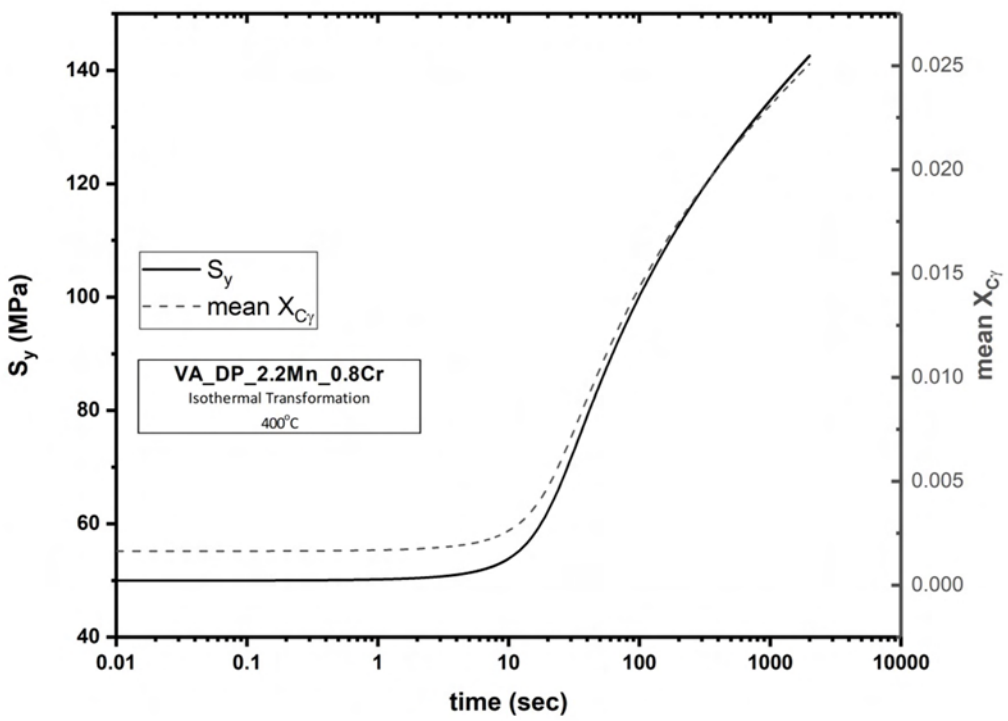

Figure 4.1-14 Yield Strength of Retained Austenite versus the Carbon enrichment of Austenite

At the last figure, we can see the relation between the Yield Strength of austenite and the mean concentration of Carbon in austenite. As the austenitic matrix gets enriched with Carbon its strength increases.

4.1.4 Summary-Comparison with Experimental Data

To summarize, the table below shows the change in volume fractions as the transformation progresses, starting from the annealing all the way to the quenching.

Table 4.1-6 Phase Transformations Results after each stage of the Heat Treatment

550 °C		**550 °C →400 °C**			**400 Isothermal °C**		
f_α	f_γ	f_α	$f_{\alpha b}$	f_γ	f_α	$f_{\alpha b}$	f_γ
0.0530231	0.9469764	0.0530231	0.080541	0.8664362	0.0530231	0.829449	0.0369878

Using the data provided by Voestalpine [39], the validity of the results can be checked. The final volume fractions of the participating phases after the completion of the thermal cycle are shown in Table 4.1-7, and the bainitic ferrite transformation regarding time is shown at Figure 4.1-15,

compared with dilatometric data from [39]. The results are in good agreement with the experimental data.

Table 4.1-7 Final Volume Fractions post Quenching

FINAL VOLUME FRACTIONS					
Simulation Data	**f_α**	**$f_{\alpha b}$ (presoaking)**	**$f_{\alpha b}$**	**f_γ**	**f_M**
	0.05302307	0.0805407	0.8294485	0.0355385	0.00144922
Experimental Data	**Transformed before soaking**		**During soaking**	**Retained austenite**	
	0.132		0.826	0.042	

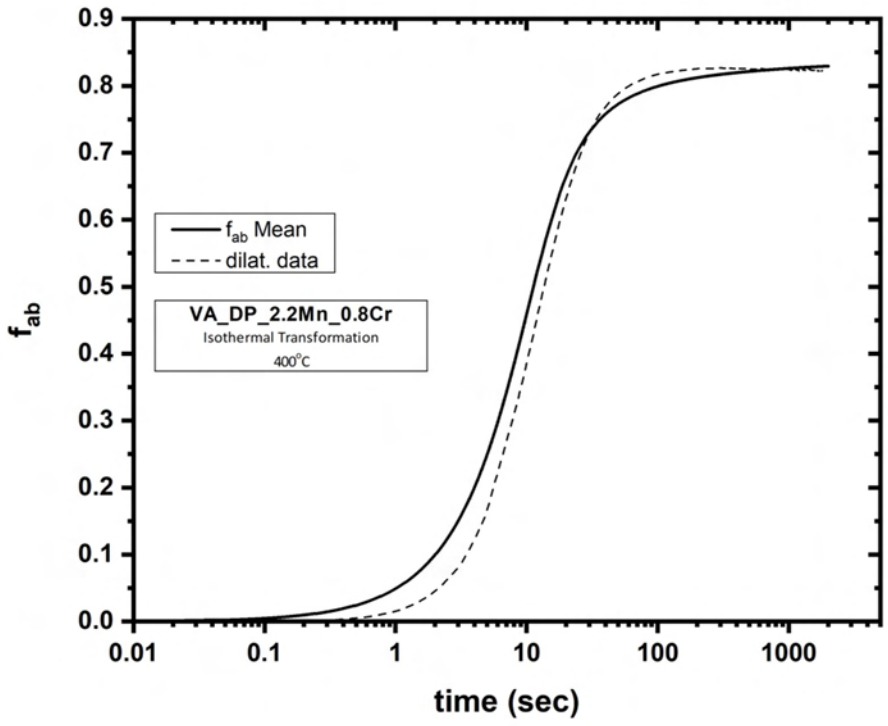

Figure 4.1-15 Comparison of Dilatometric data with Simulation

4.2 TRIP-AL

The TRIP-AL was provided by ThyssenKrupp Steel Europe AG [39] and its chemical composition is presented in the following table:

Table 4.2-1 TRIP AL Composition

C (%wt.)	Al (%wt.)	Mn (%wt.)	Cr (%wt.)	Si (%wt.)
0.219	1.35	1.6	0.033	0.122

The heat treatment for this TRIP-AL consisted of heating with 100°C/sec to the full annealing temperature of 830 °C for 60sec, subsequent cooling with a rate of 25°C/sec to the bainitic transformation temperature and isothermal holding of 400°C. The thermal cycle is depicted below in Figure 4.2-1.

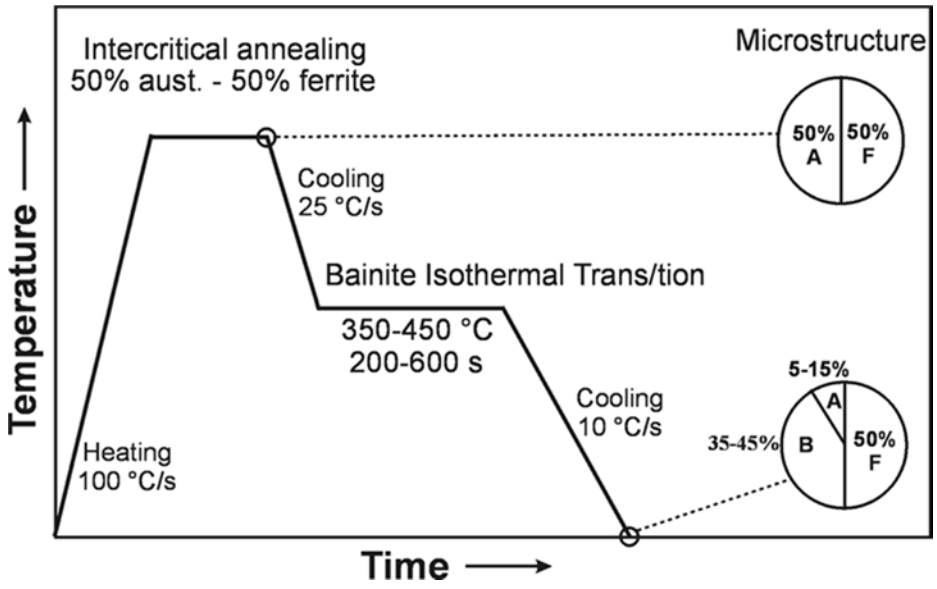

Figure 4.2-1 TRIP-AL Heat Treatment

4.2.1 Kinetic Results-Zone Division

As with the DP-steel, the initial stages of heating were investigated with the help of thermodynamics and kinetics and the commercial software Thermocalc and Dictra. The initial microstructure was ferrite-pearlite similar to that produced during hot-rolling of TRIP-steels.

Following the same procedure initial phase composition was evaluated using the thermodynamic software THERMOCALC. It was assumed that the perlite fraction of the microstructure is spontaneously converted into austenite upon exposure to the A_{C1} temperature; this is illustrated in Table 4.1-2. Kinetic calculations were performed with the software Dictra and the volume fraction of austenite (100%), as well as the composition profiles (Mn, C, Si, Al) of a supposed austenite grain was evaluated, as depicted in. The IA temperature, heating and cooling rates as well as the final temperature of the simulation is presented in Table 4.1-2. Heating and cooling rates were the same at 10K/s and the annealing holding time 60sec. It was not possible for the simulation to be performed lower than 490°C so this is the final temperature reached by cooling.

Table 4.2-2 Annealing Process

Heating		Holding		Cooling	
Initial Temp (°C)	**Rate (K/s)**	**Holding Temp (°C)**	**Holding Time (s)**	**Final Temp (°C)**	**Rate (K/s)**
0	10	830	300	490	10

At the end of cooling the element profiles are calculated. They are presented in Figure 4.2-2. As explained earlier, at the end of the IA process the forming of ferrite takes place. In our case, the ferrite phase makes up 54% of the total grain, leaving7 46% of austenite. The different profile of composition that occurred results, in 4 distinct composition zones to be developed in austenite as illustrated in Figure 4.1-3.

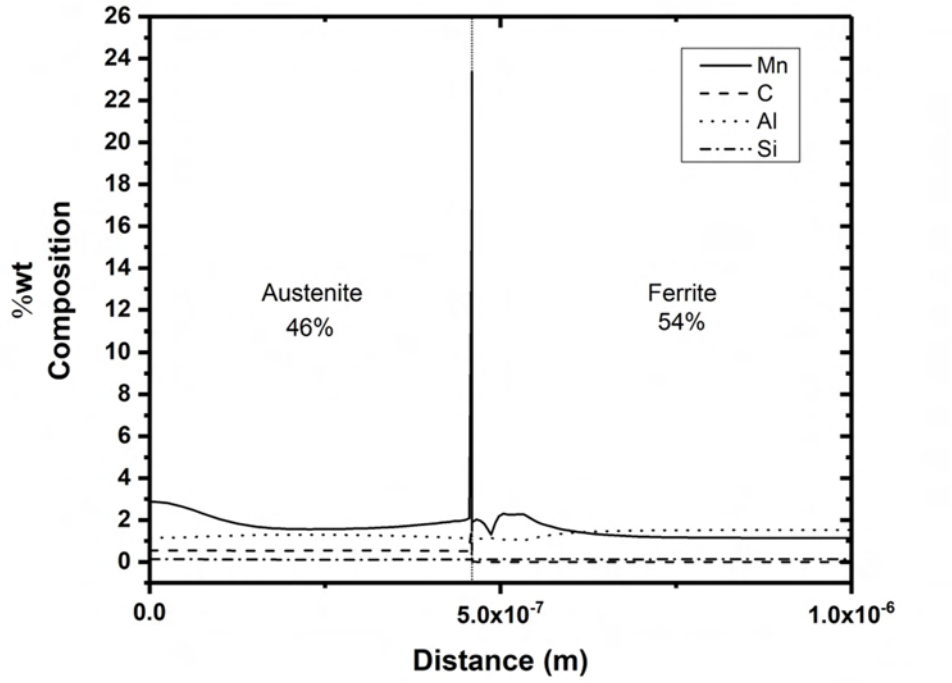

Figure 4.2-2 Element Partition after IA in TRIP-AL

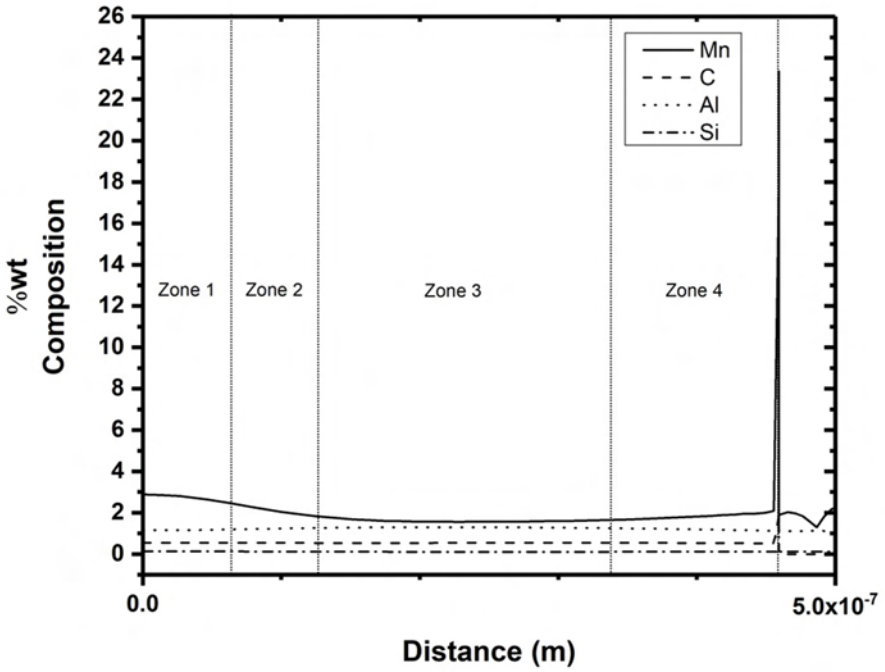

Figure 4.2-3 Zone Division of Austenite

The end of Zone 4 is defined by the boundary between the austenite that remains (on the left) and the newly formed ferrite (on the right). The volume fractions have been calculated, by dividing the distance of each phase with the total distance (Table 4.1-5).

Table 4.2-3 Volume fractions of ferrite (f_α) and austenite (f_γ) post IA

fα	fγ
0.5408298	0.4591702

Table 4.2-4 Zone Chemical Composition

	C (%wt.)	Mn (%wt.)	Cr (%wt.)	Si (%wt.)	Nb (%wt.)	Al (%wt.)
Zone 1	0.55028	2.731066	0.035	0.132222	0.001	1.163146
Zone 2	0.541268	2.058264	0.035	0.119516	0.001	1.235548
Zone 3	0.54043	1.602503	0.035	0.111271	0.001	1.289115
Zone 4	0.532148	1.849333	0.035	0.114398	0.001	1.185272

Table 4.2-5 Zone Length, Percentages and Bainite start (B_s) Temperature

	Length (nm)	Length Percentage	B_s (^oC)
Zone 1	62.45	0.14	521
Zone 2	62.81	0.14	526
Zone 3	209.19	0.46	533
Zone 4	124.85	0.26	540

4.2.2 Azuma Isothermal Transformation

The temperature is set at 400 ^oC but because the stability of the model was needed to be confirmed, the simulation run for 200000 sec.

The figures below depict the results of the isothermal Azuma simulation with respect to the four zones. The volume fraction of bainitic ferrite ($f_{\alpha b}$) for each respective zone versus time during Isothermal Holding is depicted in Figure 4.2-4. The volume fraction of austenite (f_γ) is depicted in Figure 4.2-5 and Carbon concentration ($X_{c\gamma}$) versus time is depicted in Figure 4.2-6. These results are presented in relation to every zone. In Figure 4.2-6 the mean Carbon concentration ($X_{c\gamma}$) of all participating zones is also presented versus time.

In the figures that follow the mean value of every parameter is presented. Figure 4.2-7 depicts the mean volume fraction of bainitic ferrite ($f_{\alpha b}$) and the mean volume fraction of austenite (f_γ). Figure 4.2-8 depicts the mean volume fraction of austenite (f_γ) and the corresponding austenite enrichment of all contributing zones versus time during Isothermal Holding.

During this simulation no carbides were formed in either austenite or bainitic ferrite, as is evident in Figure 4.2-9. In Figure 4.2-10 and Figure 4.2-11 the microstructural characteristics of bainitic ferrite and the mechanical characteristics of austenite. The platelet size of bainitic ferrite is presented in Figure 4.2-10 and the tensile Yield Strength of retained austenite in comparison with the enrichment of austenite in Carbon presented in Figure 4.2-11.

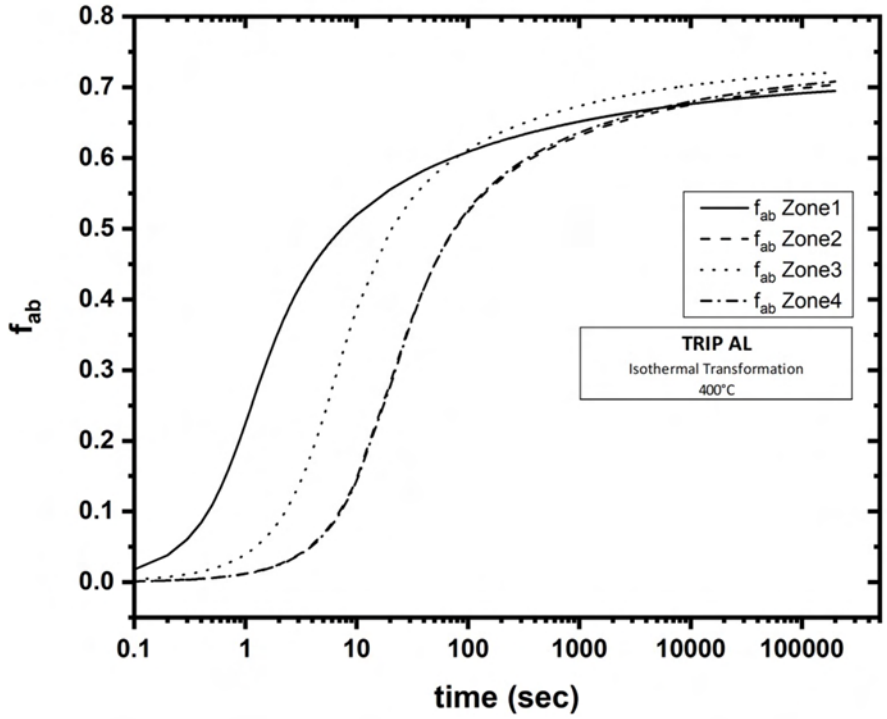

Figure 4.2-4 Volume fraction of bainitic ferrite ($f_{\alpha b}$) for each respective zone versus time during Isothermal Holding

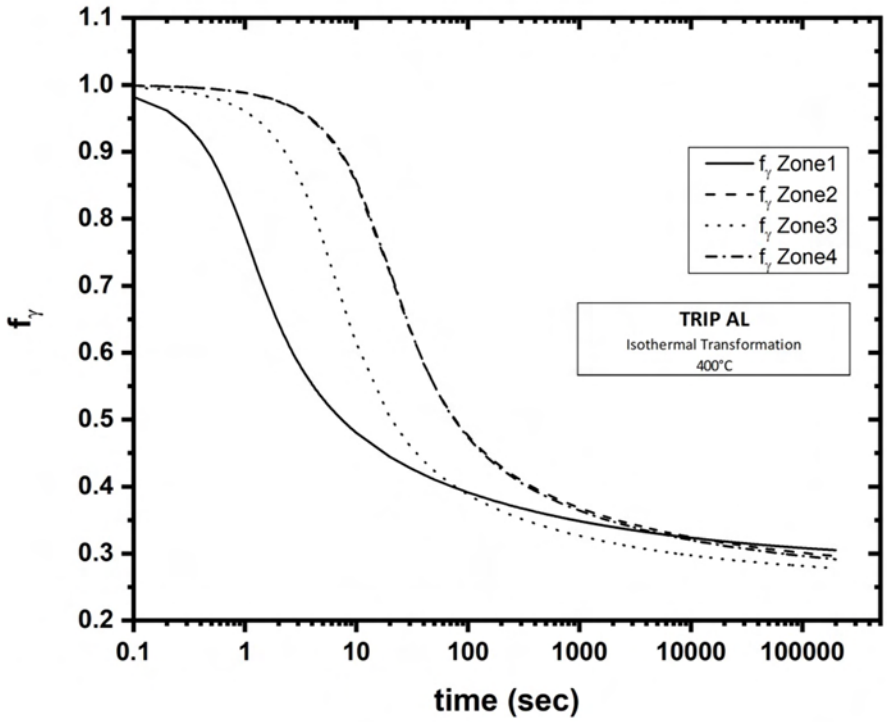

Figure 4.2-5 Volume fraction of austenite (f_γ) for each respective zone versus time during Isothermal Holding

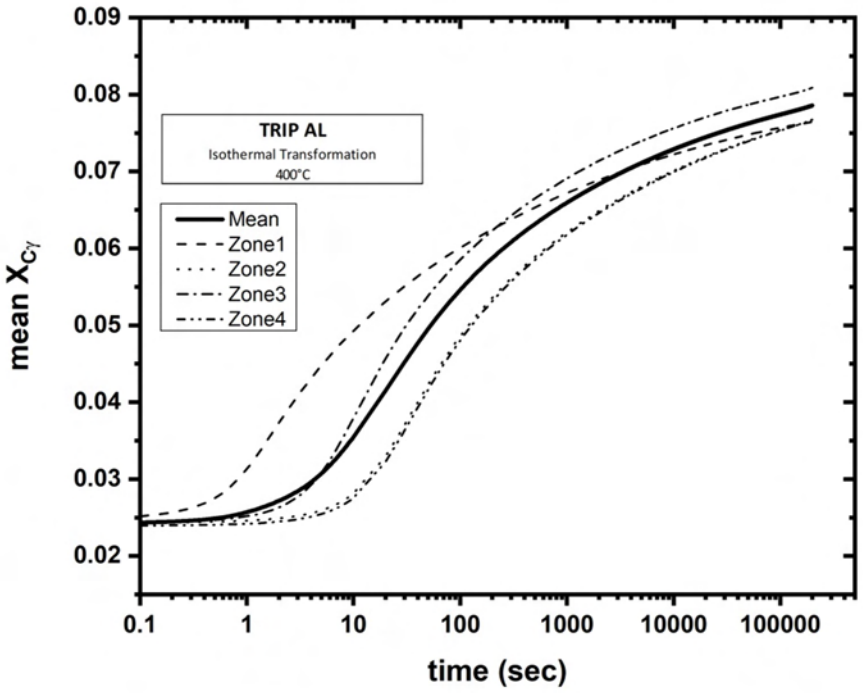

Figure 4.2-6 Mean Carbon concentration ($X_{c\gamma}$) versus time, during Isothermal Holding

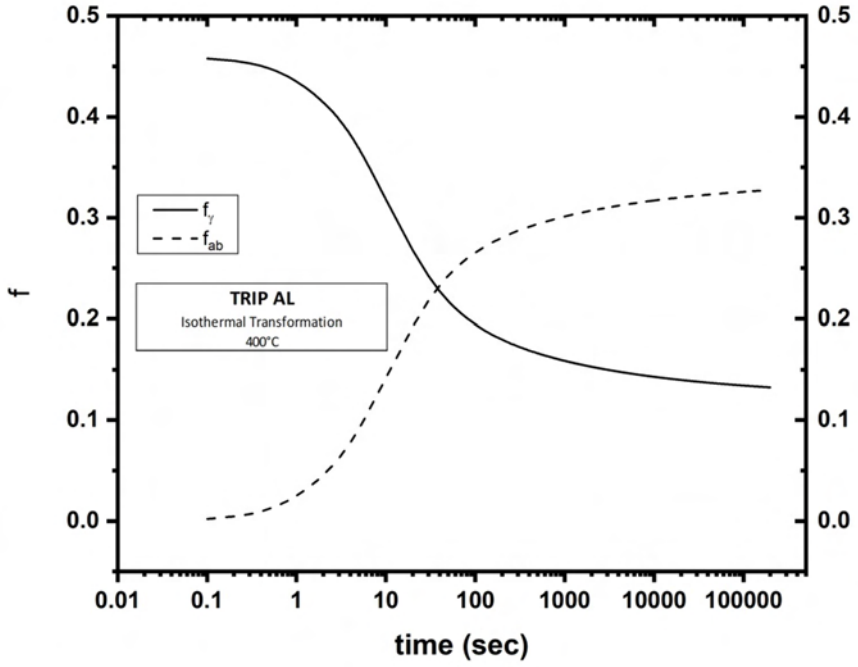

Figure 4.2-7 Mean volume fraction of bainitic ferrite ($f_{\alpha b}$) and mean volume fraction of austenite (f_γ) of all contributing zones versus time during Isothermal Holding

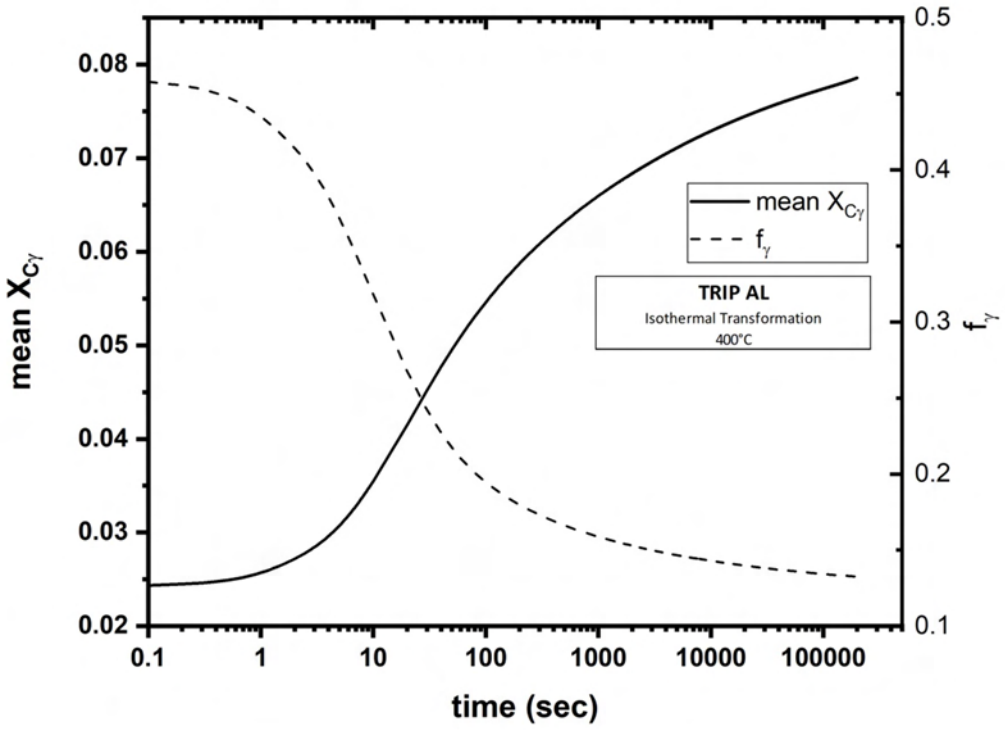

Figure 4.2-8 Mean volume fraction of austenite (f_γ) and corresponding austenite enrichment of all contributing zones versus time during Isothermal Holding

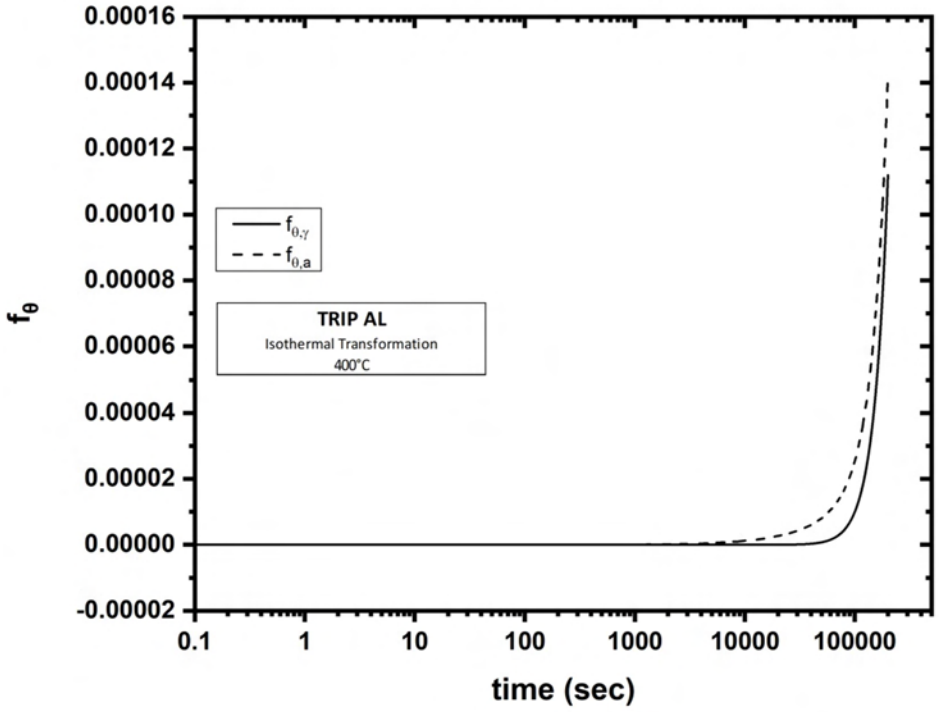

Figure 4.2-9 Cementite Precipitates: In both austenite and bainitic ferrite. There are virtually no carbides formed

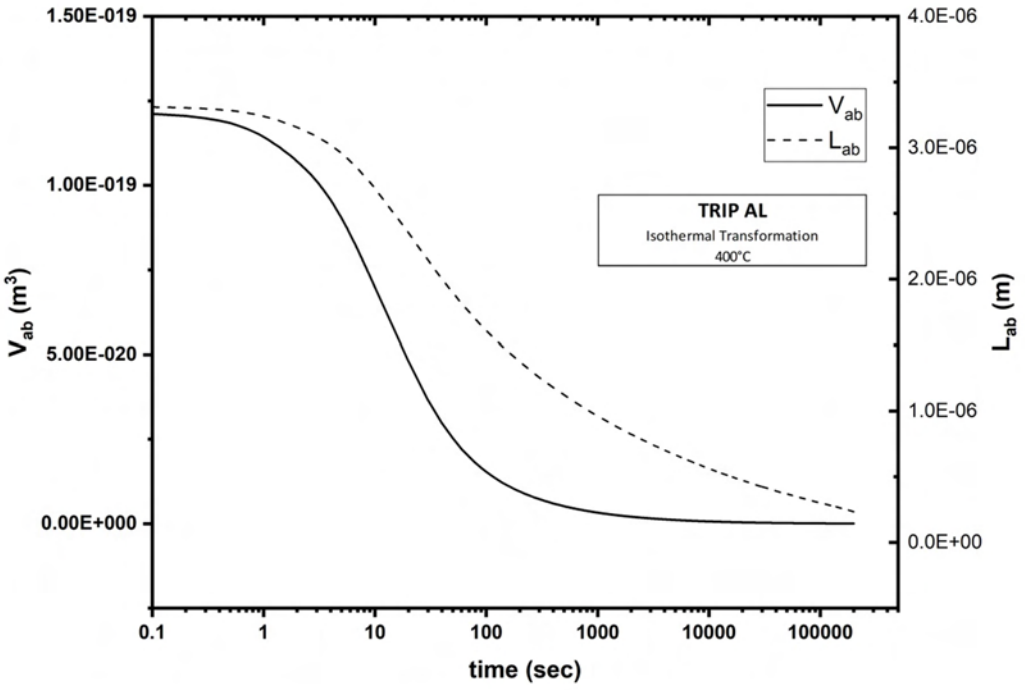

Figure 4.2-10 Platelet Size of bainitic ferrite

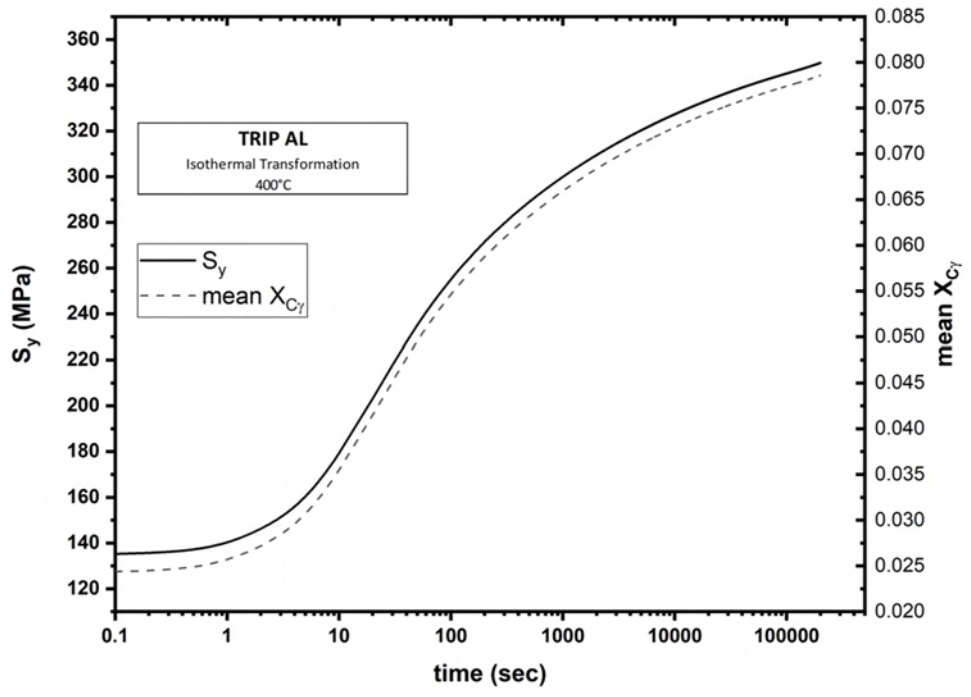

Figure 4.2-11 Yield Strength of Retained Austenite versus the Carbon enrichment of Austenite

4.2.3 Summary-Comparison with Experimental Data

Using the data provided by RWTH [39], the validity of the results can be checked. The final volume fractions of the participating phases after the completion of the thermal cycle are shown in Table 4.2-6 Final Volume Fractions post Quenching, and the bainitic ferrite transformation regarding time is shown at Figure 4.2-12, compared with dilatometric data from [39]. The results are in good agreement with the experimental data.

Table 4.2-6 Final Volume Fractions post Quenching

			Simulation Data				
time (s)	**f_α**	**$f_{\alpha b}$**	**f_γ**	**$f_{\theta,\gamma}$**	**f_M**	**mean $X_{C\gamma}$**	**mean $X_{C\alpha}$**
200000	0.5408298	0.327318	0.132428	0	0	0.078586	0.002301

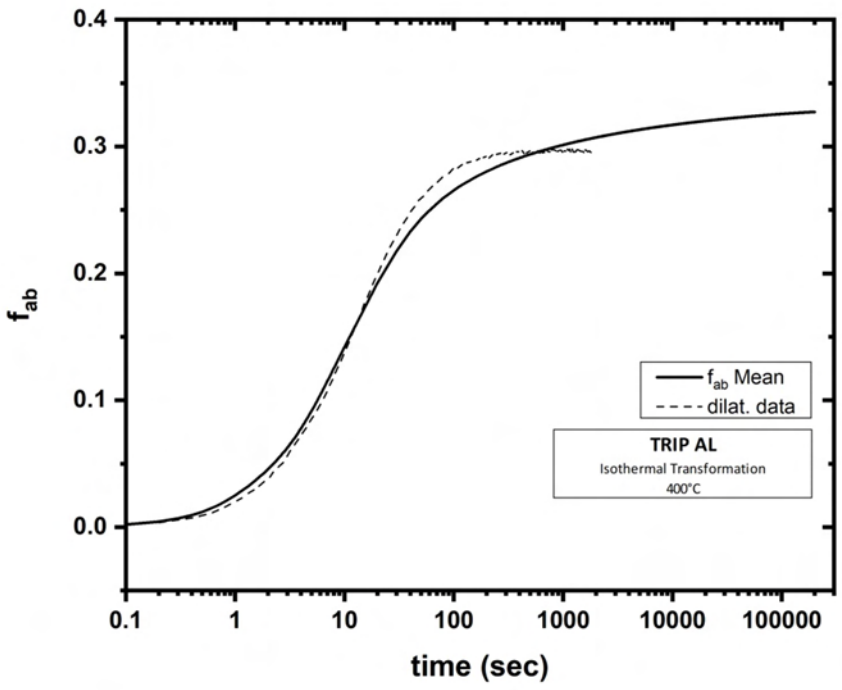

Figure 4.2-12 Comparison of Dilatometric data with Simulation

5 Results

5.1 TRIP-700

During an ongoing research program, specimens of TRIP 700 steel provided by Voestalpine were put through a series of different thermal treatments. The chemical composition of the steel is given in Table 5.1-1, and the different heat treatments are depicted in Figure 5.1-1.

Table 5.1-1 TRIP 700 Chemical Composition

C (%wt.)	Mn (%wt.)	Cr (%wt.)	Si (%wt.)	Nb (%wt.)	Al (%wt.)
0.202	1.99	0.038	0.348	0.017	1.07

The heat treatment consisted of heating with 15°C/sec to the intercritical annealing temperature of 890°C for 60sec, subsequent cooling with a rate of 60°C/sec to the bainitic transformation temperature and isothermal holding there. The thermal cycle is depicted below in Figure 5.1-1.

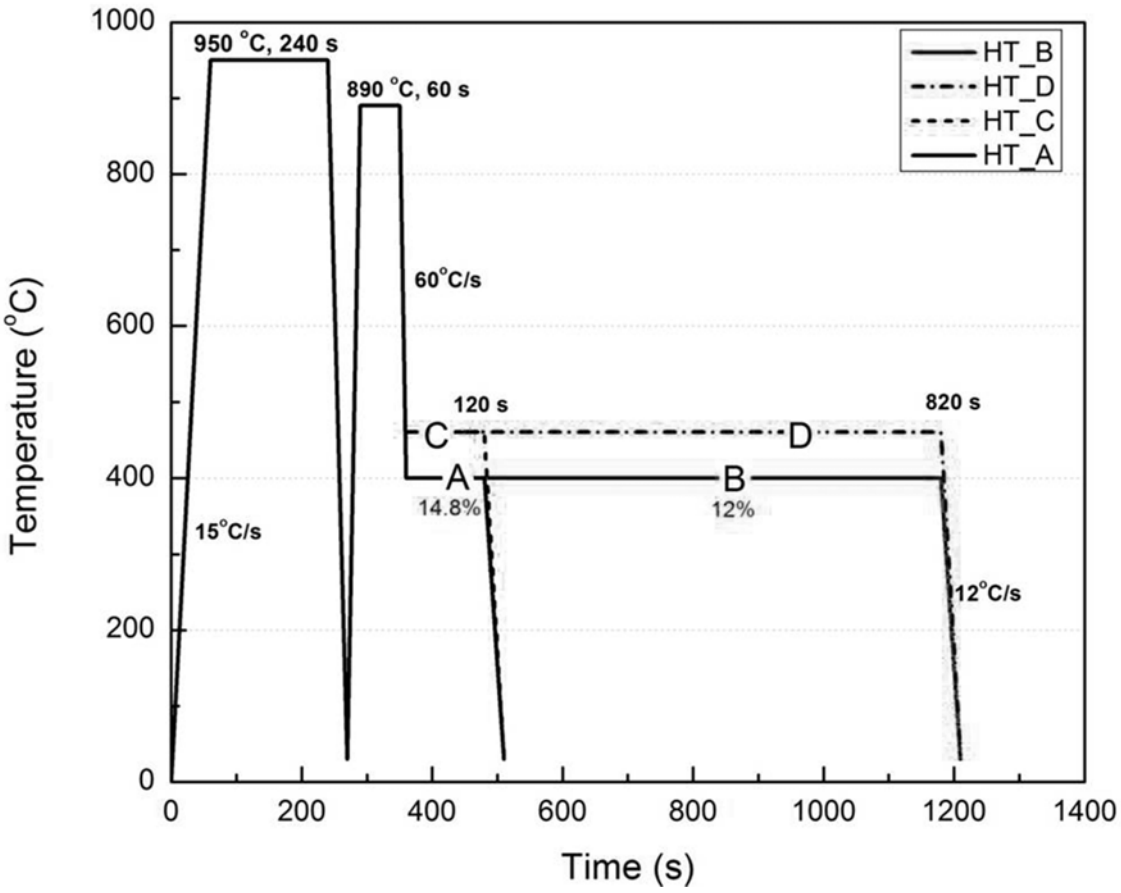

Figure 5.1-1 The 4 Heat Treatments performed on TRIP 700

5.1.1 Kinetic Results-Zone Division

As mentioned above the part of the heat treatment involving the initial stages of heating, annealing and cooling to the bainite start temperature were investigated with the help of thermodynamics and kinetics and the commercial software Thermocalc and Dictra. The initial microstructure was ferrite-pearlite.

The initial conditions (initial phase composition) were evaluated using the thermodynamic software THERMOCALC. Kinetic calculations were performed with the software Dictra and the volume fraction of austenite Figure 5.1-2, as well as the composition profiles (Mn, C, Si, Al) of a supposed austenite grain was evaluated, as depicted in Figure 5.1-3. The IA temperature, heating and cooling rates as well as the final temperature of the simulation is presented in Table 5.1-2. The heating rate was 15K/s and the cooling rate 60K/s, the annealing holding time was 60sec. It was not possible for the simulation to be performed for the cooling rate 60K/s so quenching to the bainite temperature is assumed.

Table 5.1-2 Annealing Process of TRIP 700

Heat Treatment	Austenization 950°C	Intercritical Annealing 890°C	Isothermal Transformation
A	4 min	60 sec	400°C – 120sec
B	4 min	60 sec	400°C – 820 sec
C	4 min	60 sec	460°C – 120 sec
D	4 min	60 sec	460°C – 820 sec

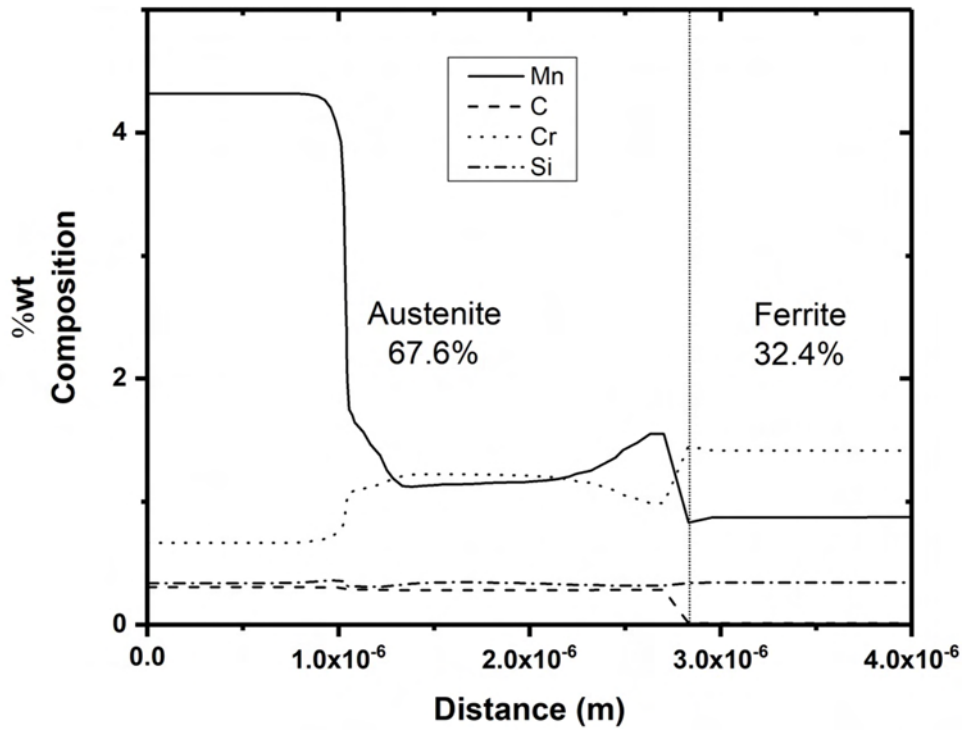

Figure 5.1-2 The evolution of austenite volume fraction for TRIP-700 after heating with a rate of 15K/sec, and isothernal holding at 890°C versus time

At the end of Intercritical Annealing the element profiles were calculated. They are presented in Figure 5.1-3. These results in four distinct composition zones to be developed in austenite as illustrated in Figure 5.1-3.

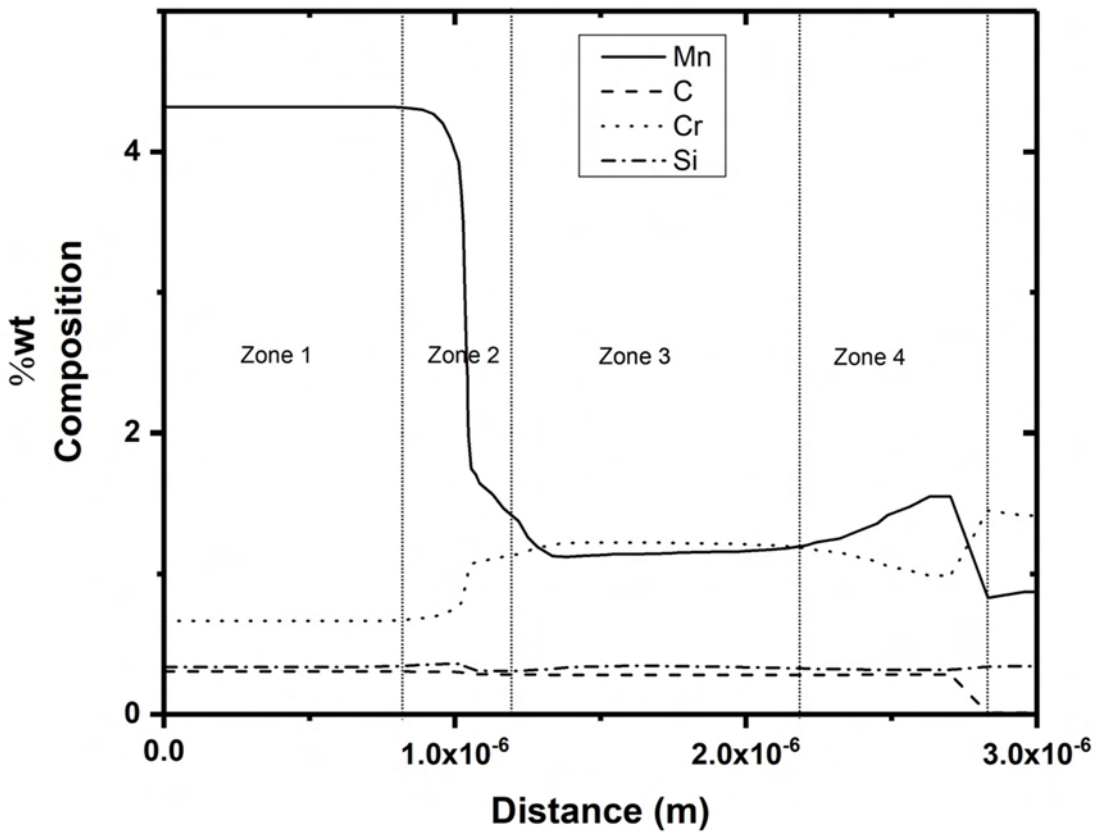

Figure 5.1-3 Composition Profiles after Annealing of TRIP 700

In this occasion, 67.6% austenite was formed during the annealing process. The region is divided in the 4 distinct zones and the composition and respective size of each zone was calculated (Table 5.1-3 and Table 5.1-4), as described previously.

Table 5.1-3 Zone Compositions

	C (%wt.)	Mn (%wt.)	Cr (%wt.)	Si (%wt.)	Nb (%wt.)	Al (%wt.)
Zone 1	0.30519	4.31505	0.03800	0.34057	0.01700	0.66760
Zone 2	0.29185	2.54001	0.03800	0.32926	0.01700	0.96214
Zone 3	0.28137	1.15424	0.03800	0.33616	0.01700	1.21261
Zone 4	0.28240	1.32177	0.03800	0.32303	0.01700	1.11463

Table 5.1-4 Zone Length, Percentages and Bainite start (B_s) Temperature

	Length (nm)	Length Percentage	B_s (°C)
Zone 1	958.72	0.24	414
Zone 2	293.29	0.07	494
Zone 3	753.67	0.19	585
Zone 4	696.58	0.17	509

5.1.2 Azuma Isothermal Transformation at 400°C

To simulate the Heat Treatments of A and B (Figure 5.1-1), the Azuma model was applied for a constant temperature of 400 °C. The figures below present the results of the model. The simulation was continued, by using the composition evaluated at the end of IA from Dictra model as the input for the isothermal bainitic transformation. The temperature is set at 400 °C and the duration is 860 sec.

The figures below depict the results of the isothermal Azuma simulation with respect to the three zones formed in austenite. The volume fraction of bainitic ferrite ($f_{\alpha b}$) for each respective zone versus time during Isothermal Holding at 400°C is depicted in Figure 5.1-4. The volume fraction of austenite (f_{γ}) is depicted in Figure 5.1-5 and Carbon concentration ($X_{c\gamma}$) versus time is depicted in Figure 5.1-6. These results are presented by relation to every zone.

In the figures that follow the mean value of every parameter is presented. Figure 5.1-7 depicts the mean volume fraction of bainitic ferrite ($f_{\alpha b}$) and the mean volume fraction of austenite (f_{γ}). Figure 5.1-8 is an enlargement of Figure 5.1-7 indicating the two values that were extracted by experimental data. For isothermal holding at 400°C for 130sec 14.9% of retained austenite remains while for holding up to 820sec 6.6% retained austenite remains.

Figure 5.1-9 depicts the mean volume fraction of austenite (f_{γ}) and the corresponding austenite enrichment of all contributing zones versus time during Isothermal Holding. During this simulation no carbides were formed in either austenite or bainitic ferrite, as is evident in Figure 5.1-10. In Figure 5.1-11 and Figure 5.1-12 the microstructural characteristics of bainitic ferrite are presented. The platelet size of bainitic ferrite is presented in Figure 5.1-11 and the tensile Yield Strength of retained austenite in comparison with the bainite platelet size presented in Figure 5.1-12.

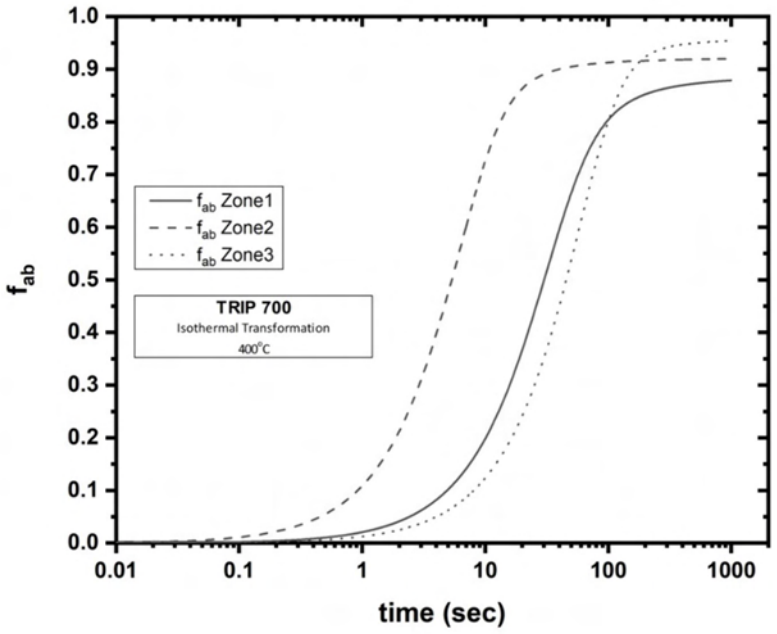

Figure 5.1-4 Volume fraction of bainitic ferrite ($f_{\alpha b}$) for each respective zone versus time during Isothermal Holding at 400°C

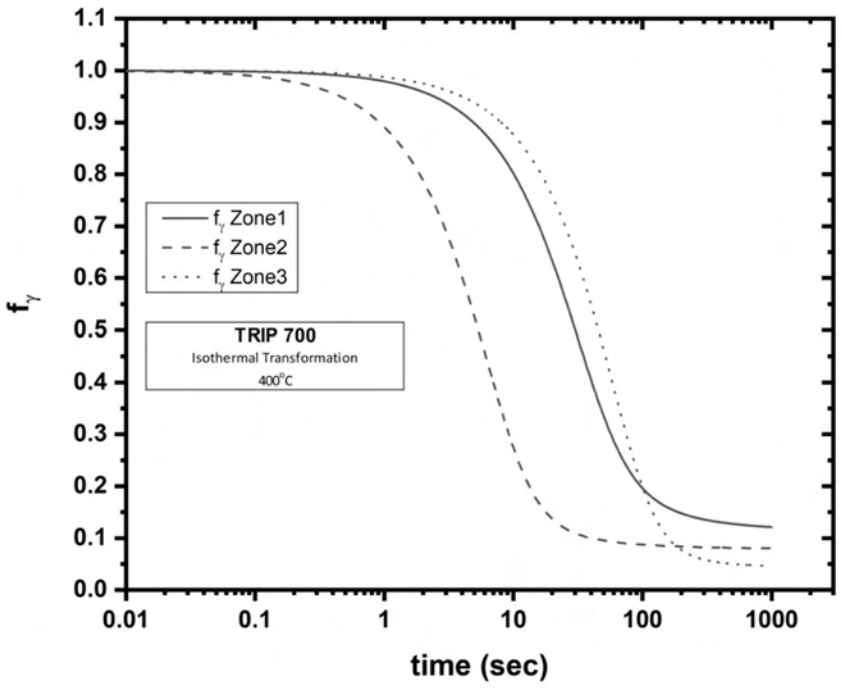

Figure 5.1-5 Volume fraction of austenite (f_γ) for each respective zone versus time during Isothermal Holding at 400°C

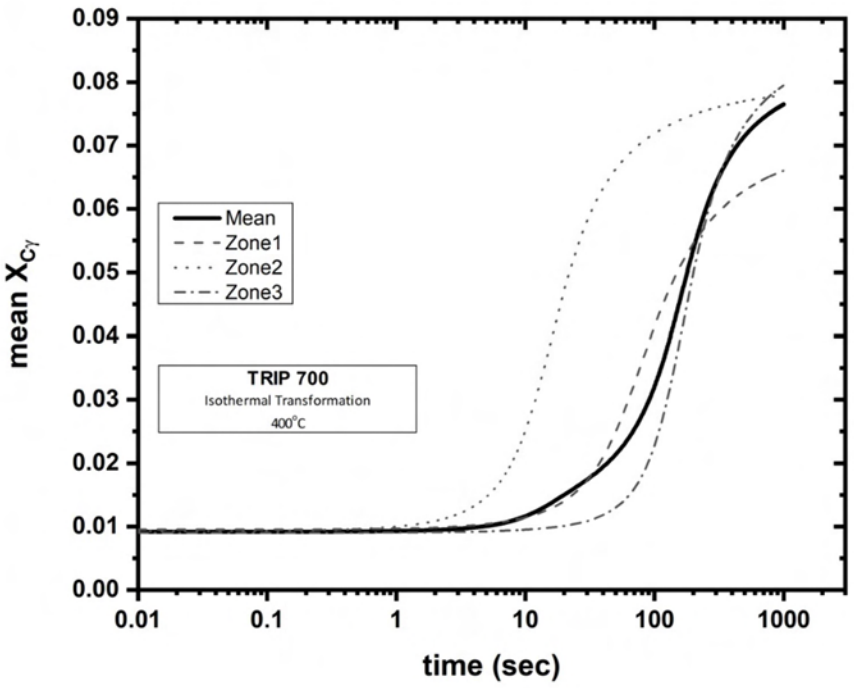

Figure 5.1-6 Mean Carbon concentration ($X_{c\gamma}$) versus time, during Isothermal Holding at 400°C

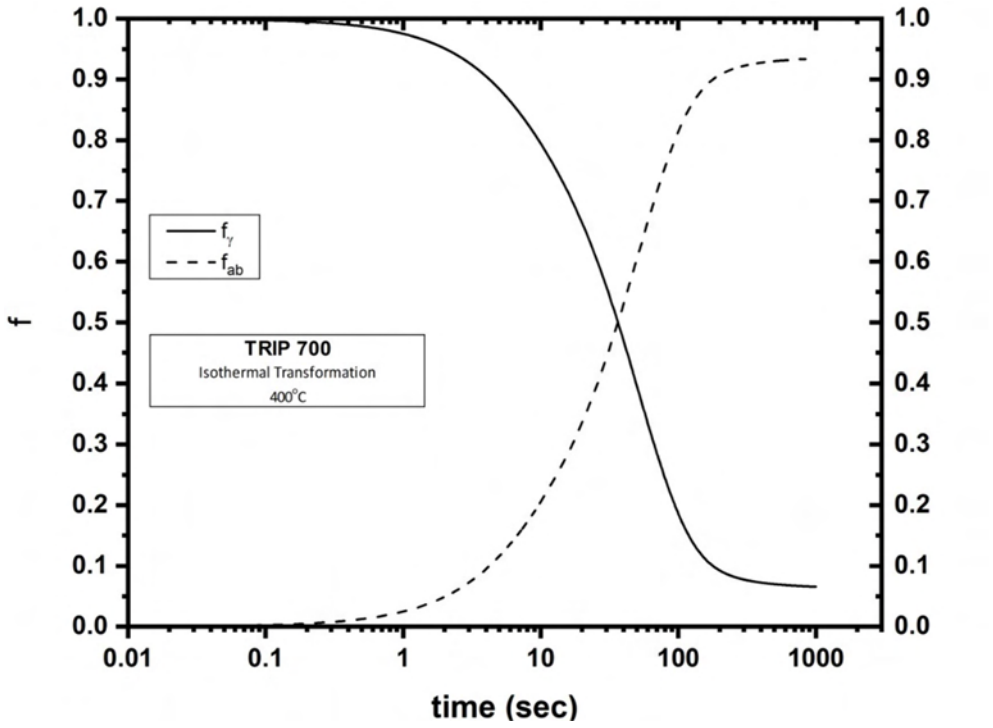

Figure 5.1-7 Mean volume fraction of bainitic ferrite ($f_{\alpha b}$) and mean volume fraction of austenite (f_γ) of all contributing zones versus time during Isothermal Holding at 400°C

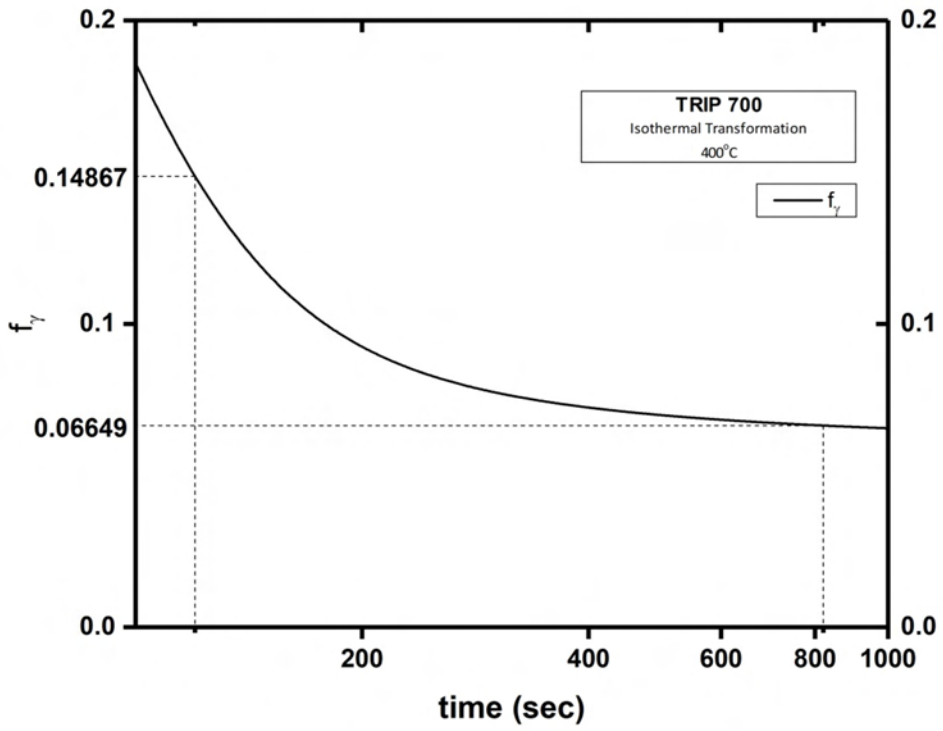

Figure 5.1-8 Mean volume fraction of austenite (f_γ) and corresponding austenite enrichment of all contributing zones versus time during Isothermal Holding at 400°C (Enlargment)

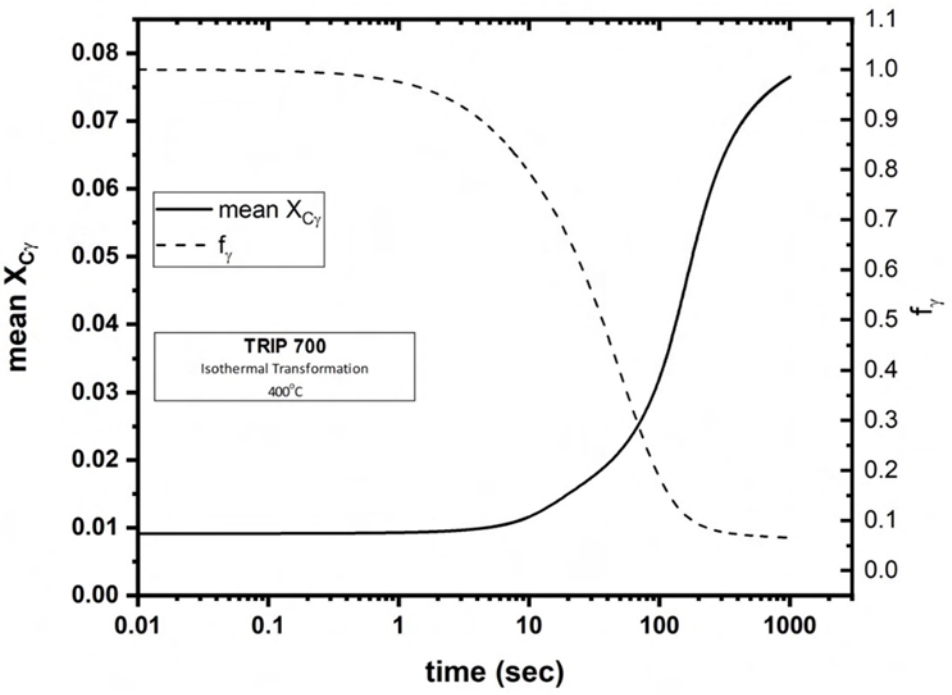

Figure 5.1-9 Mean volume fraction of austenite (f_γ) and corresponding austenite enrichment of all contributing zones versus time during Isothermal Holding at 400°C

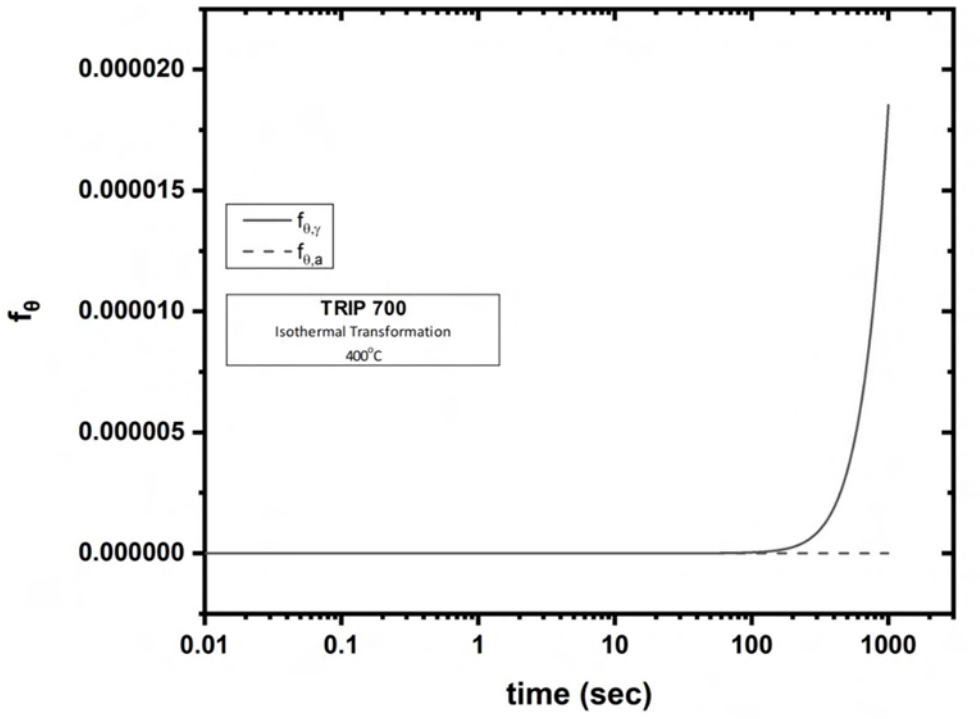

Figure 5.1-10 Cementite Precipitates: In both austenite and bainitic ferrite. There are virtually no carbides formed

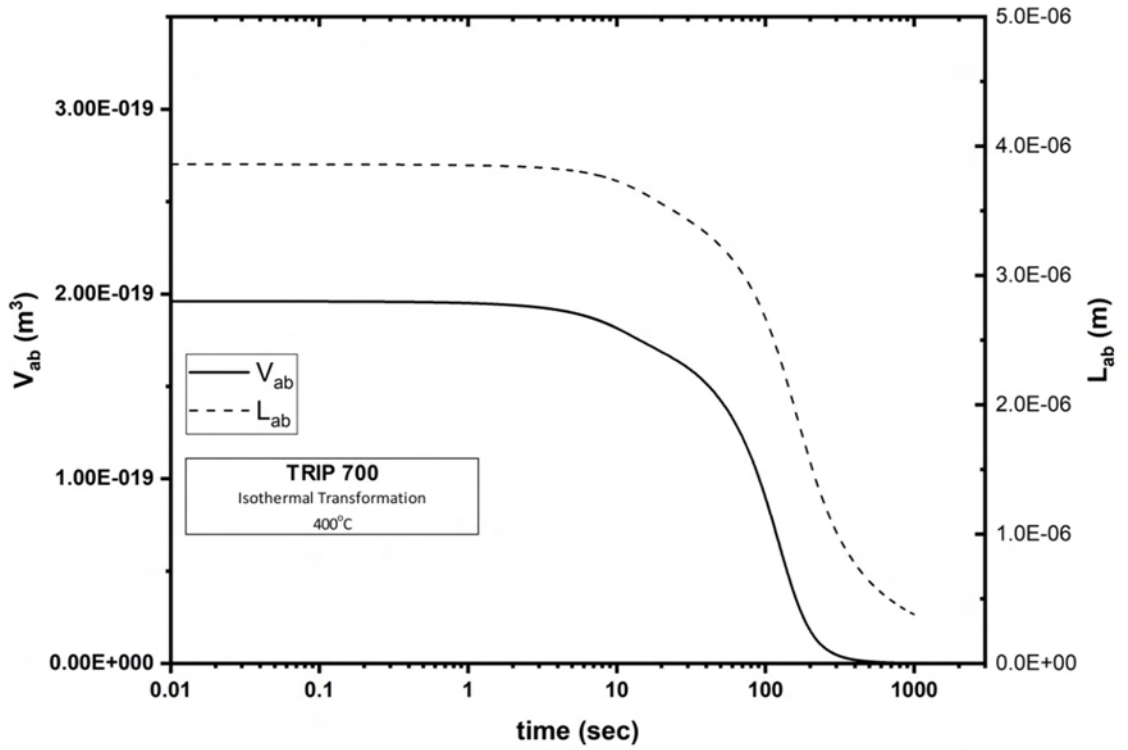

Figure 5.1-11 Platelet Size of bainitic ferrite

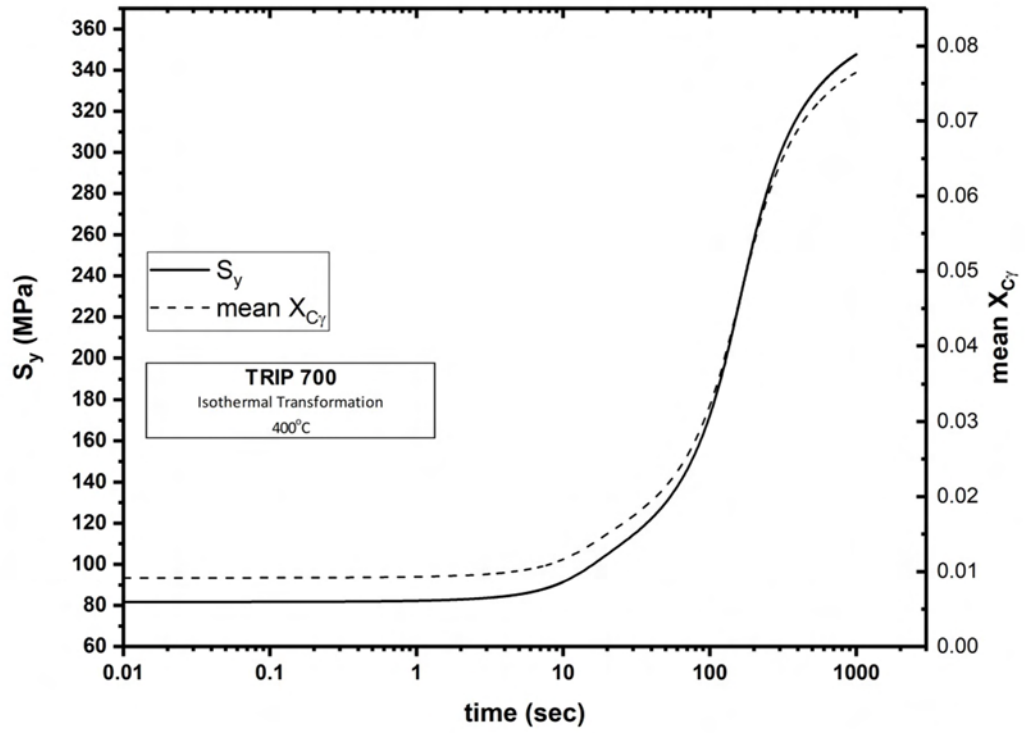

Figure 5.1-12 Yield Strength of Retained Austenite versus the Carbon enrichment of Austenite

5.1.3 Comparison with Experimental

Finally, the table below shows the change in volume fractions as the transformation progresses, starting from heating, intercritical annealing, bainitic transformation and finally quenching.

Table 5.1-5 Phase Transformations Results from the Model and experimental data

Heat Treatment		Experimental Data	Simulation Data
		Retained Austenite	Retained Austenite
A	400°C – 120sec	14.8	14.8674
B	400°C – 820 sec	12	6.6494

Using the data provided by Mechanics & Strength of Materials Laboratory, the validity of the results was checked. The final volume fractions of retained austenite after the completion of the thermal cycle are shown in Table 5.1-5, both experimental and simulation data. The simulation results for the case of isothermal holding for 120sec are in excellent agreement, while in the case of 820sec the model calculated half the measured amount of retained austenite.

5.1.4 Azuma Isothermal Transformation at 460°C

To simulate the Heat Treatments of C and D (Figure 5.1-1), the Azuma model was applied for a constant temperature of 460 °C. The figures below present the results of the model. As mentioned previously, the simulation was continued, by using the composition evaluated at the end of IA from Dictra model as the input for the isothermal bainitic transformation. The temperature is set at 460 °C and the duration is 860 sec.

The figures below depict the results of the isothermal Azuma simulation with respect to the three zones formed in austenite. The volume fraction of bainitic ferrite ($f_{\alpha b}$) for each respective zone versus time during Isothermal Holding at 460°C is depicted in Figure 5.1-13. The volume fraction of austenite (f_γ) is depicted in Figure 5.1-14 and Carbon concentration ($X_{c\gamma}$) versus time is depicted in Figure 5.1-15. These results are presented by relation to every zone.

In the figures that follow the mean value of every parameter is presented. Figure 5.1-16 depicts the mean volume fraction of bainitic ferrite ($f_{\alpha b}$) and the mean volume fraction of austenite (f_γ). Figure 5.1-17 depicts the mean volume fraction of austenite (f_γ) and the corresponding austenite enrichment of all contributing zones versus time during Isothermal Holding.

During this simulation a small amount of carbides were formed in austenite, as is evident in Figure 5.1-18. In Figure 5.1-20and Figure 5.1-21the microstructural characteristics of bainitic ferrite are presented. The platelet size of bainitic ferrite is presented in Figure 5.1-20and the tensile Yield Strength of retained austenite in comparison with the bainite platelet size presented in Figure 5.1-21.

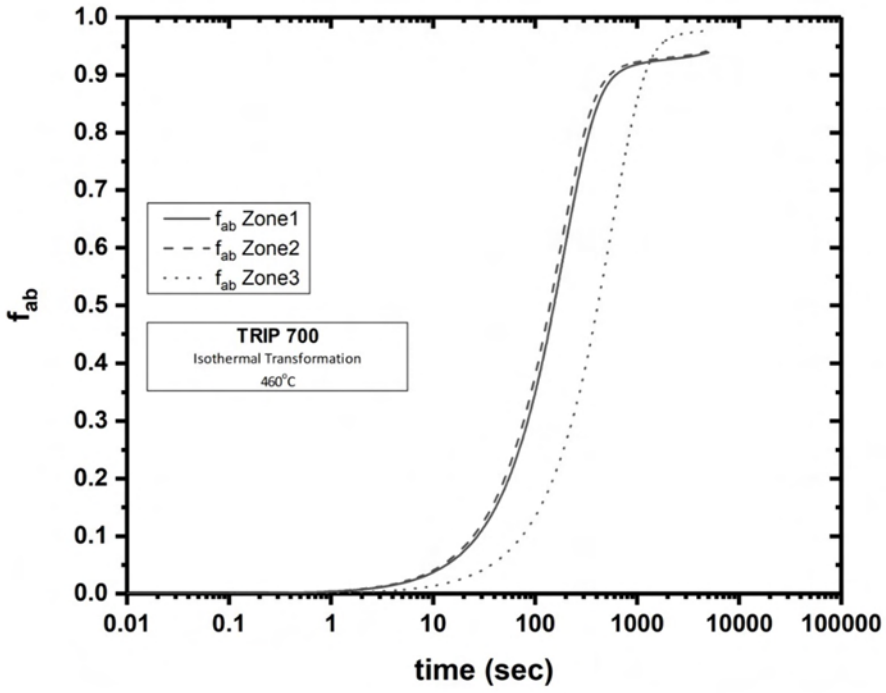

Figure 5.1-13 Volume fraction of bainitic ferrite ($f_{\alpha b}$) for each respective zone versus time during Isothermal Holding at 460°C

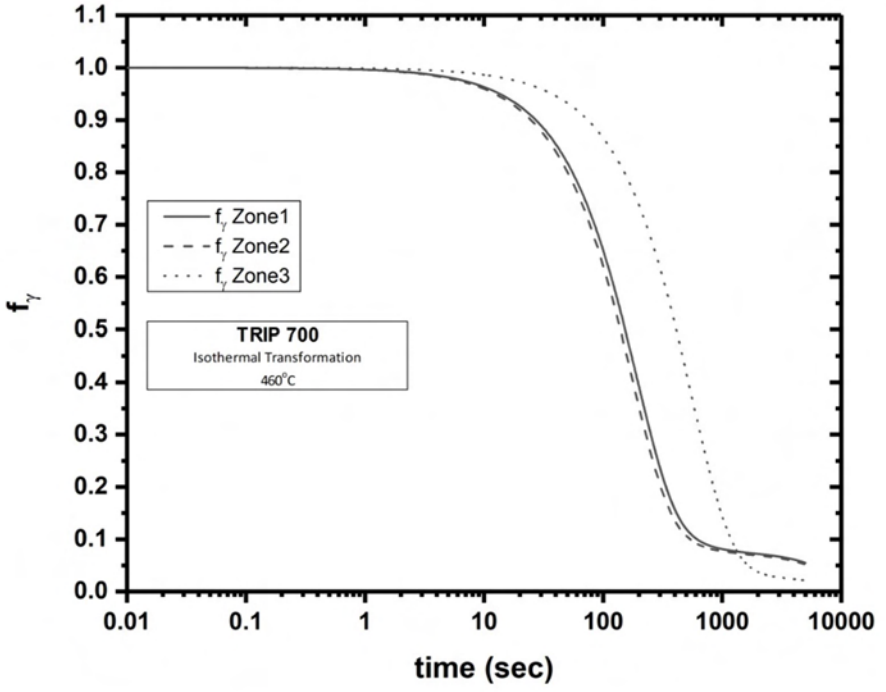

Figure 5.1-14 Volume fraction of austenite (f_γ) for each respective zone versus time during Isothermal Holding at 460°C

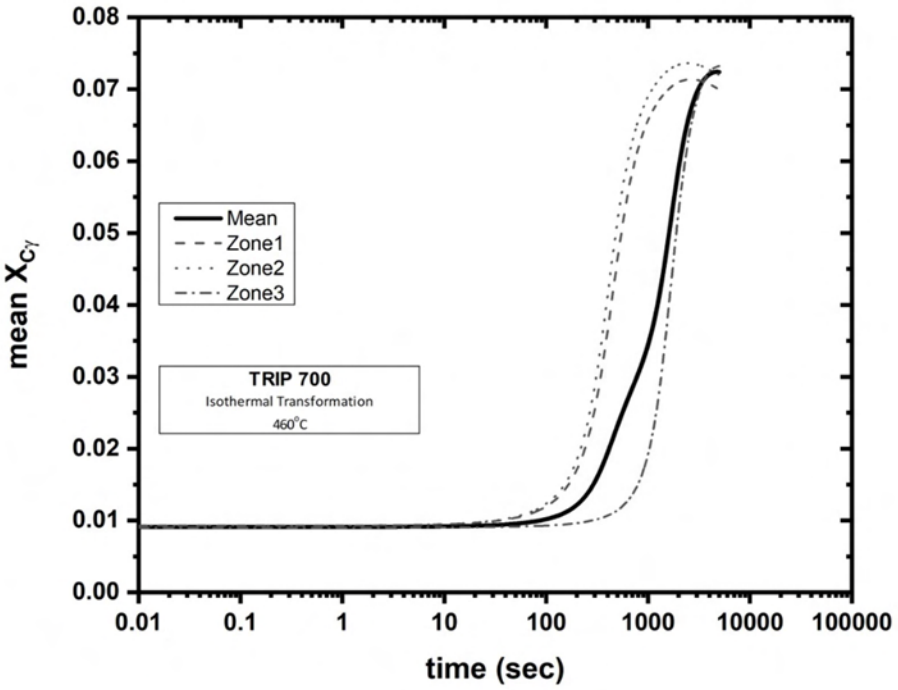

Figure 5.1-15 Mean Carbon concentration ($X_{c\gamma}$) versus time, during Isothermal Holding at 460°C

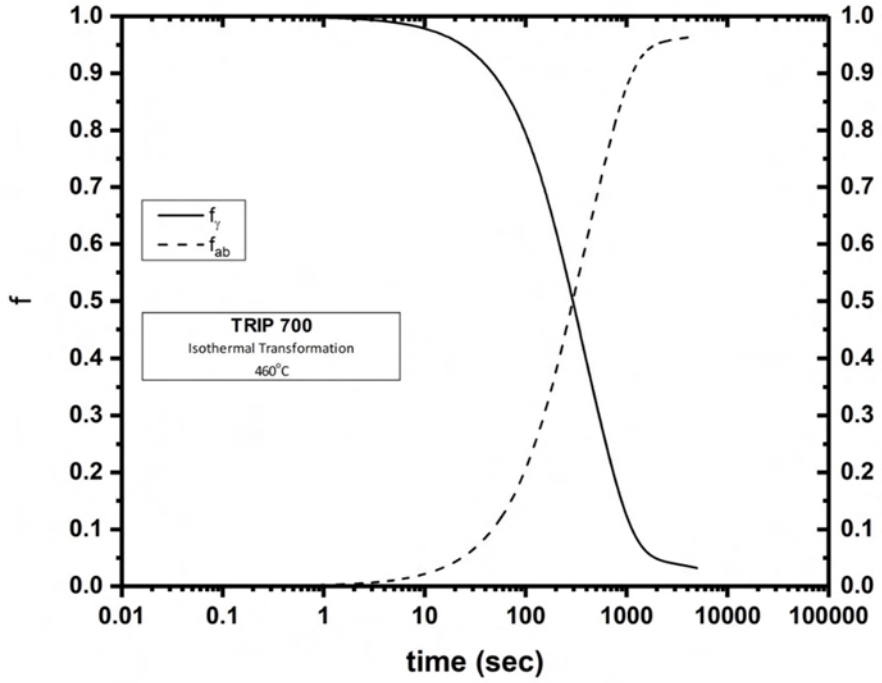

Figure 5.1-16 Mean volume fraction of bainitic ferrite ($f_{\alpha b}$) and mean volume fraction of austenite (f_γ) of all contributing zones versus time during Isothermal Holding at 460°C

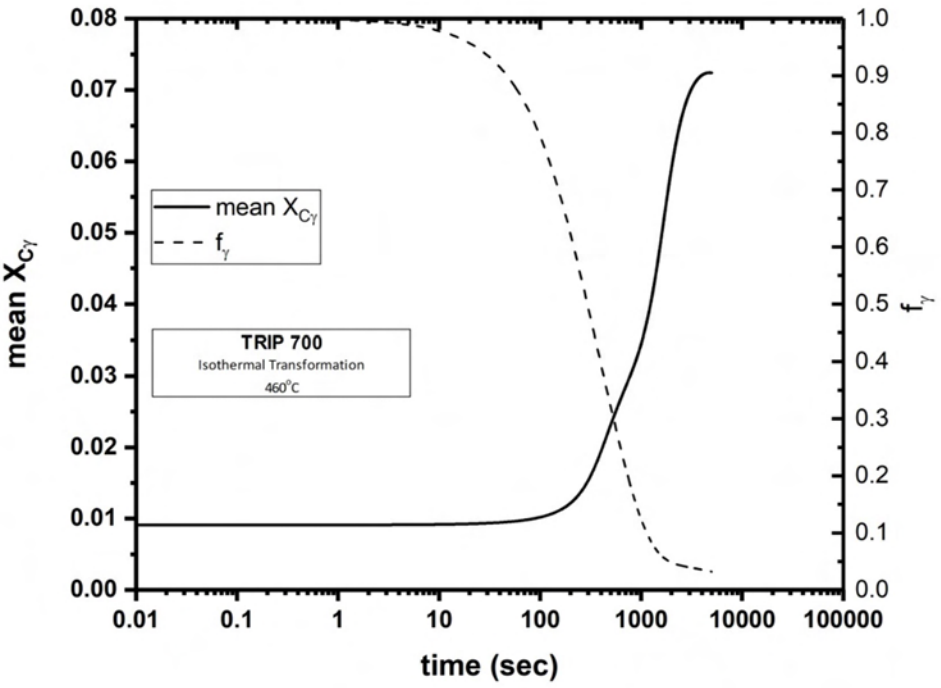

Figure 5.1-17 Mean volume fraction of austenite (f_γ) and corresponding austenite enrichment of all contributing zones versus time during Isothermal Holding at 460°C

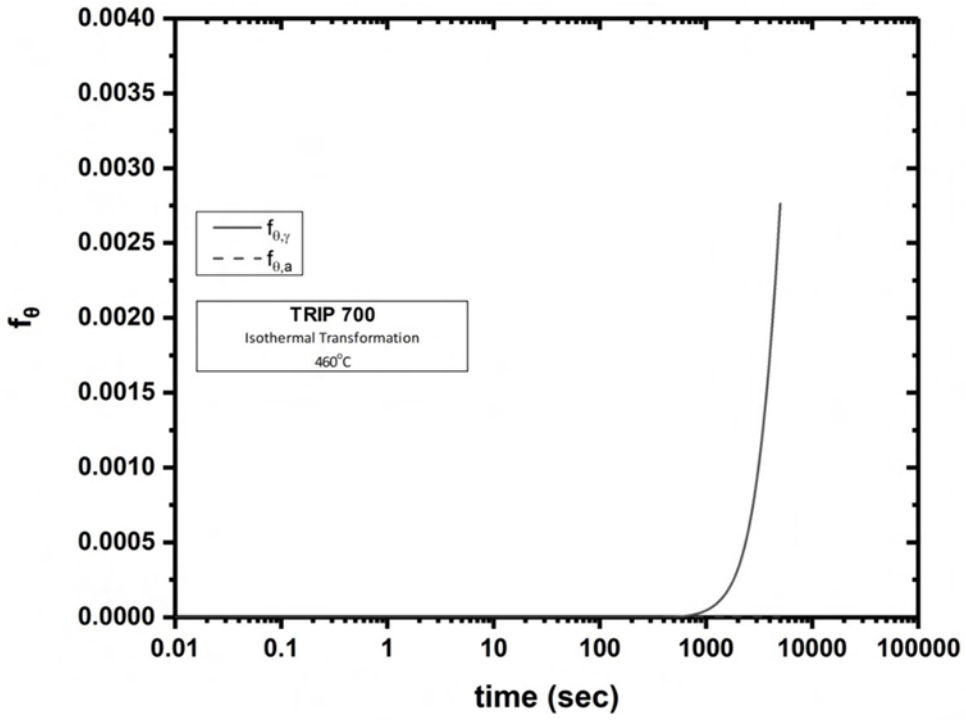

Figure 5.1-18 Cementite Precipitates: In both austenite and bainitic ferrite

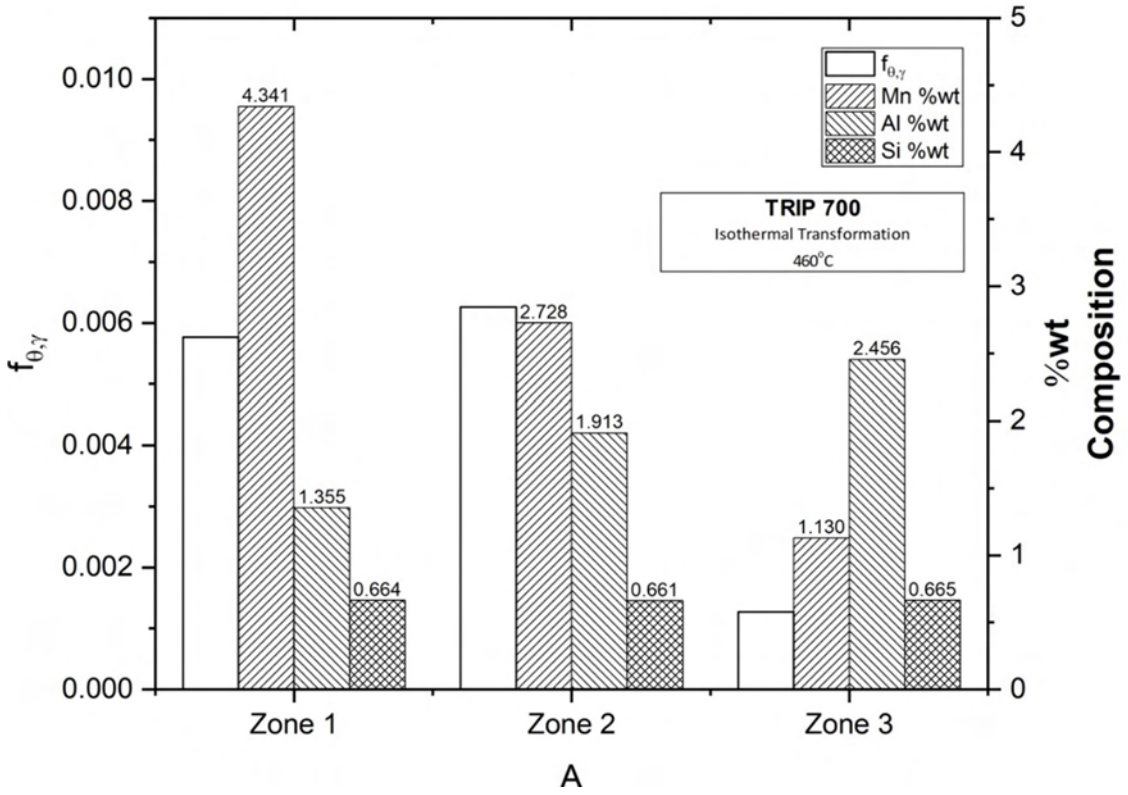

Figure 5.1-19 Mean volume fraction of carbides precipitating in austenite ($f_{\theta,\gamma}$) and mean chemical composition of each zone

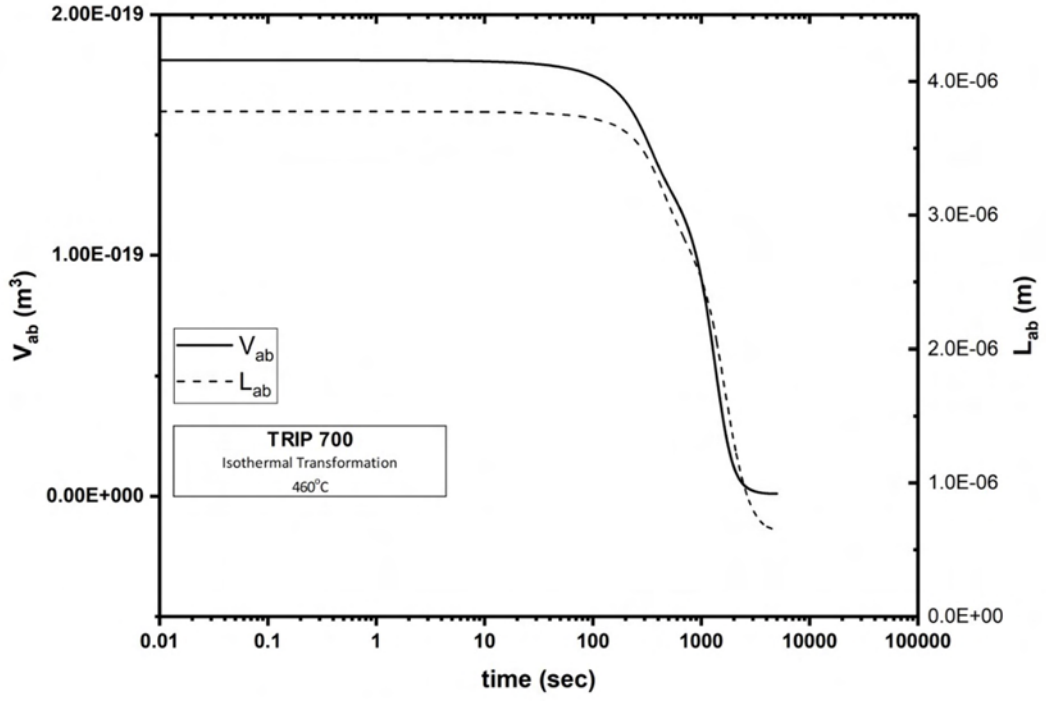

Figure 5.1-20 Platelet Size of bainitic ferrite

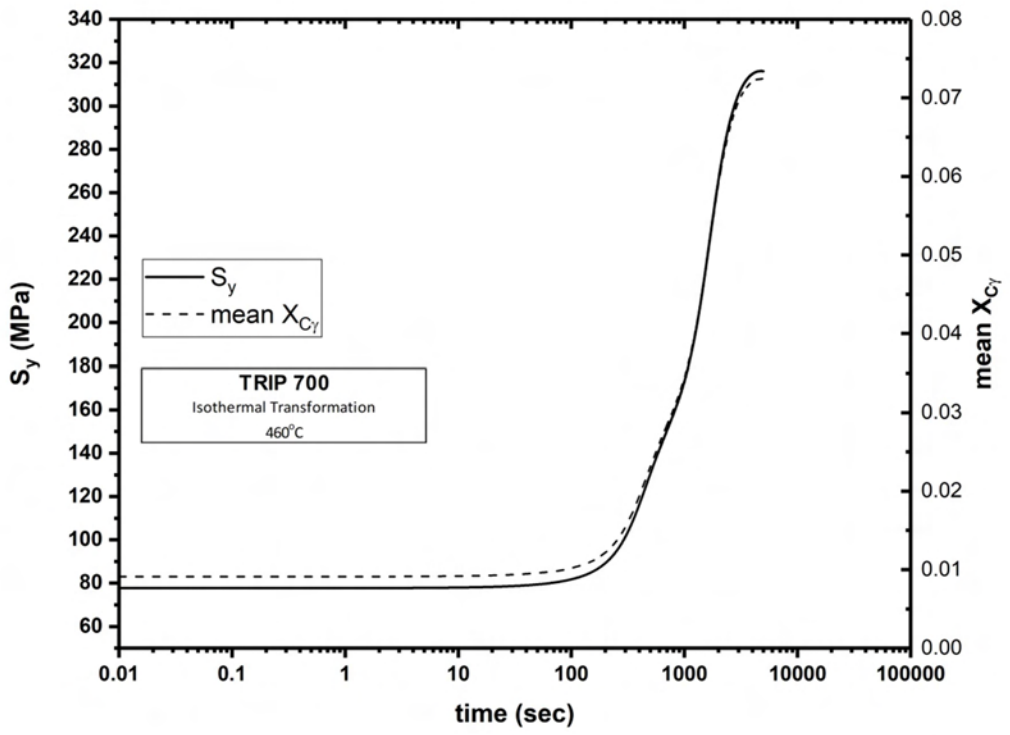

Figure 5.1-21 Yield Strength of Retained Austenite versus the Carbon enrichment of Austenite

5.1.5 Summary of Data

Finally, the table below shows the change in volume fractions as the transformation progresses, starting from heating, intercritical annealing, bainitic transformation and finally quenching.

Table 5.1-6 Phase Transformations Results from the Model

Simulation Data						
time (s)	**$f_{\alpha b}$**	**f_{γ}**	**$f_{\theta,\gamma}$**	**f_{M}**	**mean $X_{C\gamma}$**	**mean $X_{C\alpha}$**
5000	0.967172	0.029308	0.00352	0	0.071909	0.006326

The final volume fractions, calculated by the simulation, of the participating phases in the final microstructure are presented in Table 5.1-6. The microstructure consists of 2.9% retained austenite and 0.34% carbides precipitating in austenite.

5.2 Comparison of Heat Treatment Results

Figure 5.2-1 depicts a comparison between the mean volume fraction of bainitic ferrite ($f_{\alpha b}$) for isothermal holding at 400°C and 460°C. It is obvious that heat treatment at the higher temperature produces more bainitic ferrite, but the kinetics of the transformation are slower. In Figure 5.2-2 the comparison of mean volume fraction of austenite (f_{γ}) versus time during Isothermal holding at 400°C and 460°C is presented. In accordance with the previous figure less retained austenite is available at the end of isothermal holding for 460°C. This case also results in retained austenite more depleted of

Carbon, as evident from Figure 5.2-3. Although in the case of TRIP-Al steel carbides are not expected to form, Al and Si in excess of 1% retard the formation of carbides, for longer isothermal holding at 460°C some carbides appear in austenite (Figure 5.2-4)

In Figure 5.2-5 the microstructural characteristics of bainitic ferrite versus time during Isothermal Holding at 400°C and 460°C, are presented. The platelet size of bainitic ferrite starts smaller for IH at 460°C but eventually in both cases the final platelet size is extremely small. In Figure 5.2-6 the tensile Yield Strength of retained austenite for Isothermal Holding at 400°C and 460°C is illustrated. In the case of Isothermal Holding at 400°C the Yield Strength is higher.

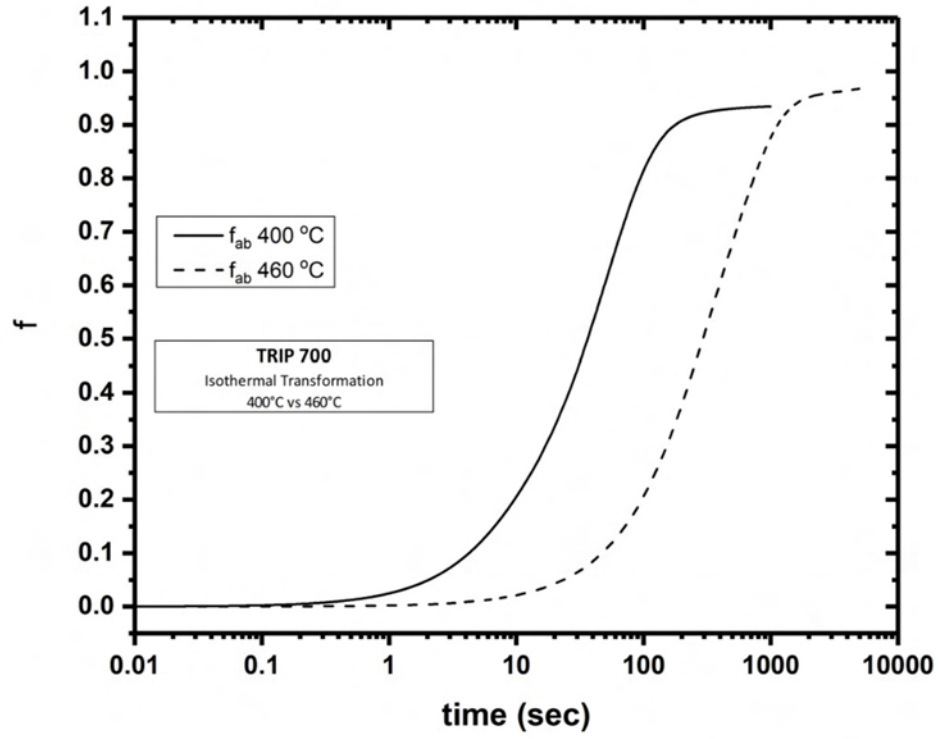

Figure 5.2-1 Comparison of mean Volume fraction of bainitic ferrite (f_{ab}) versus time during Isothermal Holding at 400°C and 460°C

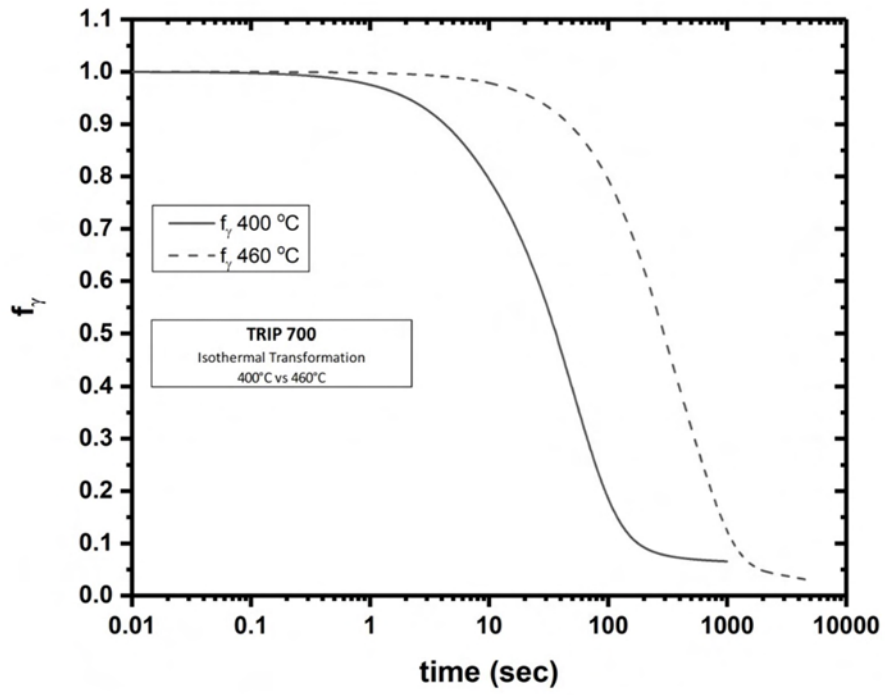

Figure 5.2-2 Comparison of mean Volume fraction of austenite (f_γ) versus time during Isothermal Holding at 400°C and 460°C

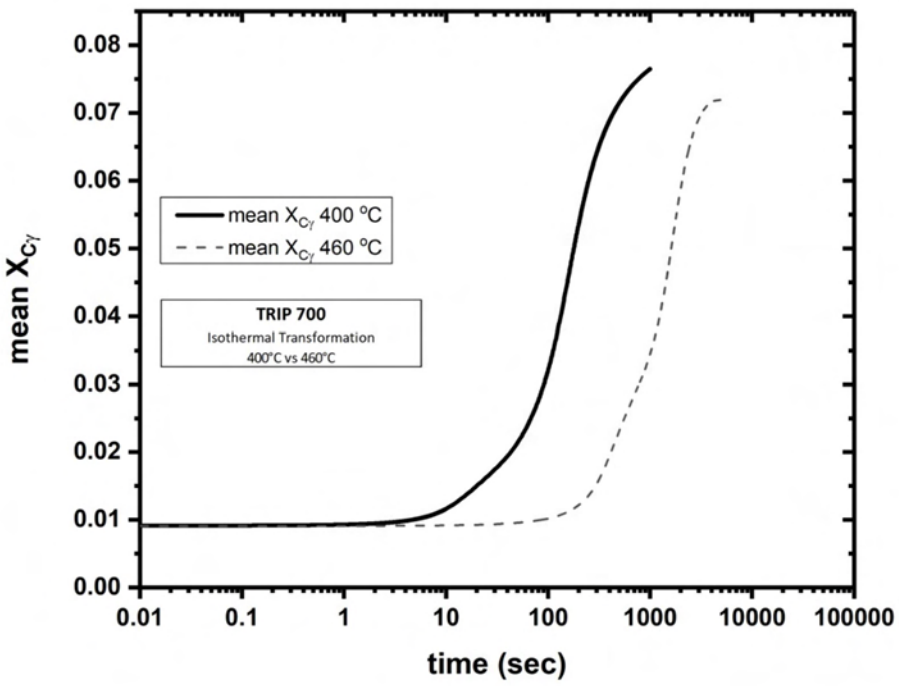

Figure 5.2-3 Comparison of mean Carbon concentration ($X_{C\gamma}$) versus time, during Isothermal Holding at 400°C and 460°C

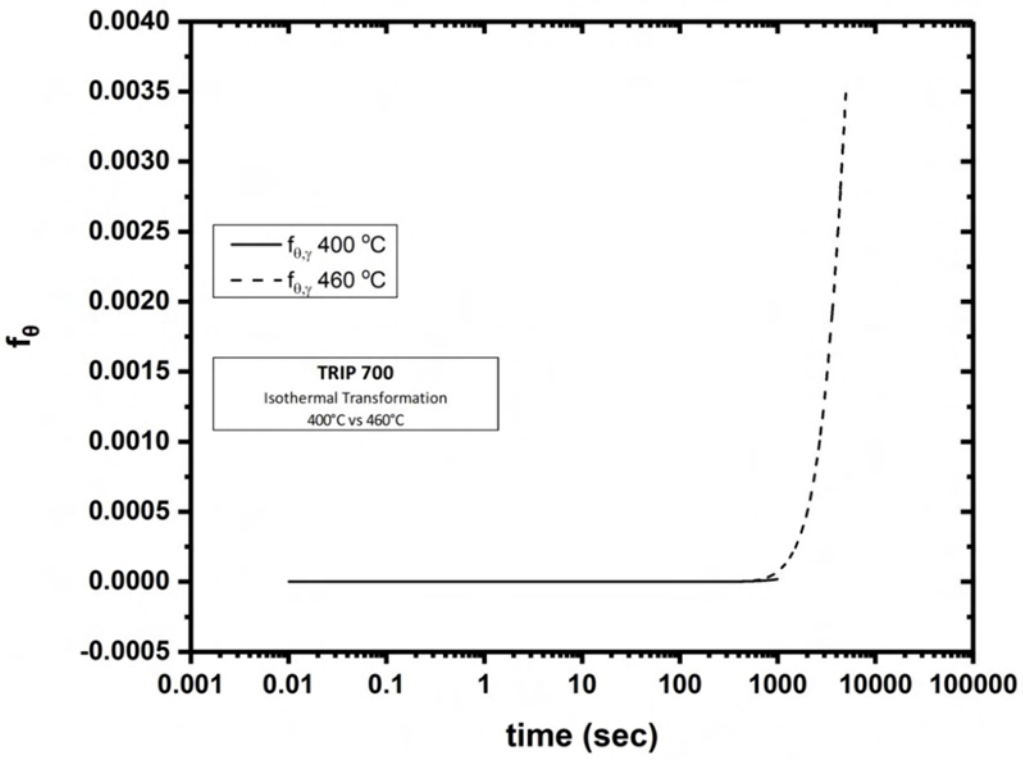

Figure 5.2-4 Comparison of carbide precipitation in austenite and versus time during Isothermal Holding at 400°C and 460°C

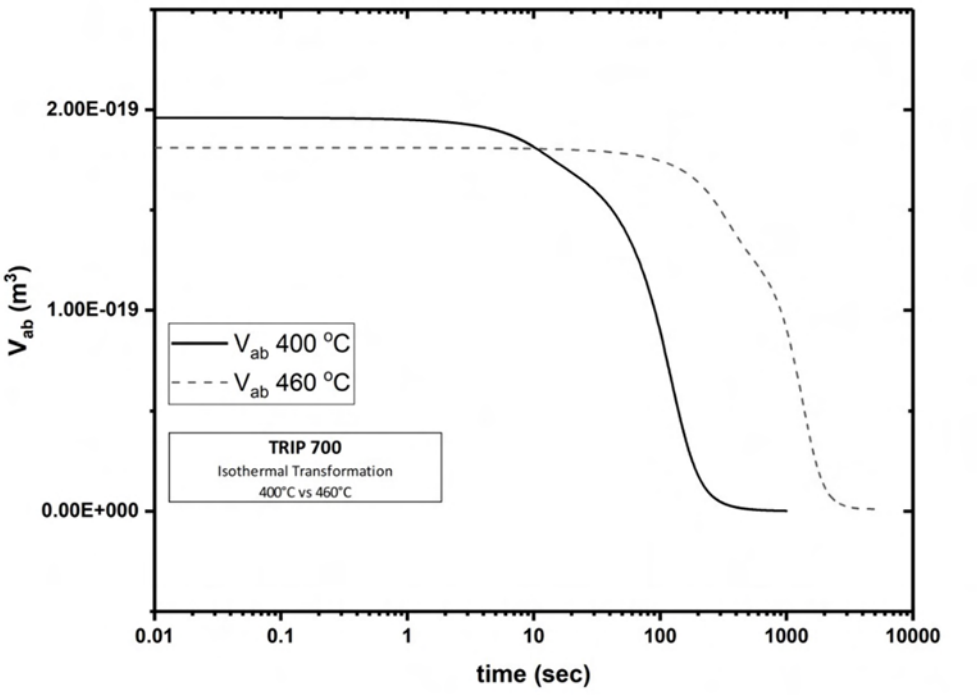

Figure 5.2-5 Comparison of platelet Size of bainitic ferrite) versus time during Isothermal Holding at 400°C and 460°C

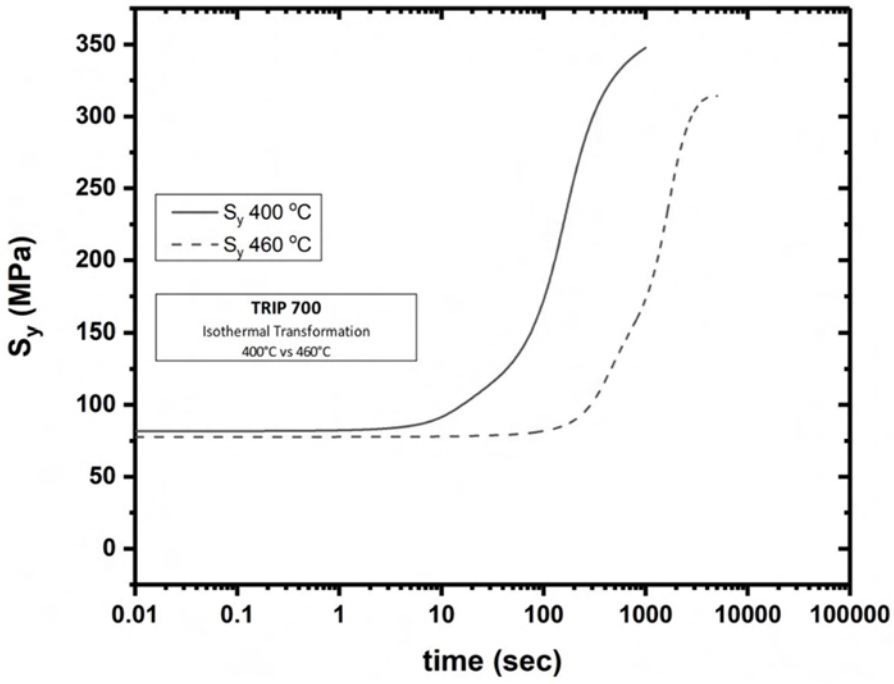

Figure 5.2-6 Comparison of Yield Strength of Retained Austenite versus time during Isothermal Holding at 400^{o}C and 460^{o}C

6 Summary - Evaluation of Method

Continuing the previous work performed by the Laboratory of Materials, an integrated thermodynamics and kinetics based modelling approached was developed, for simulating the bainitic transformation in advanced high strength steels.

The modelling approach consisted of thermodynamic calculations with the commercial software Thermocalc, kinetic calculations with the commercial software Dictra, thermodynamic calculations under paraequilibrium conditions (thermocalc and in house developed code), bainitic transformation simulation during continuous cooling and bainitic simulation during isothermal holding and finally martensitic transformation during the final quenching step. All the steps of the approach mentioned above were incorporated in a Matlab code developed during this thesis. Only the initial dictra model has not been incorporated in the final code yet.

The final code was validated by performing simulations on a Dual Phase steel containing 2.4% Mn. Experimental data were provided by Voestalpine and the simulation results were in excellent agreement. The next step consisted of evaluating the performance of the code in the case of TRIP-700 steel, with experimental results provided by the Mechanics & Strength of Materials Laboratory. The simulation results were again in very good agreement.

Finally, the output of the model includes the volume fraction of bainitic ferrite ($f_{\alpha b}$), the volume fraction of retained austenite (f_{γ}), carbides and martensite. It provides the Carbon concentration ($X_{c\gamma}$) of retained austenite, as well as the Yield Strength of retained austenite. Finally, the bainite platelet size can by calculated.

7 Future Work

Further work could focus on the initial step of the heating treatment, heating, isothermal holding and cooling to the bainitic transformation temperature. This part of the heat treatment is evaluated with the kinetics software Dictra and to this point is performed outside the integrated Matlab code. In the future, this step could be incorporated in the final Code. A great challenge for this step is the initial condition of the problem. Depending on the initial microstructure of the alloy as well as the heat treatment chosen the kinetic simulation part of the code is different.

Another useful step would be the introduction of actual composition profiles instead of mean values in the current method, as well as mapping of RA fraction and composition as a function of annealing parameters.

8 References

1. Matlock, D.K., et al., RECENT DEVELOPMENTS IN ADVANCED HIGH STRENGTH SHEET STEELS FOR AUTOMOTIVE APPLICATIONS: AN OVERVIEW. JESTECH, 2012. **15**(1): p. 1-12.

2. Kuziak, R., R. Kawalla, and S. Waengler, Advanced high strength steels for automotive industry. Archives of Civil and Mechanical Engineering, 2008. **8**(2): p. 103-117.

3. Marder, A.R. Factors Affecting the Ductility of "Dual-Phase" Alloys. in Formable HSLA and DualPhase Steels. 1979. Warrendale, PA: TMS AIME,.

4. Matlock, D.K. and J.G. Speer, Processing Opportunities for New Advanced High-Strength Sheet Steels. Materials and Manufacturing Processes, 2010. **25**(1-3): p. 7-13.

5. International Iron & Steel Institute, C.o.A.A. Advanced High Strength Steel (AHSS) Application Guidelines.

6. Kim, S.-K., G. Kim, and K.-G. Chin. Development of high Manganese TWIP Steel with 980MPa Tensile Strength. in Intl. Conf. on New Developments in Advanced High-Strength Sheet Steels, AIST,. 2008. Orlando, Fla,.

7. Gibbs, P.J., et al., Austenite Stability Effects on Tensile Behavior of Manganese-Enriched-Austenite Transformation-Induced Plasticity Steel. Metallurgical and Materials Transactions A, 2011. **42**(12): p. 3691-3702.

8. Song, R., et al., Overview of processing, microstructure and mechanical properties of ultrafine grained bcc steels. Materials Science and Engineering: A, 2006. **441**(1-2): p. 1-17.

9. Mazaheri, Y., et al., Effects of initial microstructure and thermomechanical processing parameters on microstructures and mechanical properties of ultrafine grained dual phase steels. Materials Science and Engineering: A, 2014. **612**: p. 54-62.

10. Matsumura, O., Y. Sakuma, and H. Takechi, Enhancement of elongation by retained austenite in intercritical annealed 0.4C-1.5Si-0.8Mn steel. Transactions of the Iron and Steel Institute of Japan, 1987. **27**(7): p. 570-579.

11. Matsumura, O., et al., Effect of Retained Austenite on Formability of High Strength Sheet Steels. ISIJ International, 1992. **32**(10): p. 1110-1116.

12. Perrard, F. and C. Scott, Vanadium Precipitation During Intercritical Annealing in Cold Rolled TRIP Steels. ISIJ International, 2007. **47**(8): p. 1168-1177.

13. Caballero, F.G., et al., Design of novel high strength bainitic steels: Part 2. Materials Science and Technology, 2013. **17**(5): p. 517-522.

14. Caballero, F.G., et al., Design of novel high strength bainitic steels: Part 1. Materials Science and Technology, 2013. **17**(5): p. 512-516.

15. Garcia-Mateo, C., F.G. Caballero, and H.K.D.H. Bhadeshia, Acceleration of Low-temperature Bainite. ISIJ International, 2003. **43**(11): p. 1821-1825.

16. Garcia-Mateo, C. and F.G. Caballero, Ultra-high-strength Bainitic Steels. ISIJ International, 2005. **45**(11): p. 1736-1740.

17. Speer, J., et al., Carbon partitioning into austenite after martensite transformation. Acta Materialia, 2003. **51**(9): p. 2611-2622.

18. Merwin, M.J. Low-Carbon Manganese TRIP Steels. in THERMEC 2006. 2006.

19. Miller, R.L., Ultrafine-grained microstructures and mechanical properties of alloy steels. Metallurgical and Materials Transactions B, 1972. **3**(4): p. 905-912.

20. De Moor, E., et al., Austenite stabilization through manganese enrichment. Scripta Materialia, 2011. **64**(2): p. 185-188.

21. Steven, W. and A.G. Haynes, The Temperature of Formation of Martensite and Bainite in Low-Alloy Steels. Journal of the Iron and Steel Institute, 1956. **183**(8): p. 349-359.

22. Barbier, D., Extension of the Martensite Transformation Temperature Relation to Larger Alloying Elements and Contents. Advanced Engineering Materials, 2014. **16**(1): p. 122-127.

23. Zhao, L., J. Sietsma, and S. Zwaag, Phase Transformations and Microstructural Evolution in Aluminium-Containing TRIP Steels. 2006. 77-82.

24. Girault, E., et al., Comparison of the effects of silicon and aluminium on the tensile behaviour of multiphase TRIP-assisted steels. Vol. 44. 2001. 885-892.

25. Lee, K., Y.R. Im, and K. Chin, Effect of carbon contents on the microstructure and the transformation kinetics of super bainitic TRIP steel. Vol. 3. 2008. 1785-1793.

26. Bhadeshia, H.K.D.H. and R.W.K. Honeycombe, Steels : microstructure and properties. 3rd ed. 2006, Amsterdam ; Boston ; London: Butterworth-Heinemann. xi, 344 p.

27. Azuma, M., et al., Modelling Upper and Lower Bainite Transformation in Steels. Materials Science Forum, 2003. **426-432**: p. 1405-1412.

28. Rees, G.I. and H.K.D.H. Bhadeshia, Bainite transformation kinetics Part 1 Modified model. Materials Science and Technology, 2013. **8**(11): p. 985-993.

29. Ghosh, G. and G.B. Olson, Kinetics of F.C.C. → B.C.C. heterogeneous martensitic nucleation—I. The critical driving force for athermal nucleation. Acta Metallurgica et Materialia, 1994. **42**(10): p. 3361-3370.

30. Takahashi, M. and H.K.D.H. Bhadeshia, Model for transition from upper to lower bainite. Materials Science and Technology, 1990. **6**(7): p. 592-603.

31. Ghosh, G. and G.B. Olson, Precipitation of paraequilibrium cementite: Experiments, and thermodynamic and kinetic modeling. Acta Materialia, 2002. **50**(8): p. 2099-2119.

32. Hultgren, A., Isothermal transformation of austenite. Transactions of the American Society for Metals, 1947. **39**: p. 915-1005.

33. Grujicic, M. and G.N. Haidemenopoulos, A treatment of paraequilibrium thermodynamics in AF1410 steel using the thermocalc software and database. Calphad, 1988. **12**(3): p. 219-224.

34. Ghosh, G. and G. Olson, Simulation of paraequilibrium growth in multicomponent systems. Metallurgical and Materials Transactions A, 2001. **32**(3): p. 455-467.

35. Sundman, B., B. Jansson, and J.-O. Andersson, The Thermo-Calc databank system. Calphad, 1985. **9**(2): p. 153-190.

36. Lee, Y.K., Empirical formula of isothermal bainite start temperature of steels. Journal of Materials Science Letters, 2002. **21**(16): p. 1253-1255.

37. Sonderegger, B. and E. Kozeschnik, Generalized Nearest-Neighbor Broken-Bond Analysis of Randomly Oriented Coherent Interfaces in Multicomponent Fcc and Bcc Structures. Metallurgical and Materials Transactions a-Physical Metallurgy and Materials Science, 2009. **40a**(3): p. 499-510.

38. Aristeidakis, J.S. and G.N. Haidemenopoulos, Alloy Design Based on Computational Thermodynamics and Multi-objective Optimization: The Case of Medium-Mn Steels. Metallurgical and Materials Transactions A, 2017. **48**(5): p. 2584-2602.

39. Design of bainite in steels from homogeneous and inhomogeneous microstructures using physical approaches - Bainite Design -, E.C.a.s. Community, Editor. 2010, RFCS: Brussels.

9 Appendix

9.1 Main Code

```
%                                MAIN CODE
%
%--------------------------------------------------------------------------
%--------------------------------------------------------------------------
%--------------------------------------------------------------------------

clear;clc;close all;

%--------------------------------------------------------------------------
%--------------------------------------------------------------------------
%
%                                INPUTS
%
%--------------------------------------------------------------------------
%                      Enter Zones Compositions in %wt
%                            C/Mn/Cr/Si/Nb/Al

alloycomp=[ 0.951575331 4.34135111  0.038   0.66385291  0.017   1.35472386;
            0.927262866 2.72846661  0.038   0.66098325  0.017   1.91289496;
            0.902966545 1.12967619  0.038   0.66495939  0.017   2.45590698;];

%--------------------------------------------------------------------------
%                            Enter Name of Zones

zones=['Zone01_400';'Zone02_400';'Zone03_400';];

%--------------------------------------------------------------------------
%                            General Constants

Temp=400;           %(C)
duration=2E3;       %(sec)
step=0.01;          %(sec)

R=8.3145;           %(J/mol*K)
k=1.38065E-23;      %(J/K)
No=1E+19;           %(1/m3)
No_cem_a=1E+10;     %(1/m3)
No_cem_y=1E+10;     %(1/m3)
NA=6.023E+23;       %(1/mol)
h=6.62607E-34;      %(J*sec)
b=1;                %(-)
QC_a=8.03E+04;      %(J/mol)
QC_y=1.35E+05;      %(J/mol)

%--------------------------------------------------------------------------
```

```
%-------------------------------------------------------------------------
%-------------------------------------------------------------------------
%                              Interface Code
%-------------------------------------------------------------------------
%-------------------------------------------------------------------------
%-------------------------------------------------------------------------

for i=1:size(zones,1)
    if ((exist(['RESULTS\',zones(i,:)],'dir'))==7)
        disp('One or more directories with the same name already exists')
        disp('Choose a different folder name for results')
        return
    end
end

disp('You entered the following %wt compositions:')
fprintf('\n')

fprintf('\n')
disp(['C  =  ',num2str(alloycomp(:,1)','%.4f\t\t')])
disp(['Mn =  ',num2str(alloycomp(:,2)','%.4f\t\t')])
disp(['Cr =  ',num2str(alloycomp(:,3)','%.4f\t\t')])
disp(['Si =  ',num2str(alloycomp(:,4)','%.4f\t\t')])
disp(['Nb =  ',num2str(alloycomp(:,5)','%.4f\t\t')])
disp(['Al =  ',num2str(alloycomp(:,6)','%.4f\t\t')])
fprintf('\n')

disp('Under the conditions:')
fprintf('\n')
disp(['Temp=',num2str(Temp),' C   Duration=',num2str(duration,'%2.1G'),...
     ' sec   Step=',num2str(step),' sec'])
 fprintf(['\n','No=',num2str(No,'%2.1G'),' 1/m3\n','No_cem_a=',...
     num2str(No_cem_a,'%2.1G'),' 1/m3\n','No_cem_y=',...
     num2str(No_cem_a,'%2.1G'),' 1/m3\n\n'])
disp('If your inputs are false, STOP NOW and correct them')

disp('Calculations will begin in 30 sec')
n=7;

for i=29:-1:0
    pause(1)
    fprintf(repmat('\b',1,n));
    fprintf([num2str(i),' sec']);
    n=size([num2str(i),' sec'],2);
end

addpath Source
Temp=Temp+273.15;     %(K)

tic
```

```
% %------------------------------------------------------------------------
% %------------------------------------------------------------------------
% %                          Zone Calculations
% %------------------------------------------------------------------------
for i=1:size(zones,1)

    zonecomp=alloycomp(i,:);
    resultsfolder=zones(i,:);
    mkdir(['RESULTS/',resultsfolder]);

    %------------------------------------------------------------------------
    %                          Fitting Equations Constants

    %Calculation of Xi Range
    mean_XC_y=XiCreation(zonecomp,resultsfolder);
    mean_XC_y=repmat(mean_XC_y,1,2);

    %Paraequilibrium Calculations
    XC_cem_y=Thermocalc('Xc_(cem-y)',resultsfolder);

    XC_cem_a=Thermocalc('Xc_(cem-a)',resultsfolder);

    poly_DGn_y_ab=Thermocalc('DGm_(a-y)',resultsfolder);

    poly_Vm_a=Thermocalc('Vm_x(bcc-a2)',resultsfolder);

    poly_DGn_y_cem=Thermocalc('DGm_(y-cem)',resultsfolder);

    poly_Vm_cem=Thermocalc('Vm_x(cem)',resultsfolder);

    poly_DGn_a_cem=Thermocalc('DGm_(a-cem)',resultsfolder);

    poly_XC_y_cem=Thermocalc('Xc_(y-cem)',resultsfolder);

    poly_XC_a_y=Thermocalc('Xc_(a-y)',resultsfolder);

    poly_XC_a_cem=Thermocalc('Xc_(a-cem)',resultsfolder);

    %Interfacial Energies
    s_polynomial=S_fitting;
    poly_s_cem_a=s_polynomial(1,:);
    poly_s_cem_y=s_polynomial(2,:);
    poly_s_ab_y=s_polynomial(3,:);
    clear s_polynomial

    %------------------------------------------------------------------------

    % Save Constants
    constants=['RESULTS\',resultsfolder,'\',resultsfolder,'.mat'];
    save(constants, '-regexp',...
        '^(?!(i|Temp|duration|step|alloycomp|varstore|resultsfolder|)$).' )
```

```
    %-------------------------------------------------------------------------
    %                                  AZUMA
    %-------------------------------------------------------------------------

    [data,timeaxis]=Azuma_ConstantTemp(Temp,duration,step,constants);


    %Create Excel with Azuma Results
    copyfile('Source\Azuma.xlsx',['RESULTS\',resultsfolder,'\Constant_',...
        resultsfolder,'.xlsx'])

    xlswrite(['RESULTS\',resultsfolder,'\Constant_',resultsfolder,'.xlsx'],..
        [timeaxis(:),data(:,:)'],'Data','A4')

    %-------------------------------------------------------------------------
    %                                QUENCHING
    %-------------------------------------------------------------------------


    T_R=25; % Room Temperature

    %Ms Calculation
    Ms=545-601.2*(1-exp(-0.868*100*...
        Final_wt([data(1,size(data,2)),zonecomp(2:6)],resultsfolder)))...
        -34.4*zonecomp(2)-13.7*zonecomp(4)-9.2*zonecomp(3);
    Ms(Ms<-273)=-273;

    % K-M Model (Transformation Fraction as a function of austenite)
    f_M=(Ms>=T_R).*(1-exp(-0.011*(Ms-T_R)));
    f_M=data(4,size(data,2))*f_M;

    % Total Retained Austenite Fraction
    data(4,size(data,2))=data(4,size(data,2))-f_M;

    %Create .dat with final Results
    final=fopen(['RESULTS\',resultsfolder,'\Quenching_Results',...
        resultsfolder,'.dat'],'w');
    titles={'mean_XC_y','mean_XC_a','f_ab','f_y','f_cem_y','f_cem_a',...
        'L_ab','W_ab','S_ab','Vsu','Sy','f_m'};

    fprintf(final,'%s\n\n\n','FINAL RESULTS AFTER QUENCHING');
    for j=1:(size(titles,2)-1)
        fprintf(final,'%s%s%g\n',titles{j},'=',data(j,size(data,2)));
    end
    fprintf(final,'%s%s%g\n',titles{size(titles,2)},'=',f_M);
    fclose(final);

end

clc;
disp('Calculations are complete.')

toc
```

9.2 Paraequilibrium Calculations

```
%This Function Calculates all Constants Using Thermocalc
%
%-------------------------------------------------------------------------
%                                  INPUT
%
%CalculationType = {'DGm_(a-cem)','DGm_(a-y)','DGm_(y-cem)',
%                   'Vm_x(bcc-a2)','Vm_x(cem)','Xc_(a-cem)','Xc_(a-y)',...
%                   'Xc_(cem-a)','Xc_(cem-y)','Xc_(y-cem)'};
%
%-------------------------------------------------------------------------

function result = Thermocalc(CalculationType,resultsfolder)

cd(['RESULTS\',resultsfolder]);

cleardir(CalculationType);

for i=1:15
%     Run Calculations for i Composition

    [X(i,:),WComp]=ReadComp(i);

    y=AssignVariables(WComp);

    ThermoCalculate(y,X(i,:),CalculationType);
end

result=FitData(CalculationType,X(:,2));
cd ../..
end

%-------------------------------------------------------------------------
%                               FUNCTIONS
%-------------------------------------------------------------------------

function cleardir(folder)
%This function clears the Thermocalc directories

if ((exist(['Thermocalc\',folder],'dir'))==7)
    originalpath=cd;
    cd(['Thermocalc\',folder]);
    delete *.dat *.tcm *.POLY3
    cd(originalpath)
end

end
```

```
function [X,Y]=ReadComp(j)
originalpath=cd;
cd 'Xi'

if ((exist(['x',int2str(j),'.PLE'],'file'))~=2)
    disp(['Could Not Find ','"x',int2str(j),'"'])
    return
end
fid=fopen(['x',int2str(j),'.PLE'],'r');

%Skip unnecessary lines
for k=1:12
    fgets(fid);
end

%Keep lines with Composition
for k=1:7
    A(k,:)=fgets(fid);
end
fclose(fid);
clear ans

%Manipulate Data
A=str2num(A(:,26:35));
X=A;
Y=A/(1-A(2));
cd(originalpath);
end
```

```
function x=AssignVariables(A)
%Assign Variables
x=zeros(55,1);
% ------------------------------------------------------------------------
x(1)=A(4);x(2)=A(5);x(3)=A(3);x(4)=A(7);x(5)=A(6);x(6)=A(1);

x(7)=x(1)*x(2);x(9)=x(1)*x(3);x(11)=x(1)*x(4);x(13)=x(1)*x(5);
x(15)=x(1)*x(6);

x(17)=x(2)*x(3);x(19)=x(2)*x(4);x(21)=x(2)*x(5);x(23)=x(2)*x(6);

x(25)=x(3)*x(4);x(27)=x(3)*x(5);x(29)=x(3)*x(6);

x(31)=x(4)*x(5);x(33)=x(4)*x(6);

x(35)=x(5)*x(6);
% ------------------------------------------------------------------------
x(8)=x(7)*(abs(x(1)-x(2)));x(10)=x(9)*(abs(x(1)-x(3)));
x(12)=x(11)*(abs(x(1)-x(4)));x(14)=x(13)*(abs(x(1)-x(5)));
x(16)=x(15)*(abs(x(1)-x(6)));

x(18)=x(17)*(abs(x(2)-x(3)));x(20)=x(19)*(abs(x(2)-x(4)));
x(22)=x(21)*(abs(x(2)-x(5)));x(24)=x(23)*(abs(x(2)-x(6)));

x(26)=x(25)*(abs(x(3)-x(4)));x(28)=x(27)*(abs(x(3)-x(5)));
x(30)=x(29)*(abs(x(3)-x(6)));

x(32)=x(31)*(abs(x(4)-x(5)));x(34)=x(33)*(abs(x(4)-x(6)));

x(36)=x(35)*(abs(x(5)-x(6)));
% ------------------------------------------------------------------------
m=37;
for i=1:4
    for j=i+1:5
        for k=j+1:6
            if((i~=j)&&(j~=k)&&(i~=k)&&m<55)
                x(m)=x(i)*x(j)*x(k);
                m=m+1;
            end
        end
    end
end
x(m)=x(4)*x(5)*x(6);
end
```

```
function ThermoCalculate(y,Comp,filename)
originalpath=cd;

%Open 'filename' Source File e.g. DGm
cd ../..
cd Source
readid=fopen([filename,'.txt'],'r');

%Create Thermocalc File
folder=[originalpath,'\Thermocalc\',filename];
if ((exist(folder,'dir'))~=7)
    mkdir(folder);
end
cd(folder);

writeid=fopen([filename,'.tcm'],'w');

%Copy Source File but change the Values of Y
k=1;
while ~feof(readid)
   tline=fgetl(readid);
   if strcmp(tline,['Y',int2str(k)])
      fprintf(writeid,'%s\n',tline);
      fgetl(readid);
      fprintf(writeid,'%d%s\n',y(k),';');
      k=k+1;
   elseif strcmp(tline,'am-el')
       fprintf(writeid,'%s\n',tline);
       tline=fgetl(readid);
       fprintf(writeid,'%s\n',tline);
       tline=fgetl(readid);
       fprintf(writeid,'%s\n',tline);
       g1=Comp(4)*55.847+Comp(5)*54.938+Comp(3)*51.996+Comp(7)*28.085+...
           Comp(6)*92.906+Comp(1)*26.982;
       g2=Comp(4)*4489+Comp(5)*4996+Comp(3)*4050+Comp(7)*3217.5+...
           Comp(6)*5220+Comp(1)*4577.296;
       g3=Comp(4)*27.28+Comp(5)*32.008+Comp(3)*23.56+Comp(7)*18.82+...
           Comp(6)*36.27+Comp(1)*28.322;
       fprintf(writeid,'%d\n%d\n%d\n',g1,g2,g3);
       fgetl(readid);
       fgetl(readid);
       fgetl(readid);
   elseif strcmp(tline,'ma')
      fprintf(writeid,'%s\n',tline);
      fgetl(readid);
      fprintf(writeid,'%s%g%s\n',filename,Comp(2),'.dat');
   else
      fprintf(writeid,'%s\n',tline);
   end
end
    fclose('all');

    %Run the Thermocalc File
    system(['"',filename,'.tcm"']);
    cd(originalpath);
end
```

```
function poly=FitData(filename, Comp)
%Read the Values of files for Every Composition
%and applies the correct Fit
originalpath=cd;
cd(['Thermocalc\',filename]);

for i=1:size(Comp,1)
    clear A;
    if ((exist([filename,num2str(Comp(i)),'.dat'],'file'))~=2)
        disp(['Could Not Find ','"',filename,num2str(Comp(i)),'"'])
        return
    end
    fid=fopen([filename,num2str(Comp(i)),'.dat'],'r');

    %Find the lines containing the Results
    %Dismiss any other line
    k=1;
    A=[''];
    while ~feof(fid)
        tline=fgetl(fid);
        if size(tline,2)>2 && strcmp(tline(1:3),'   ')
            A(k,:)=tline(1:38);
            k=k+1;
        end
    end

    fclose(fid);
    if isempty(A)
        Comp(i)=100;
        continue
    end

    A=unique(A,'rows');

    %Only for the first run, set the Temp Axis
    %and allocate the size of the Value Array
    Temp_new=str2num(A(:,4:19));
    toDelete=round(mod(Temp_new,10),3)~=3.1500&...
        round(mod(Temp_new,10),3)~=0;
    A(toDelete,:) = [];
    Temp_new(toDelete,:)=[];

    if i==1
        Temp=Temp_new;
    end

    if size(Temp,1)<size(Temp_new,1)
        for j=1:size(Temp,1)
            comparison=Temp(j,:)==Temp_new(j,:);
            if comparison==0
                break
            end
        end
        A(j,:)=[];
```

```
    elseif size(Temp,1)>size(Temp_new,1)
        Temp=Temp_new;
        for j=1:size(Temp,1)
            comparison=Temp(j,:)==Temp_new(j,:);
            if comparison==0
                break
            end
        end
        FitValue(j,:)=[];
    end

    FitValue(:,i)=str2num(A(:,23:38));
end

%Decide the Type of Fit
if strcmp(filename,'Xc_(cem-a)')||strcmp(filename,'Xc_(cem-y)')
    FitType='poly00';
elseif strcmp(filename,'Xc_(a-cem)')||strcmp(filename,'Xc_(a-y)')
    FitType='poly42';
elseif strcmp(filename(1:3),'DGm')||strcmp(filename,'Xc_(y-cem)')
    FitType='poly45';
elseif strcmp(filename,'Vm_x(bcc-a2)')
    FitType='poly11';
elseif strcmp(filename,'Vm_x(cem)')
    FitType='poly21';
end

warning('off','all')

Comp(Comp(:)==100)=[];
if isempty(Comp)
    poly=0;
    return
end

[Xaxis,Yaxis,Zaxis]=prepareSurfaceData(Temp,Comp,FitValue);
Fitted=fit([Xaxis,Yaxis],Zaxis,FitType,'Normalize','off');
poly=coeffvalues(Fitted);

syms f(x,y)
if strcmp(FitType,'poly00')
    f(x,y)=real(poly);
elseif strcmp(FitType,'poly11')
    f(x,y)=poly(1)+poly(2)*x+poly(3)*y;
elseif strcmp(FitType,'poly21')
    f(x,y)=poly(1)+poly(2)*x+poly(3)*y+poly(4)*x^2+poly(5)*x*y;
elseif strcmp(FitType,'poly41')
    f(x,y)=real(poly(1)+poly(2)*x+poly(3)*y+poly(4)*x^2+poly(5)*x*y+...
        poly(6)*x^3+poly(7)*x^2*y+poly(8)*x^4+poly(9)*x^3*y);
elseif strcmp(FitType,'poly42')
    f(x,y)=real(poly(1)+poly(2)*x+poly(3)*y+poly(4)*x^2+poly(5)*x*y+...
        poly(6)*y^2+poly(7)*x^3+poly(8)*x^2*y+poly(9)*x*y^2+...
        poly(10)*x^4+poly(11)*x^3*y+poly(12)*x^2*y^2);
elseif strcmp(FitType,'poly45')
    f(x,y)=real(poly(1)+poly(2)*x+poly(3)*y+poly(4)*x^2+poly(5)*x*y+...
```

```
        poly(6)*y^2+poly(7)*x^3+poly(8)*x^2*y+poly(9)*x*y^2+...
poly(10)*y^3 +poly(11)*x^4+poly(12)*x^3*y+poly(13)*x^2*y^2+...
        poly(14)*x*y^3+poly(15)*y^4+poly(16)*x^4*y+poly(17)*x^3*y^2+...
        poly(18)*x^2*y^3+poly(19)*x*y^4+poly(20)*y^5);
end


figure('Name',filename,'NumberTitle','off','Units','Pixels',...
'OuterPosition',[0 0 1920 1080],'Visible', 'off')
fsurf(f,[400 800 Comp(1) Comp(size(Comp,1))])
hold on
scatter3(Xaxis,Yaxis,Zaxis)
hold off
print(filename,'-dpng','-r300')

warning('on', 'all')
cd(originalpath);
end
```

9.3 Azuma model for constant temperature transformation

```
%            AZUMA MODEL FOR CONSTANT TEMPERATURE TRANSFORMATION
%-------------------------------------------------------------------------
%-------------------------------------------------------------------------
%-------------------------------------------------------------------------

function [datastore,timeaxis]=Azuma_ConstantTemp(Temp,duration,step,...
    Constants)

load(Constants)

loops=duration/step+1;

%Definition of Variables used for Storing Data
datanum=20000;
datastore=zeros(11,datanum);
timeaxis=zeros(1,datanum);
datacount=0;


%-------------------------------------------------------------------------
%                           Azuma Calculations
%-------------------------------------------------------------------------



XC_y_cem=Fit(Temp,mean_XC_y(2),poly_XC_y_cem);

XC_a_y=Fit(Temp,mean_XC_y(2),poly_XC_a_y);

XC_a_cem=Fit(Temp,mean_XC_y(2),poly_XC_a_cem);

Vm_cem=Fit(Temp,mean_XC_y(2),poly_Vm_cem);

%Variable Initialization
mean_XC_a=[XC_a_y 0];
f_ab=[0 0];
f_cem_y=[0 0];
f_cem_a=[0 0];
Df_ab_ext=0;
Df_ab=0;
I_cem_y_Dt=0;
I_cem_y=0;
I_cem_a_Dt=0;
I_cem_a=0;
f_y=1;
```

```
%First Step of ab Calculations
Vm_a=Fit(Temp,mean_XC_y(2),poly_Vm_a);
DGn_y_ab=-R*400*Fit(Temp,mean_XC_y(2),poly_DGn_y_ab);

DGv_y_ab=DGn_y_ab/Vm_a;
s_ab_y=Fit(Temp,mean_XC_y(2),poly_s_ab_y);
DG_y_ab=(16*pi*s_ab_y^3*NA)/(3*DGv_y_ab^2)-(3.637*(Temp-273.15)-2540);
I_ab=(1+b*f_ab(2))*No*k*Temp/h*exp((-QC_y-DG_y_ab)/(R*Temp));
Sy=(1-0.0026*(Temp-298.15)+(4.7E-6)*(Temp-298.15)^2-...
    (3.26E-9)*(Temp-298.15)^3)*15.4*(3.6+23*(21.69631*mean_XC_y(2)-...
    (1.77636E-15))+0.65*zonecomp(2)+1.3*zonecomp(4));
if(((0.478+0.00012*Temp+0.000125*(Temp-DGn_y_ab)-0.0022*Sy)*1E-6)>0)
    W_ab=(0.478+0.00012*Temp+0.000125*(Temp-DGn_y_ab)-0.0022*Sy)*1E-6;
else
    W_ab=0;
end
L_ab=6*W_ab;
S_ab=0.12*W_ab;
Vsu=W_ab*L_ab*S_ab;


for j=1:loops

    if(j~=1)
        Df_ab_ext=I_ab*Vsu*step;
    end
    Df_ab=Df_ab_ext*(1-f_ab(1)-f_cem_y(1)-f_cem_a(1));
    f_ab(2)=f_ab(1)+Df_ab;

    %Calculations for ab
    Vm_a=Fit(Temp,mean_XC_y(2),poly_Vm_a);
    DGn_y_ab=-R*400*Fit(Temp,mean_XC_y(2),poly_DGn_y_ab);

    DGv_y_ab=DGn_y_ab/Vm_a;
    s_ab_y=Fit(Temp,mean_XC_y(2),poly_s_ab_y);
    DG_y_ab=(16*pi*s_ab_y^3*NA)/(3*DGv_y_ab^2)-(3.637*(Temp-273.15)-2540);


    I_ab=(1+b*f_ab(2))*No*k*Temp/h*exp((-QC_y-DG_y_ab)/(R*Temp));
    Sy=(1-0.0026*(Temp-298.15)+(4.7E-6)*(Temp-298.15)^2-...
        (3.26E-9)*(Temp-298.15)^3)*15.4*(3.6+23*(21.69631*mean_XC_y(2)-...
        (1.77636E-15))+0.65*zonecomp(2)+1.3*zonecomp(4));
    if(((0.478+0.00012*Temp+0.000125*(Temp-DGn_y_ab)-0.0022*Sy)*1E-6)>0)
        W_ab=(0.478+0.00012*Temp+0.000125*(Temp-DGn_y_ab)-0.0022*Sy)*1E-6;
    else
        W_ab=0;
    end
    L_ab=6*W_ab;
    S_ab=0.12*W_ab;
    Vsu=W_ab*L_ab*S_ab;

    %Calculations for y_cem
    DGn_y_cem=-R*400*Fit(Temp,mean_XC_y(2),poly_DGn_y_cem);
    DGv_y_cem=DGn_y_cem/Vm_cem;
    s_cem_y=Fit(Temp,mean_XC_y(2),poly_s_cem_y);
```

```
    DG_y_cem=(16*pi*s_cem_y^3*NA)/(3*DGv_y_cem^2);

    I_cem_y_Dt=I_cem_y_Dt+I_cem_y*step;
    I_cem_y=No_cem_y*k*Temp/h*exp((-QC_y-DG_y_cem)/(R*Temp));
    f_cem_y(2)=f_cem_y(1)+19.634954085*I_cem_y_Dt*...
        ((mean_XC_y(2)-XC_y_cem)^2/((XC_cem_y-mean_XC_y(2))*...

        (XC_cem_y-XC_y_cem))*step*1E-8)^(1.5)*...
        (1-f_ab(1)-f_cem_y(1)-f_cem_a(1));

    %Calculations for a_cem
    DGn_a_cem=-R*400*Fit(Temp,mean_XC_y(2),poly_DGn_a_cem);
    DGv_a_cem=DGn_a_cem/Vm_cem;
    s_cem_a=Fit(Temp,mean_XC_y(2),poly_s_cem_a);
    DG_a_cem=(16*pi*s_cem_a^3*NA)/(3*DGv_a_cem^2);

    I_cem_a_Dt=I_cem_a_Dt+I_cem_a*step;
    I_cem_a=No_cem_a*k*Temp/h*exp((-QC_a-DG_a_cem)/(R*Temp));
    f_cem_a(2)=f_cem_a(1)+19.634954085*I_cem_a_Dt*...
        ((mean_XC_a(2)-XC_a_cem)^2/((XC_cem_a-mean_XC_a(2))*...
        (XC_cem_a-XC_a_cem))*step*0.00000062)^(1.5)*...
        (1-f_ab(1)-f_cem_y(1)-f_cem_a(1));

    %General Calculations
    mean_XC_y(2)=(mean_XC_y(1)-f_ab(2)*XC_a_y-...
        f_cem_y(2)*XC_cem_y)/(1-f_ab(2)-f_cem_y(2));
    mean_XC_a(2)=(mean_XC_a(1)-f_cem_a(2)*XC_cem_a)/(1-f_cem_a(2));
    mean_XC_a(2)=(mean_XC_a(2)>=0)*mean_XC_a(2);
    f_y=1-f_ab(2)-f_cem_y(2)-f_cem_a(2);

    %Progression of Loop
    f_ab(1)=f_ab(2);
    f_cem_y(1)=f_cem_y(2);
    f_cem_a(1)=f_cem_a(2);

    %Storing Data for Graphs
    dataskip=1E2;

    if(mod(j,dataskip)==0||(step*(1+j))<10||j==loops)
        datacount=datacount+1;
        datastore(:,datacount)=[mean_XC_y(2),mean_XC_a(2),...
            f_ab(2), f_y, f_cem_y(2),f_cem_a(2), L_ab, W_ab,...
            S_ab, Vsu, Sy];
        timeaxis(datacount)=(j-1)*step;
    end
end

datanum=datacount;
datastore=datastore(:,1:datanum);
timeaxis=timeaxis(:,1:datanum);

end
```

```
%--------------------------------------------------------------------------
%                               Functions
%--------------------------------------------------------------------------

function result = Fit(x,y,poly)

if size(poly,2)==1
    result=real(poly);
elseif size(poly,2)==3
    result=poly(1)+poly(2)*x+poly(3)*y;
elseif size(poly,2)==5
    result=poly(1)+poly(2)*x+poly(3)*y+poly(4)*x^2+poly(5)*x*y;
elseif size(poly,2)==9
    result=real(poly(1)+poly(2)*x+poly(3)*y+poly(4)*x^2+poly(5)*x*y+...
        poly(6)*x^3+poly(7)*x^2*y+poly(8)*x^4+poly(9)*x^3*y);
elseif size(poly,2)==12
    result=real(poly(1)+poly(2)*x+poly(3)*y+poly(4)*x^2+poly(5)*x*y+...
        poly(6)*y^2+poly(7)*x^3+poly(8)*x^2*y+poly(9)*x*y^2+...
        poly(10)*x^4+poly(11)*x^3*y+poly(12)*x^2*y^2);
elseif size(poly,2)==20
    result=real(poly(1)+poly(2)*x+poly(3)*y+poly(4)*x^2+poly(5)*x*y+...
        poly(6)*y^2+poly(7)*x^3+poly(8)*x^2*y+poly(9)*x*y^2+...
        poly(10)*y^3 +poly(11)*x^4+poly(12)*x^3*y+poly(13)*x^2*y^2+...
        poly(14)*x*y^3+poly(15)*y^4+poly(16)*x^4*y+poly(17)*x^3*y^2+...
        poly(18)*x^2*y^3+poly(19)*x*y^4+poly(20)*y^5);
end


end
```